Welding Research

SPONSORED BY THE WELDING RESEARCH COUNCIL
OF THE ENGINEERING FOUNDATION

W. SPRARAGEN, DIRECTOR

SUPPLEMENT TO THE WELDING JOURNAL, OCTOBER, 195

IMPACT PERFORMANCE OF SYNTHETICALLY REPRODUCED HEAT-AFFECTED-ZONE MICROSTRUCTURES IN "T-1" STEEL

Laboratory investigation indicates that, based on results with particular heat tested, "T-1" steel is not embrittled by the thermal cycles of welding

BY ERNEST F. NIPPES AND CRAIG R. SIBLEY

ABSTRACT. When a low-alloy steel which has been quenched and tempered to obtain its optimum properties is to be welded, consideration must be given to the metallurgical changes which occur in the heat-affected zone as a result of the welding thermal cycle.

Certain low-alloy steels have exhibited poor performance after welding due to the presence of an embrittled microstructure in some region of the heat-affected zone. Such behavior can be determined experimentally by synthetic production of heat-affected-zone microstructures and subsequent testing of these microstructures to determine if they are embrittled.

"T-1" steel, a low-alloy quenched-and-tempered steel, was subjected to heat-affected-zone thermal cycles attending a weld made in ½-in. plate. The resultant microstructures were evaluated by impact testing of Charpy vee-notch specimens. The impact strength of various heat-affected-zone structures revealed that there was only slight loss in toughness for these microstructures compared to the unaffected plate material.

The results obtained show that the particular heat of "T-1" steel tested herein is not embrittled by the thermal cycles of welding.

Ernest F. Nippes is associated with the Department of Metallurgical Engineering, Rensselaer Polytechnic Institute, Troy, N. Y.; **Craig R. Sibley** was formerly Research Fellow at Rensselaer Polytechnic Institute and is now with Air Reduction Research Laboratories, Murray Hill, N. J.

Presented at the 1956 AWS National Spring Meeting in Buffalo, N. Y., May 7–11.

Introduction

The industrial demand for storage vessels for subzero service has increased and is expected to grow continuously in the future. The increasing demand has offered a challenge to steel producers to supply an economical plate material which can be readily fabricated by welding and will deform in a ductile fashion at subzero temperature.

The low-alloy steels, as a class, are known to be capable of exhibiting higher yield strengths and increased notch toughness when compared to mild steel. However, for the most efficient utilization of alloying elements in steels, the proper heat treatment should be used. The optimum combination of strength and notch toughness in low-alloy steels is obtained from a quenched-and-tempered microstructure, provided the steel has adequate hardenability for through-hardening. Improved properties obtained by heat treatment have been shown by Seens, Jensen, and Miller[1] for various nickel-alloy steels, and by Rickett and Hodge[2] for various low-alloy steels.

Satisfactory yield strength and low-temperature notch toughness for subzero service are exhibited by many low-alloy steels in plate form prior to welding fabrication. However, exposure to welding thermal cycles may so alter the plate microstructure that the resultant properties of the weld-heat-affected zone are markedly impaired. Thus it is apparent that weldability, as well as strength and notch toughness, must be considered in the design of a low-alloy-steel plate material if the necessity for post-treatment is to be eliminated.

Bibber, Hodge, Altman and Doty[3] reported a new steel, "T-1," having a high yield strength and possessing good weldability. The properties of welded pressure vessels made from this material, with and without subsequent thermal stress relief, have been extensively studied.[4–6]

The present investigation concerns the Charpy-impact test behavior of "T-1" steel after exposure to a variety of thermal cycles equivalent to those found in the heat-affected zone of an arc weld. The high-speed time-temperature-control device, developed in the Welding Laboratories at Rensselaer Polytechnic Institute,[7] has been employed to duplicate the thermal cycles found at various points in the weld-heat-affected zone. Sufficient specimens were subjected to each thermal cycle of interest to permit determination

of the transition behavior using the Charpy impact test.

Object

The object of this program was to determine the effect of the thermal cycles experienced in the weld-heat-affected zone on the impact properties of a recent heat of "T-1" steel.[3, 4]

Scope

The present investigation was limited to the reproduction of heat-affected-zone microstructures in plate material of one thickness, 1/2 in., for one energy input value, 47,000 joules per inch of weld. Charpy-type specimens with an Izod vee notch were tested over a temperature range of −240 to +120° F. The fracture-transition and ductility-transition temperatures were obtained for the microstructures characteristic of eight peak temperatures in the range of 1000 to 2400° F.

Material

The following summarizes the chemical composition and mechanical properties of the plate material used in this investigation. The following data were provided by the supplier of the steel.

Plate thickness, 1/2 in.
Heat No., 74 L 236
Slab No., 62678
Check analysis, %:

C,	0.15	Cr,	0.53
Mn,	1.00	V,	0.05
P,	0.014	Cu,	0.34
S,	0.022	Mo,	0.45
B,	0.0014	Sn,	0.008
Si,	0.23	Ti,	0.004
Ni,	0.94		

Mechanical properties:

Test location	*Yield strength 0.2% offset, psi*	*Tensile strength, psi*	*Elongation, % in 8 in.*	*Elongation, % in 2 in.*	*Reduction of area, %*
Long., bottom	114,500	122,400	13.1	27.0	54.3
Long., top	111,600	120,900	10.7	25.0	52.8
Trans., top	113,900	123,600	11.5	29.0	50.1

Transition temperatures (as-received condition), Charpy keyhole impact (longitudinal specimen, notch perpendicular to rolled surface):
Ductility-transition temp. = −208° F (selected at center of scatter band; 12 ft-lb)
Fracture-transition temp. = −110° F (selected at 50% shear level)
Hardness:
Rockwell C scale, 27.5
Brinell hardness no., 278 (3000 kg load)

Procedure

The method used by the authors for duplicating the microstructures found in weld-heat-affected zones has been described in detail previously.[7-9] Cams were constructed to reproduce the heating and cooling cycles attending a weld deposit made at an energy input of 47,000 joules per inch of weld in 1/2-in. plate with the plate initially at 72° F. Thermal cycles were chosen having peak temperatures differing by 200° F over a range of 1000 to 2400° F. Figure 1 illustrates the time-temperature cycles employed, and indicates schematically the relative location of the equivalent positions in the heat-affected zone of a weld.

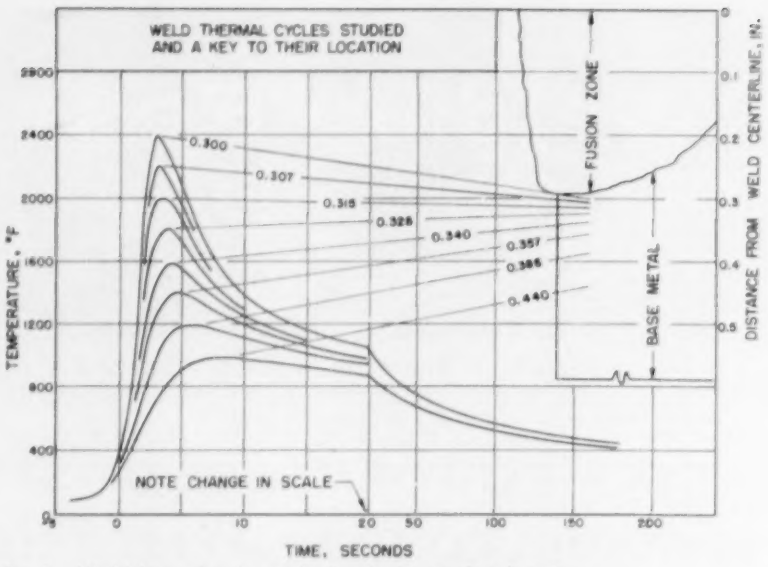

Fig. 1 Weld thermal cycles studied and a key to their location

Blanks, 0.42 x 0.42 x 2 3/4 in., were machined from the 1/2-in. thick as-received plate stock of "T-1" steel in preparation for heat treatment. As shown in Fig. 2, the longitudinal axis of each blank was in the rolling direction. A 0.052-in. diam hole, 0.050 in. deep, was drilled in the approximate center of the length of each blank to permit attachment of a chromel-alumel thermocouple for controlling the thermal cycle. The hole was located on a surface perpendicular to the original plate surface and served to locate the vee notch of the impact test specimen after heat treatment. The thermocouples were attached to the bottom of the hole by means of a capacitor-discharge weld using 150 microfarads charged to approximately 400 v.

The heat-treated blanks were machined to Charpy vee-notch dimensions, and the notch was located at the centerline of the thermocouple hole, perpendicular to the original plate surface. One heat-treated blank from each thermal cycle was used for metallographic studies. After a minimum time lapse of 21 days' storage at room temperature following heat treatment, the Charpy vee-notch specimens were fractured in a 220 ft-lb impact testing machine, following the procedure and precautions outlined by Driscoll.[10]

Denatured alcohol cooled with solid CO_2 was used to obtain testing tempera-

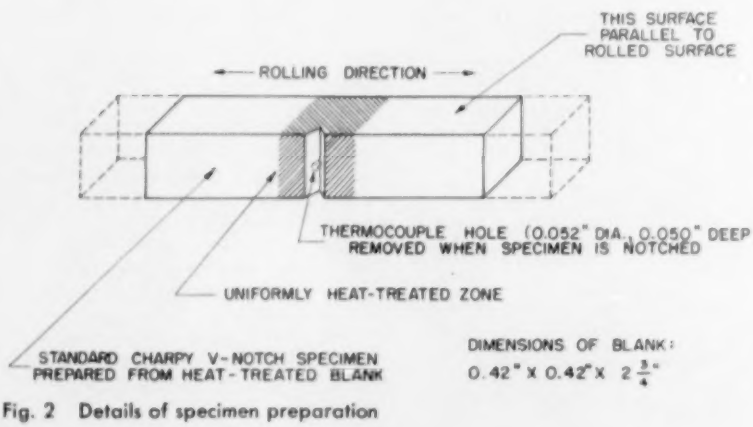

Fig. 2 Details of specimen preparation

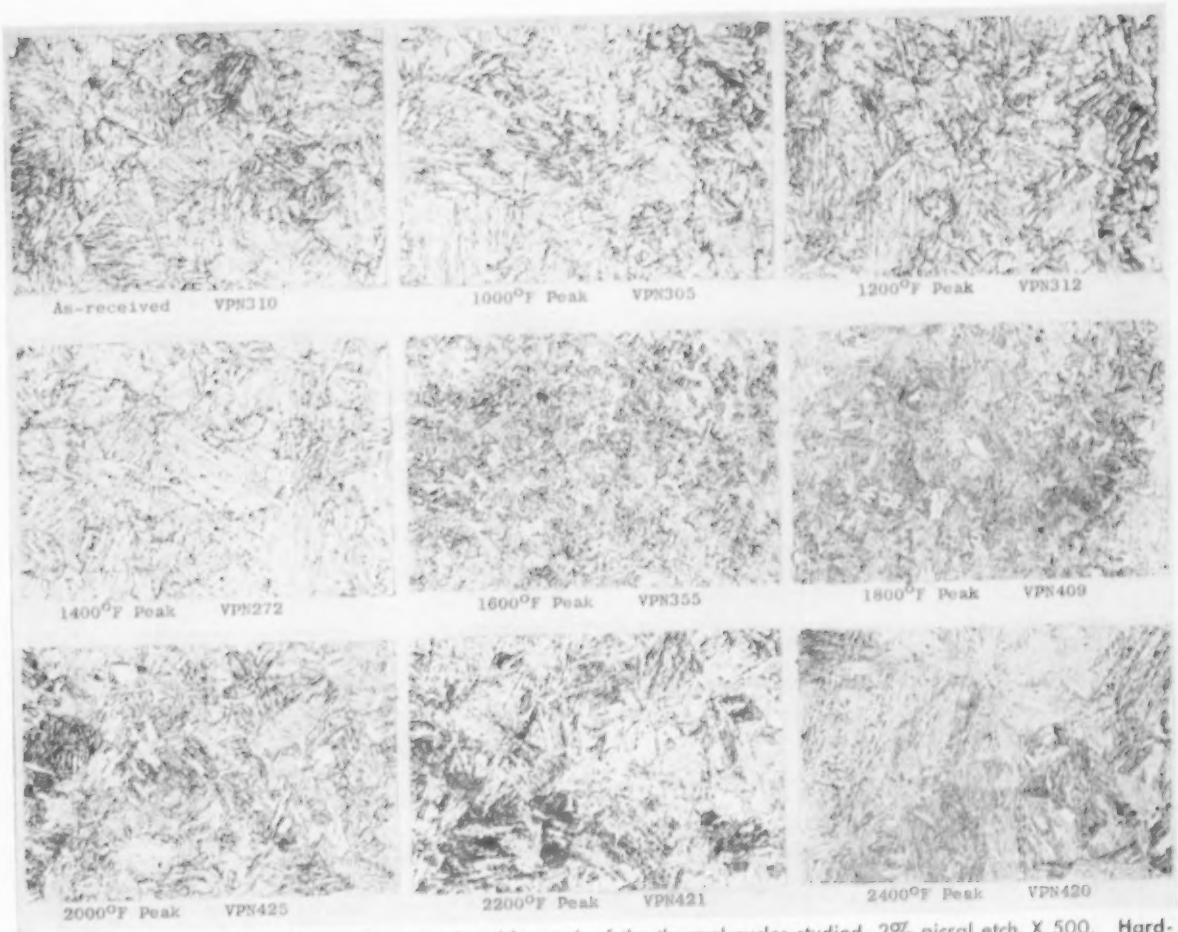

Fig. 3 Photomicrographs of the structures produced by each of the thermal cycles studied, 2% picral etch, X 500. Hardness, Vickers Pyramid Numerals, (VPN), is given for each microstructure. (Reduced by 1/2 upon reproduction)

tures between 0 and −80° F. Isopentane, cooled by liquid nitrogen passing through a heat exchanger, was used to obtain testing temperatures below −80° F. Water was used for testing temperatures above 32° F.

Three specimens were tested at each testing temperature for each thermal cycle investigated, and three samples of the as-received plate material were tested at each testing temperature for comparison. A minimum of 10 testing temperatures was used in obtaining the impact strength-temperature curves. Each fractured specimen was examined to determine the mode of failure. The fracture-transition temperature was evaluated as the temperature at which the fracture area showed 50% brittle fracture. The testing temperature at which the fracture required 10 ft-lb was chosen as the ductility-transition temperature.

Results

Metallographic Examination

The microstructure of the as-received plate material is shown in Fig. 3, together with typical examples of the microstructure produced by each of the thermal cycles studied. All photomicrographs show the structure as revealed at × 500 magnification after etching with 2% picral. Also presented with each microstructure in this figure is the hardness expressed in terms of Vickers Pyramid Numerals (VPN).

Marked changes in the tempered martensite structure of the original plate were produced whenever the peak temperature of the thermal cycle under investigation exceeded the effective value of the A_1 transformation temperature. Below the transformation temperature (1000 and 1200° F peak temperature) the change in the microstructure and hardness was negligible. No change would be expected at 1000° F and only a slight change at 1200° F, since the as-received material had been tempered at 1150° F by the manufacturer. A significant change in microstructure and hardness was produced by the thermal cycle having a peak temperature of 1400° F. The 1400° F peak temperature exceeded the equilibrium value of the A_1 temperature (1316° F),[4] but the time at temperature was apparently too short to allow appreciable transformation prior to cooling.

The thermal cycle with a peak temperature of 1600° F exceeded the A_3 temperature (1570° F)[4] and produced a fine-grained martensitic microstructure as may be seen by inspection of Fig. 3. Thorough metallographic examination revealed a tendency for a "ghost-structure," reflecting the fact that while austenitization was nearly complete during this thermal cycle, the time at temperature was insufficient to produce homogeneous austenite. The supposition of inhomogeneous austenitization is substantiated by the fact that the hardness of this structure (VPN 355) is lower than that expected (VPN 425) from martensite produced from homogeneous austenite of 0.15% carbon content.

The 1800° F peak-temperature thermal cycle caused grain refinement as compared with the as-received structure, but the grain size of the martensitic structure was not completely uniform. Extensive metallographic examination led to the conclusion that homogeneity was not quite attained during this ther-

mal cycle, presumably because of insufficient time at temperature for diffusion.

The 2000° F peak temperature thermal cycle produced a grain size slightly smaller than the original grain size but larger than the grain size of the material subjected to a peak temperature of 1800° F. With the thermal cycles having peak temperatures of 2200 and 2400° F, a progressive increase in grain size of the martensitic structure was noted.

Excellent correlation was observed in the comparison between the synthetic-specimen microstructures, discussed above, and the corresponding microstructures adjacent to a bead weld made at 47,000 joules per inch.

Impact Testing

The impact strength-temperature curves for each microstructure are presented in Figs. 4 through 12, along with percentage-shear-fracture data.

The plate material in the as-received condition, Fig. 4, exhibited a sharp fracture-transition at a temperature of about −50° F and a ductility-transition temperature of approximately −140° F. In the 1000 and 1200° F peak temperature specimens, Figs. 5 and 6, respectively, fracture- and ductility-transition

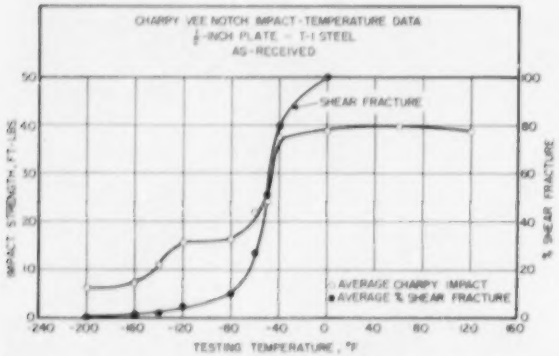

Fig. 4 Charpy vee-notch impact-temperature data for as-received plate

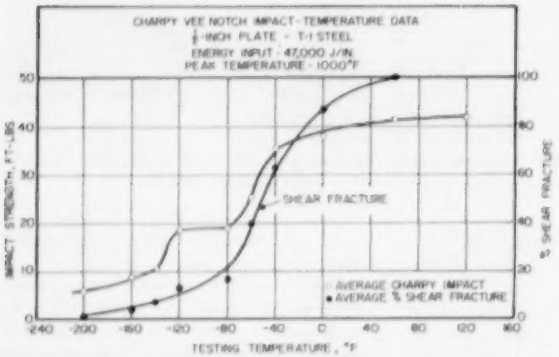

Fig. 5 Charpy vee-notch impact-temperature data for specimens produced by the thermal cycle with 1000° F peak temperature

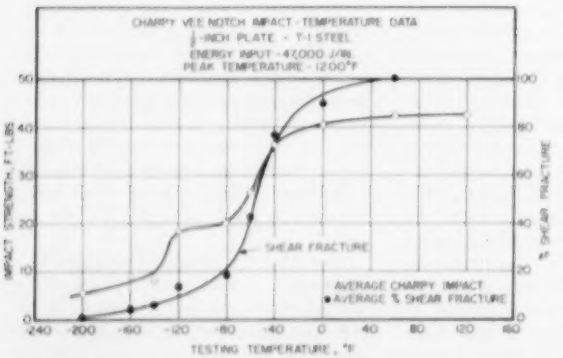

Fig. 6 Charpy vee-notch impact-temperature data for specimens produced by the thermal cycle with 1200° F peak temperature

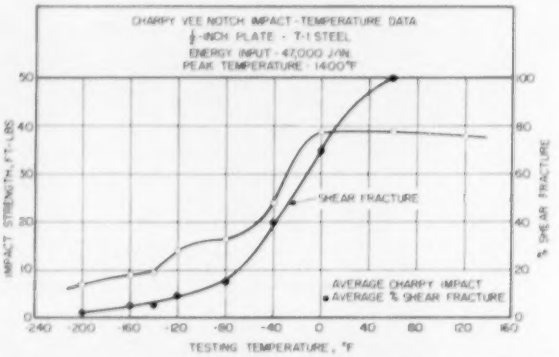

Fig. 7 Charpy vee-notch impact-temperature data for specimens produced by the thermal cycle with 1400° F peak temperature

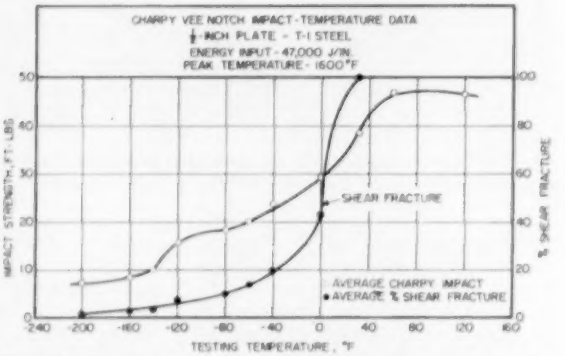

Fig. 8 Charpy vee-notch impact-temperature data for specimens produced by the thermal cycle with 1600° F peak temperature

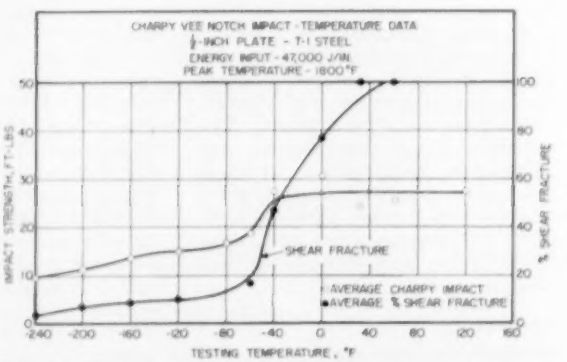

Fig. 9 Charpy vee-notch impact-temperature data for specimens produced by the thermal cycle with 1800° F peak temperature

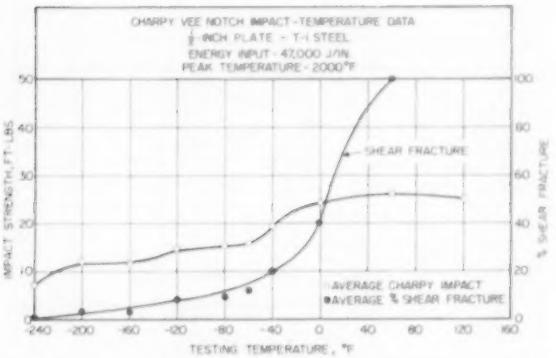

Fig. 10 Charpy vee-notch impact-temperature data for specimens produced by the thermal cycle with 2000° F peak temperature

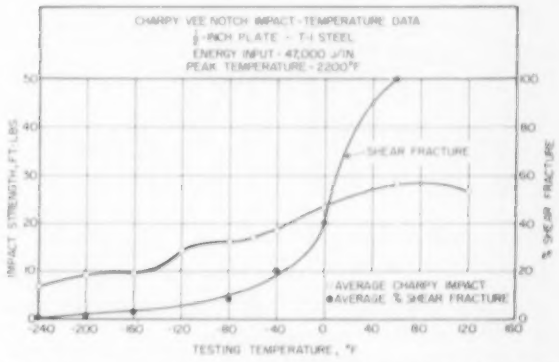

Fig. 11 Charpy vee-notch impact-temperature data for specimens produced by the thermal cycle with 2200° F peak temperature

temperatures remained virtually unchanged.

The 1400° F peak temperature thermal cycle produced a shift in the fracture-transition temperature to approximately −15° F, as shown in Fig. 7. The ductility-transition temperature and the upper and lower levels of impact strength were consistent with the values obtained with the lower peak temperature tests, however. This thermal cycle exceeded the equilibrium value of the A_1 transformation temperature, and the microstructure indicated a general increase in the tempered products with evidence of partial transformation.

The results of impact tests on the material subjected to the 1600° F peak temperature thermal cycle are shown in Fig. 8 and indicate a further increase in the fracture-transition temperature as well as an increase in the energy required to fracture at the higher testing temperatures. The fine-grained structure, shown previously in Fig. 3, undoubtedly caused the increase in fracture energy at the higher testing temperature. Below 0° F the impact strength falls off gradually to a level of brittle failure. Again, little change in ductility-transition temperature resulted from exposure to this thermal cycle.

The specimens subjected to the 1800° F peak temperature thermal cycle, Fig. 9, gave results unlike those at lower peak temperatures. Both the fracture- and ductility-transition temperatures were lower than the corresponding values for material subjected to thermal cycles with peak temperatures of 1400 and 1600° F, and the ductility-transition temperature was considerably lower than that of the as-received plate. However, above the fracture-transition temperature, the value of impact strength (25–30 ft-lb) was lower than that of the as-received plate (approximately 40 ft-lb).

The results of the impact tests on material subjected to the 2000 and 2200° F peak temperature thermal cycles were similar, as illustrated in Figs. 10 and 11. Both impact strength curves showed low values of impact strength (25 to 30 ft-lb) above the fracture-transition temperature, which was slightly above 0° F in both cases. The increased grain size caused a higher ductility-transition temperature for the samples heated to a peak temperature of 2200° F. Further increase in grain size with the 2400° F peak temperature caused a still higher ductility-transition temperature, as shown in Fig. 12.

Discussion of Results

The weldability of the low-alloy steels within the range of 0.10 to 0.30% carbon is generally considered good, provided proper care is exercised to eliminate underbead cracking. If underbead cracking is avoided, hardening of the heat-affected zone is usually not of great concern since most weldments are thermally "stress-relieved" prior to service. In the case of heat-treatable steels, welding is often done in normalized plate and the weldment is given subsequent thermal treatments to obtain desirable strengths and ductility; thus the heat-affected microstructures attending welding are altered in part or completely by the post-treatment.

If a quenched-and-tempered low-alloy steel, such as "T-1", is to be used in welded fabrication without thermal "stress-relief," the metallurgical changes occurring in the heat-affected zone become quite important because this area must remain tough and ductile in the as-welded condition. Tempering is not always a necessity, however, because the impact properties of low-carbon martensites are outstanding in the as-quenched condition for both plain-carbon and low-alloy steels.[11]

In the summary plot of the transition-temperature data, Fig. 17, changes are evident in fracture-transition temperature (or 50% shear fracture) as the peak temperature increases. The general trend indicates a steady rise in fracture-transition temperature as the structure approaches the weld fusion zone. An exception to this general trend results from the fine-grained structure obtained

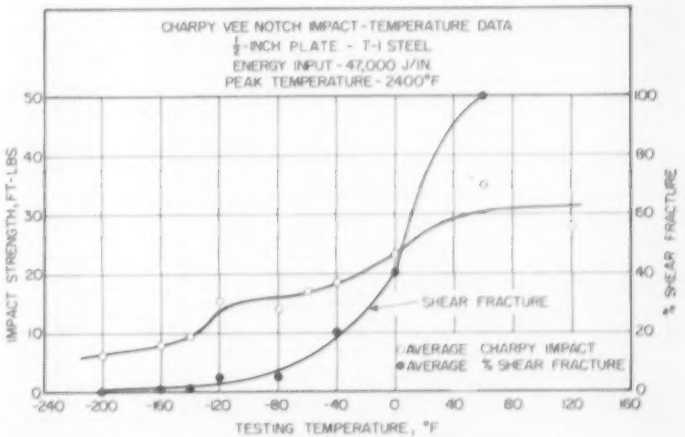

Fig. 12 Charpy vee-notch impact-temperature data for specimens produced by the thermal cycle with 2400° F peak temperature

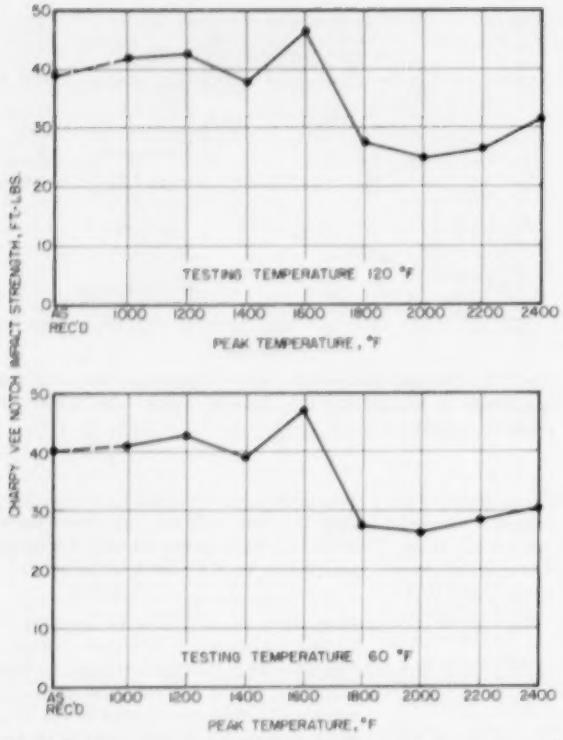

Fig. 13 Impact strength vs. peak temperature of thermal cycle for 120 and 60° F testing temperatures

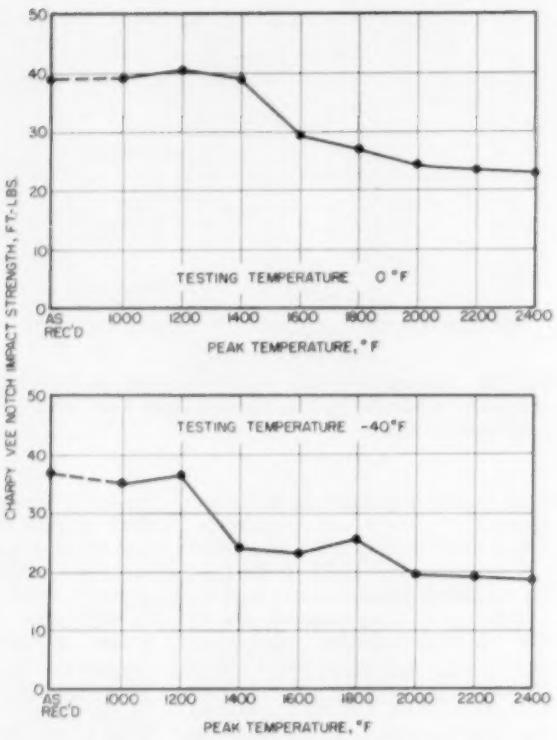

Fig. 14 Impact strength vs. peak temperature of thermal cycle for 0 and −40° F testing temperatures

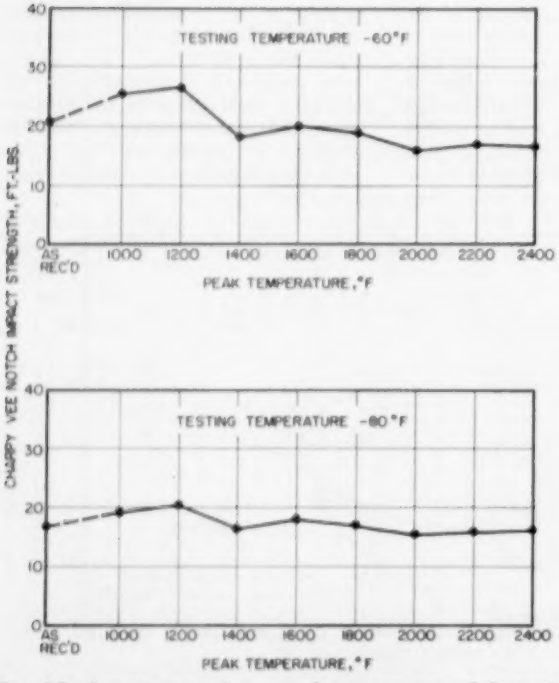

Fig. 15 Impact strength vs. peak temperature of thermal cycle for −60 and −80° F testing temperatures

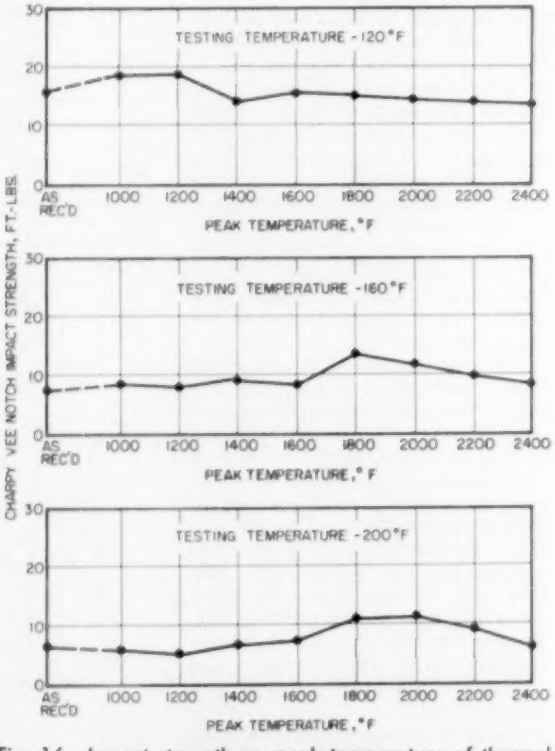

Fig. 16 Impact strength vs. peak temperature of thermal cycle for −120, −160 and −200° F testing temperatures

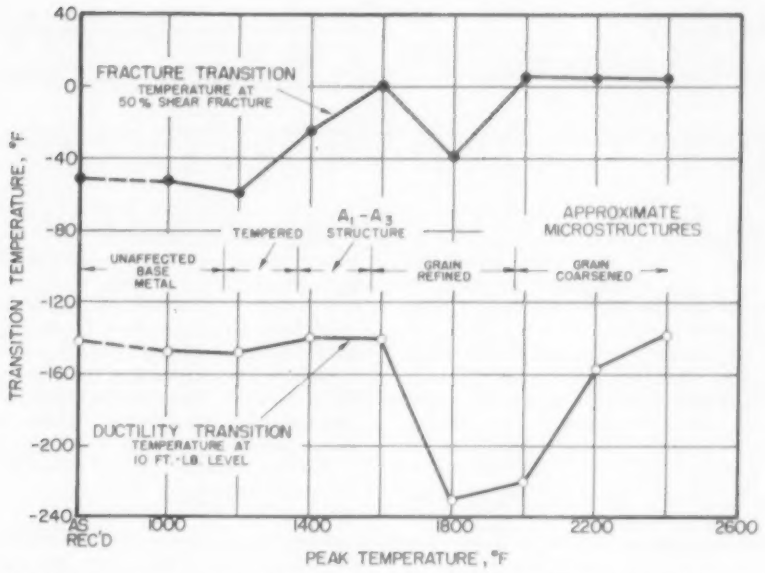

Fig. 17 Summary curves of fracture- and ductility-transition temperatures vs. peak temperature of thermal cycle. Approximate microstructures resulting from these thermal cycles are also presented

by heating to 1800° F. The ductility-transition (or 10 ft-lb) temperature is also plotted as a function of peak temperature in Fig. 17. A general lowering of the ductility-transition temperature is indicated in the structures receding from the weld fusion zone. At a greater distance from the weld zone, the ductility-transition temperature gradually increases to that of the unaffected plate. A tabulation of the ductility-transition and fracture-transition temperatures is given in Table 1 along with hardness data. Using the ductility-transition temperature as the criterion of toughness, the obtained data indicate that all the produced microstructures are as tough as the plate material. Also included in Fig. 17 are the approximate microstructures resulting from the exposure of "T-1" to the thermal cycles employed in this investigation.

When the impact strength at the various testing temperatures is plotted against the peak temperature attained in producing the heat-affected-zone microstructures, Figs. 13 through 16, it is evident that all the microstructures behave in a similar manner below a testing temperature of −60° F. The decrease in impact strength shown at testing temperatures above 0° F by the specimens heated above 1600° F does not indicate embrittlement since shear-type fractures were predominant above 0° F. This decrease in energy absorption is the result of the change in microstructure and increased hardness of specimens heated above 1600° F. No loss in hardness occurred until the peak temperature exceeded the equilibrium A_1 transformation temperature, 1316° F. The initial loss of hardness in the specimens heated to 1400° F resulted from tempering effects rather than transformation effects. Further heating caused increased transformation of the original plate structure with an accompanying increase in hardness. The hardness of the specimens heated above 1800° F is characteristic of the maximum hardness obtainable with the carbon content of this steel. The fact that these untempered martensitic structures remained tough is clear evidence of the outstanding heat-affected-zone performance of "T-1" steel.

Table 1 Fracture- and Ductility-Transition Temperatures and Hardness Data

Charpy vee-notch specimens with notch perpendicular to rolled surface

Peak temperature, ° F	*Fracture transition temperature, ° F**	*Ductility transition temperature, ° F†*	*Hardness VPN (30 kg)*
As-received	−50	−142	310
1000	−52	−148	305
1200	−58	−148	312
1400	−24	−140	272
1600	1	−140	355
1800	−38	−230	409
2000	5	−220	425
2200	4	−156	421
2400	5	−138	420

* 50% shear criterion.
† Ten ft-lb criterion.

Summary and Conclusions

1. "T-1," a low-alloy, quenched-and-tempered steel, was subjected to a variety of welding thermal cycles, using the RPI synthetic-specimen technique.

2. A systematic survey was made of the Charpy vee-notch impact properties of the various microstructures which duplicated those found in the heat-affected zone of an arc weld made in ½-in. "T-1" steel with an energy input of 47,000 joules per inch.

3. The ductility-transition temperature (10 ft-lb level criterion) of the "T-1" steel was not adversely affected by the weld thermal cycles.

4. The fracture transition temperature (50% shear fracture criterion) was increased somewhat by the thermal cycles experienced in the weld-heat-affected zone.

5. Specimens which were exposed to thermal cycles which exceeded the effective A_3 temperature of the "T-1" steel exhibited a low-carbon martensitic structure. The impact properties of these low-carbon martensites in the as-quenched condition were outstanding.

Acknowledgments

The authors wish to acknowledge the sponsorship of this research program by the Chicago Bridge and Iron Co. and the United States Steel Corp. through the Welding Research Council. They are also indebted to Leonard Zick of the Chicago Bridge and Iron Co. and Dr. W. D. Doty of the U. S. Steel Corp. for their assistance and advice. In addition, the authors wish to express their appreciation to the members of the Fellowship Board of the University Research Committee for their guidance and suggestions.

References

1. Seens, W. B., Jensen, W. L., and Miller, O. O., "Notch Toughness of Four Alloy Steels at Low Temperatures," *Proc. ASTM*, **51**, 918–930 (1951).

2. Rickett, R. L., and Hodge, J. M., "Notch Toughness of Fully Hardened and Tempered Low-Alloy Steels," *Proc. ASTM*, **51**, 931–944 (1951).

3. Bibber, L. C., Hodge, J. M., Altman, R. C., and Doty, W. D., "A New High-Yield Strength Alloy Steel for Welded Structures," *Trans. ASME* (April 1952), reprinted July 1952, *Welding Research Council Bull. Ser.*, No. 15.

4. Doty, W. D., "Properties and Characteristics of a Quenched Tempered Steel for Pressure Vessels," THE WELDING JOURNAL, **34** (9), Research Suppl., 425-s to 441-s (1955).

5. Zick, L. P., "Design of Welded Pressure Vessels Using Quenched and Tempered Steel," *Ibid.*, **34** (9), Research Suppl., 442-s to 448-s (1955).

6. Bibber, L. C., "Suitability of Quenched and Tempered Steels for Pressure-Vessel Construction," *Ibid.*, **34** (9), Research Suppl., 449-s to 464-s (1955).

7. Nippes, E. F., and Savage, W. F., "Development of Specimen Simulating Weld Heat-Affected Zones," *Ibid.*, **28** (11), Research Suppl., 534-s to 546-s (1949).
8. Nippes, E. F., Merrill, L. L., and Savage, W. F., "Cooling Rates in Arc Welds in 1/2-In. Plate," *Ibid.*, **28** (11), Research Suppl., 556-s to 564-s (1949).
9. Nippes, E. F., and Savage, W. F., "Tests of Specimens Simulating Weld Heat-Affected Zones," *Ibid.*, **28** (12), Research Suppl., 599-s to 616-s (1949).
10. Driscoll, D. E., "The Charpy Impact Machine and Procedure for Inspection and Testing Vee Notch Specimens," *ASTM Bull.*, No. 191, 60–64 (July 1953).
11. Aborn, R. H., "Low Carbon Martensites," *Trans. Am. Soc. Metals*, **48**, 51–85 (1956).

DISCUSSION BY K. WINTERTON

The authors are to be congratulated on this correlation of properties with microstructure, these structures being notoriously difficult for exact interpretation.

It would be interesting if the authors could be persuaded to undertake an examination of the effect of hydrogen, introduced by electrolysis, on the properties of the simulated heat-affected zone, and in particular its effect on static fatigue rather than the ductile/brittle transition.

A similar investigation by Cottrell (*Brit. Welding Jnl.*, April 1954, p. 167) showed that hydrogen depressed the end-of-transformation temperature for martensite formation, and that this was accompanied by a deleterious effect on static fatigue strength. Impact strength was comparatively little affected. Even very small quantities of hydrogen comparable with that produced with a low-hydrogen electrode could have a marked effect, depending on the steel composition.

Though it is realized that the authors had a specific objective in the investigation described, an extension might be found profitable, with the technique of simulating welding thermal cycles already established.

K. Winterton is Assistant Director, Department of Engineering and Metallurgy, Ontario Research Foundation, Toronto, Canada.

AUTHOR'S REPLY

The authors wish to thank Mr. Winterton for his suggestions regarding the influence of hydrogen on the properties of the simulated heat-affected zone. Future investigations in this laboratory on the weldability of "T-1" steel might well include work similar to that described by Cottrell. It would be of great interest to determine the effect of steel composition on the influence of hydrogen, since the deleterious effect may be not so pronounced at lower carbon contents.

RESEARCH ON OXYGEN CUTTING

BY K. TESKE

Abstract of "Beitrag zur Klarung der Vorgange beim Brennschneiden," published in *Schweissen und Schneiden*, 8, 122–129 (April 1956).

In order to start a cut, the steel must be heated to its ignition temperatures. Measurements showed this to be 1150° C for pure iron, 1210° C for 0.25% carbon and 1230° C for 0.90% carbon steel. These measurements were made with electrically-heated steel on which a cutting torch was directed. The results agreed with ignition tests on closely-coiled wire filaments heated by resistance in an oxygen chamber. The results were corrected for emissivity.

The temperature of cutting slag which was largely FeO, was found to be 1600° C. If all the reaction heat was absorbed by the slag its temperature would be 3600° C. Only about half of the heat of cutting is absorbed by the slag.

The maximum linear-cutting speed was calculated from the number and speed of oxygen atoms in the gas, and the number of iron atoms in an iron surface. A maximum cutting speed of 160 ipm. was calculated. Under exceptional conditions, oxygen cuts were made in 0.04-in. thick steel at 80 ipm. In practice, not over 1/4 of the calculated maximum speed is achieved.

Abstracted by Dr. G. E. Claussen, Metals Research Laboratories, Electrometallurgical Co., Niagara Falls, N. Y.

PROBLEMS INVOLVED IN SPOT WELDING TITANIUM TO OTHER METALS

Properties and problems of spot welding commercially-pure titanium to stainless steel and several other metals are examined. General information concerning the nature of these welds is provided

BY FRANK W. McBEE, Jr., JIMMY HENSON AND L. R. BENSON

Introduction

Since the recent commercial appearance of titanium, great enthusiasm has been shown regarding the potentialities of this metal. This enthusiasm has led to numerous investigations relative to the techniques for producing satisfactory titanium welds. However, very little information is available concerning dissimilar welds involving titanium. The material contained in this paper was collected in an effort to examine the properties and problems of spot welding commercially-pure titanium to stainless steel and several other metals. It was not intended to establish welding schedules but only to provide a wide variety of general information concerning the nature of these welds.

Scope of the Investigation

The ultimate objective of this research was the successful spot welding of titanium to stainless steel; preliminary investigation indicated these welds to be extremely poor. Weld indentation was low and ductility was poor. The welds could be broken with light hand pressure in a simple peel test. In view of the above, the investigation was expanded to three principal paths. The first phase of study deals entirely with the properties of titanium-stainless steel type 301 welds. The second phase is concerned with the welds produced between titanium and the principal components of stainless steel. Here each component (iron, chromium and nickel) was investigated independently to determine if one particular element might be responsible for the undesirable weld characteristics. The welds of titanium to a group of miscellaneous metals are studied in the third phase. The metals used throughout this study were varied in physical properties as well as properties relative to resistance welding. Selection of these metals was on the basis of melting point, thermal conductivity, electrical resistivity, crystalline structure, location in the periodic table, and atomic diameter. Table 1 contains the above information for each metal of the selected group while the chemical analysis of the titanium and stainless steel used is shown in Table 2.

Table 1—Properties of Metal

Metal	*Melting point (approximate)* ° *C*	° *F*	*Thermal conductivity, cal/sq cm/cm/° C/sec (approximate)*	*Electrical resistivity microhm-cm (approximate at ambient temperature)*	*Crystalline structure (ambient temperature)*	*Periodic group*	*Atomic diameter A.*
Titanium (A-55)	1800	3200	0.035	80	C.P.H.	IVa	2.91
Iron (chemically pure)	1500	2800	0.18	9.7	B.C.C.	VIIIa	2.48
Chromium (Pure)	1890	3400	0.16	13	B.C.C.	VIa	2.49
Nickel (Pure)	1450	2650	0.22	6.8	F.C.C.	VIIIa	2.50
Zirconium (Pure)	1750	3200	0.045	41	C.P.H.	IVa	3.16
Aluminum (24ST-3)	650	1220	0.50	2.9	F.C.C.	III	2.86
Magnesium (FS1)	640	1200	0.35	4.6	C.P.H.	II	3.20
Stainless (301 Austenitic)	1400	2550	0.04	60	...	...	...
Stainless (446 Ferritic)	1450	2650	0.04	75	...	...	...

Description of Equipment

All welding operations were performed on a 75-kva spot welder. Two hundred and twenty-volt, 60-cycle, single-phase alternating current was supplied to the welder. For controlling weld time and current magnitude a thyratron control panel was used; squeeze time, hold time, and off time were controlled by a sequence control panel.

Weld strengths were obtained on a

Table 2—Analysis of Metals

Certified Analysis of Titanium RC-55	
Grade and condition	A-55 (Annealed)
C, %	0.1
N, %	0.015
Mn, %	0
Al, %	0
Nominal Analysis of Stainless Steel 301-B	
C, %	0.08-0.20
Mn, %	2.00
Si, %	1.00
P, %	0.040
S, %	0.030
Cr, %	16.0-18.0
Ni, %	6.0-8.0

Frank W. McBee, Jr., and **Jimmy Henson** are Research Engineers, Defense Research Laboratory, and **L. R. Benson** is Assistant Professor of Mechanical Engineering, The University of Texas, Austin, Tex.

Presented at 1956 AWS National Fall Meeting in Cleveland, Ohio, October 8th to 12th.

This work was supported by the Navy Bureau of Ordnance under the basic research phase of its Contract NOrd-16498 and the Mechanical Engineering Department of The University of Texas, Austin, Tex.

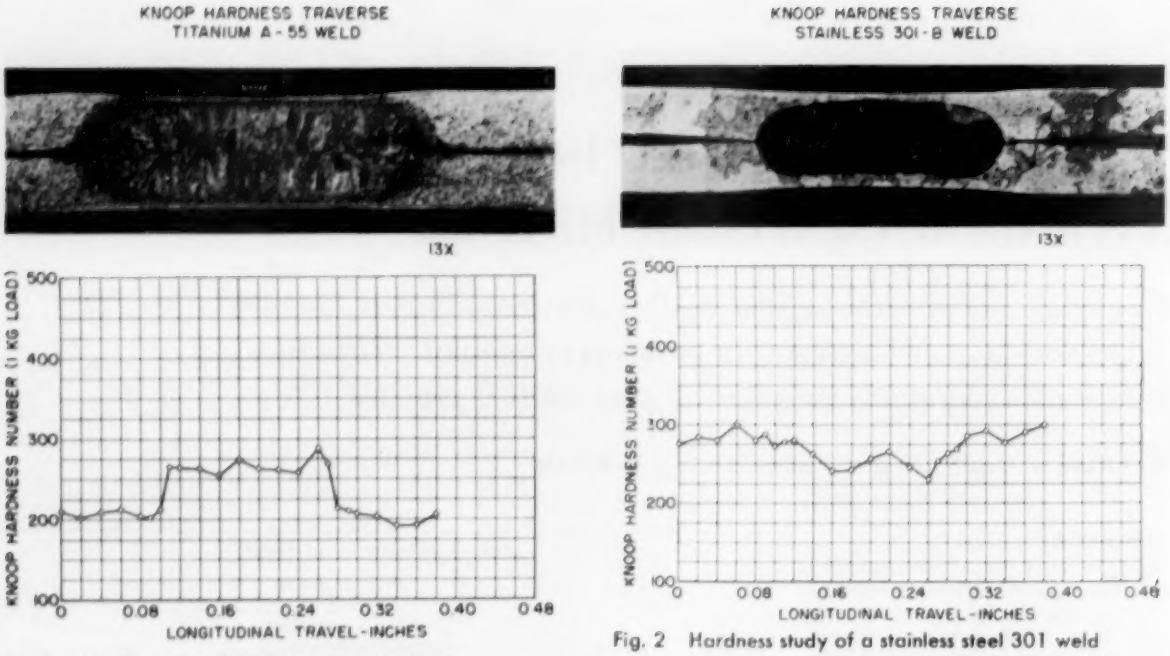

Fig. 1 Hardness study of a titanium A-55 weld

Fig. 2 Hardness study of a stainless steel 301 weld

120,000 lb capacity hydraulic testing machine using sheet-metal grips. The welded specimens were so held that the nature of failure was primarily shear. Except for the titanium-stainless steel 301 specimens, all welds were made using standard RWMA Class I electrode tips with 6-in. radius dome. The electrode arrangement for the titanium-stainless steel 301 welds will be discussed in detail later. A Tukon hardness tester, was used with a Knoop indenter at one kilogram load to obtain weld hardness traverses. All hardness traverses originate in the base metal adjacent to the heat-affected zone and proceed across the weld nugget terminating in the base metal.

Materials and Their Preparation

Commercially-pure titanium sheet 0.031 in. thick was used throughout this investigation. The metal was designated as A-55 annealed. Unless otherwise noted, all other metal sheet was also 0.031 in. thick (22 gage).

The tension-shear specimens were cut to $2^3/_4$ in. by $^3/_4$ in. and thoroughly degreased with carbon tetrachloride. No further cleaning was attempted except for the welds involving titanium to magnesium and aluminum, in which instances it was necessary to remove the oxide film from the metals. In welding, a $^3/_4$-in. overlap was used to conform with good practice.

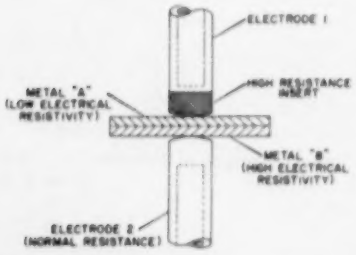

Fig. 3 Electrode arrangement for effecting a better heat balance in metals of different electrical resistivity

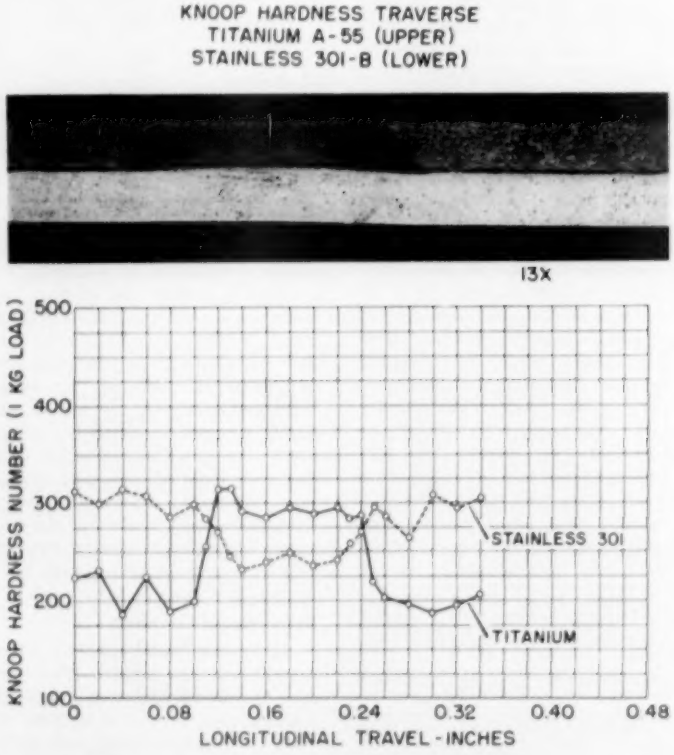

Fig. 4 Hardness study of a titanium-stainless steel weld

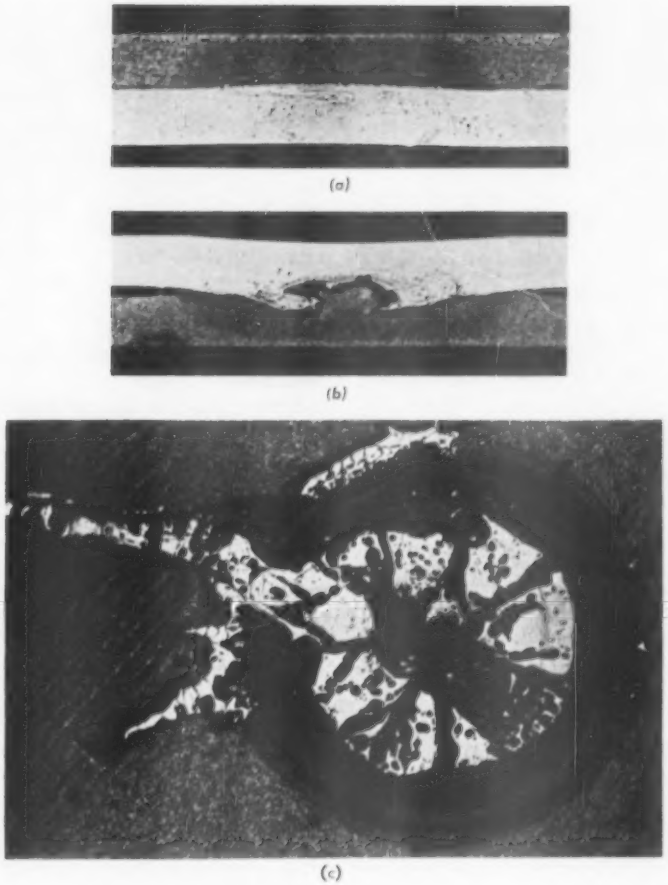

(a)

(b)

(c)

Fig. 5 Progressive steps in the formation of a titanium-stainless steel weld nugget with increasing heat

(a) Low heat (4 cycles, 3000 amp). (b) Medium heat (4 cycles, 3800 amp). (c) High heat (4 cycles, 4500 amp). X 13.

Welding Variables

The minor welding variables were held constant at the following values:

Squeeze time, cycles	20
Hold time, cycles	20
Electrode closing rate, fps	3
Throat depth, in.	12
Horn gap, in.	8
Electrode stroke, in.	1/4

Because of the vast differences in the properties of the metals welded to titanium, a wide range of weld current, weld time, and tip force was used.

Procedure

As no information was available for dissimilar welds involving titanium, preliminary investigations were necessary to determine a reasonable range of welding currents. After this range had been determined for a given weld time, five specimens were welded at most preselected machine setting. Three of these were utilized in the tension-shear tests; two, in metallurgical studies.

Polishing of the metallurgical specimens proved most difficult. The brittle nature of the weld nugget material of many of the dissimilar welds caused large chips to break from the nugget particularly during the final polishing operation. If the nugget material did not tend toward chipping, the difference in the abrading properties of the metals and the nugget caused uneven polishing. As a result, the specimens were polished to produce flat surfaces for photography and hardness studies rather than for scratch-free surfaces. Etching also proved to be a problem as the chemical activity of the metals often varied greatly. In all instances the specimens were etched to favor the titanium; 15 sec. in 5% hydrofluoric acid usually provided a satisfactory surface.

Spot Welds of Titanium and Stainless Steel

The physical and metallurgical characteristics of titanium-stainless steel welds are of primary interest in this phase of the investigation. Spot welds involving only titanium and only stainless steel are compared to those involving both metals. Of particular interest is the effect of increasing heat on the physical and metallurgical properties of titanium-stainless welds. It was hoped that a thorough knowledge of the weld characteristic would suggest a possible solution to the problem.

Titanium-Titanium Welds

The weld cross section and Knoop hardness traverse shown in Fig. 1 serves to illustrate the weldability of titanium to titanium. Note the typical dendritic structure of the nugget, the high penetration, and the low indention. The hardness traverse shows the weld nugget to have an average Knoop number of approximately 260 with a base metal hardness of about 200. This hardness increase in the nugget area is typical of most metals. Welds of this nature involving commercially pure titanium were shown by a previous investigation to have a tension-shear strength of about 1400 lb. Physical appearance and ductility of the welds were satisfactory.

Stainless Steel-Stainless Steel Welds

Figure 2 shows a stainless steel type 301 weld with accompanying Knoop hardness traverse. Again note the nugget structure, the good penetration, and low indention. Observe also the nugget shrinkage cavity which is quite common to this type of weld. The Knoop traverse shows the weld nugget to have an average hardness of approximately 245 while the base-metal hardness is about 285. Since stainless 301 is an austenitic alloy to well below room temperature, no heat effect hardening occurred. The hardness decrease of the nugget material could have been caused by the relieving of stresses due to rolling and working of the metal. In any event, the weld possesses good metallurgical and physical properties, welds of this character having tension-shear strengths in excess of 1000 lb.

High-Resistance Electrodes

If the difference in the electrical resistivity of the two metals is great enough to cause nugget offset, a satisfactory heat balance may be produced through the use of one high-resistance electrode. Figure 3 is a schematic sketch of such an electrode arrangement. The high-resistance tungsten insert of electrode 1 causes a larger portion of the heat to be generated at the point of contact between the electrode and "metal A." The result is that approximately equal heating of each metal occurs thus effecting a better heat balance. By use of this arrangement, it is often possible to weld certain combinations of metals that otherwise produce undesirable weld characteristics.

Because of the poor characteristics of titanium-stainless welds, it was

decided to apply the high-resistance electrode arrangement to this phase of the research. In the initial stages of investigation, the location of the high-resistance electrode was varied, but positioning adjacent to the stainless seemed to produce somewhat better results. This was anticipated as the electrical resistance of the stainless was considerably less than that of titanium. Used adjacent to the stainless was a high-resistance electrode with 8-in. radius dome.

Titanium-Stainless Steel Welds

Figure 4 is a macrograph and hardness traverse of a titanium-stainless weld made at low heat (4 cycles at approximately 3000 amp). Very little melting of either metal occurred even though the high-resistance electrode was placed next to the stainless steel. Penetration and indentation were essentially zero and bonding was of a solid phase nature. In appearance the weld was quite good, and no flashing occurred at this current setting. The heat-affected zone of the titanium was considerably harder than the nugget zone of the titanium-titanium weld, (Knoop 295 compared to 260), indicating some sort of molecular intermingling. The behavior of the stainless steel was about the same as in the stainless-stainless weld.

The effect of increasing heat on weld structure is shown in Fig. 5, *a* through *c*. Figure 5*a* is identical to the photograph of Fig. 4. Welds of this character (solid-phase bonding) produced the

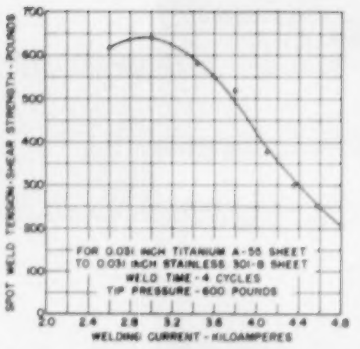

Fig. 6 Effect of variable weld current upon the tension-shear strength of titanium-stainless steel welds

best shear strength, the reason for this to be pointed out later. The apparent incompatibility of the metals can be seen in Fig. 5*b* by noting strange nugget appearance. Here again the indentation was low but penetration had increased to about 30%. This weld, produced at 4 cycles and 3800 amp, was the highest heat weld that could be cross sectioned and polished with any degree of success. Figure 5*c* is a plan view of a polished high-heat weld (4 cycles at 4500 amp) looking into the titanium. The polishing of a cross section of a weld of this character proved extremely difficult because, as previously mentioned, chips would break from the nugget during the polishing operation. The dark spots and radial lines are holes and cracks and are not the result of etching. Expulsion of metal (flashing) occurred at this condition as can be observed. The average Knoop hardness of the weld nugget material of Fig. 5*c* was 786 (Rockwell C of 66) compared with a sheet titanium hardness of 200 and a stainless steel 301 hardness of about 285. This drastic hardness increase and the crystalline appearance of the titanium-stainless steel weld nugget leads to the conclusion that an intermetallic compound was formed.

Tension-Shear Strength of Titanium-Stainless Steel Welds

Even though an attempt was made to effect a better heat balance through use of a high-resistance electrode, welds of titanium to stainless steel showed little or no improvement when placed in shear. The simple peel test caused weld failures with only light hand pressure. In view of this condition, a spot weld tension-shear strength curve was obtained for titanium-stainless steel welds. Figure 6 shows the results of this phase of the investigation. The point at 2600 amp was the minimum current setting for obtaining any bonding of the metals. The weld of 3000 amp with macrograph shown in Fig. 4, produced the maximum shear strength of 640 lb. Radiographs revealed that minute cracks appeared in the weld as the current was increased, thus accounting for the rapid decline of the curve.

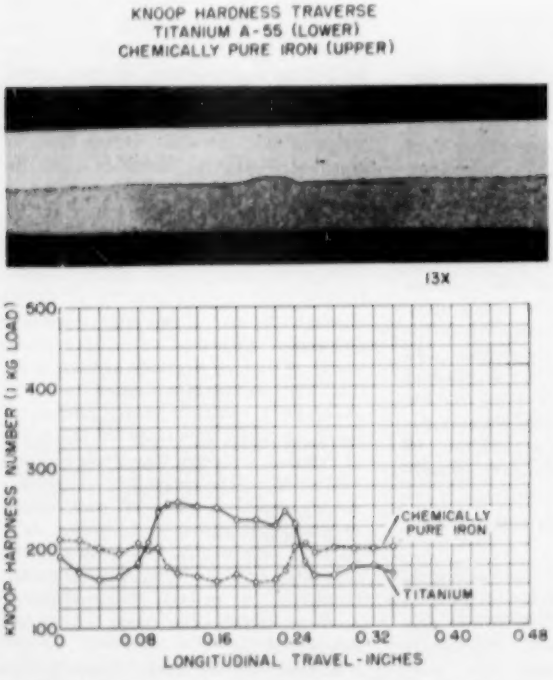

Fig. 7 Hardness study of a titanium-pure iron weld

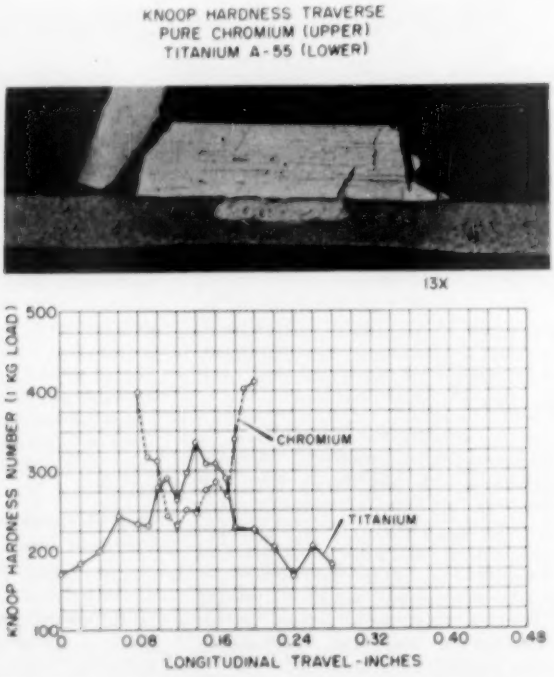

Fig. 8 Hardness study of a titanium-chromium weld

Welds of Titanium to the Components of Stainless Steel

In the resistance welding of alloys, it is conceivable that one metal or component of the alloy could be responsible for producing undesirable characteristics of the weld nugget material. For instance, if the solubility of one metal in another is very limited, the resulting structure could exhibit unusual crystalline properties. On the other hand, if two metals exhibit a chemical affinity for each other resulting in an intermetallic compound, the elimination or increase of one of these might improve the weld properties. The object of this phase of research was to investigate the welds of titanium to the components of stainless steel to see if one component might be responsible for the undesirable weld characteristics. Since the principal stainless steel components are iron, chromium, and nickel, these metals in their pure form were utilized in this phase of study.

Welds of Titanium to Chemically-Pure Iron (99.7)

A macrograph of a titanium-iron weld is shown in Fig. 7 with accompanying Knoop hardness traverses. These traverses revealed an increase in titanium hardness with a decrease in the pure iron hardness. Since the iron contained no carbon, this hardness decrease, due to the annealing effect of the welding heat, might be expected. This weld, made at approximately 4000 amp, exhibited the same general characteristics as the titanium-stainless steel weld. Indentation and penetration were essentially zero, and the best welds were produced in the solid-phase bonding region. Fracture occurred on the application of light hand pressure, and weld ductility was very poor. Increasing heat resulted in the formation of hard, brittle nugget material similar to that of the titanium-stainless steel weld. The average tension-shear strength of this combination was 675 lb.

Welds of Titanium to Chromium

The pure chromium as utilized in this study was a hard, brittle metal that could not be machined. The surface of this metal as obtained was very rough and the thickness quite irregular. However, surface grinding of the metal proved fairly successful in producing a smooth surface as long as the thickness was kept above about 0.030 in. With thickness below 0.030 in., it became increasingly difficult to hold the chromium and prevent cracking while grinding.

Because of the difficulty in obtaining suitably smooth chromium, small pieces of the metal 0.045 in. thick were used in making the metallurgical specimen welds. Shear specimens utilizing chromium were not feasible as the metal was extremely brittle.

Of considerable interest is the chromium-titanium macrograph and hardness traverse of Fig. 8. Observe the heat-affected zone of the titanium with the obviously new material in the center of this zone. Reference to the titanium traverse shows this new substance to have an average Knoop hardness of approximately 300. While the titanium hardness increased due to heating, the hardness of the chromium dropped from a Knoop number of approximately 400 to about 250. Both the moderate increase in the titanium hardness and the decrease in the chromium hardness served to indicate more compatibility between titanium and chromium than any other metal combination tested. The cracking of the chromium perpendicular to the parallel sides was caused by the electrode force even though this was reduced to approximately 300 lb while making these welds.

Simple destructive tests involving hand tools showed the chromium to be very securely bonded to the titanium. On the basis of the foregoing information it seemed reasonable that the titanium-stainless weld characteristics might be improved by somehow injecting additional chromium into the weld. Attempts were made toward this end; the results are included in a later paragraph.

Welds of Titanium to Nickel

A typical macrograph and Knoop hardness traverses for the titanium-nickel weld are shown in Fig. 9. The nugget offset in this instance is due to the difference in the electrical resistivity of the metals as both electrodes were RWMA class 1 with 6-in. radius dome. Note the porosity and strange appearance of the nugget material. Indentation was quite low but penetration was approximately 70%. This weld, made at 5000 amp, did not flash and had an average shear strength of 705 lb compared to maximum of 640 for titanium-

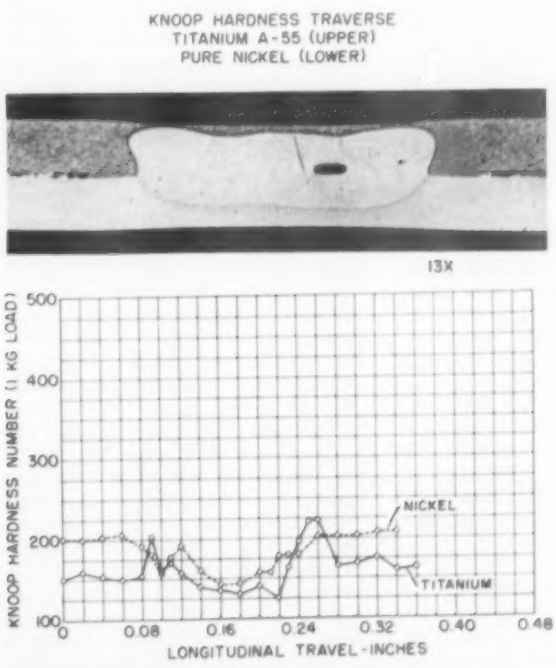

Fig. 9 Hardness study of a titanium-nickel weld

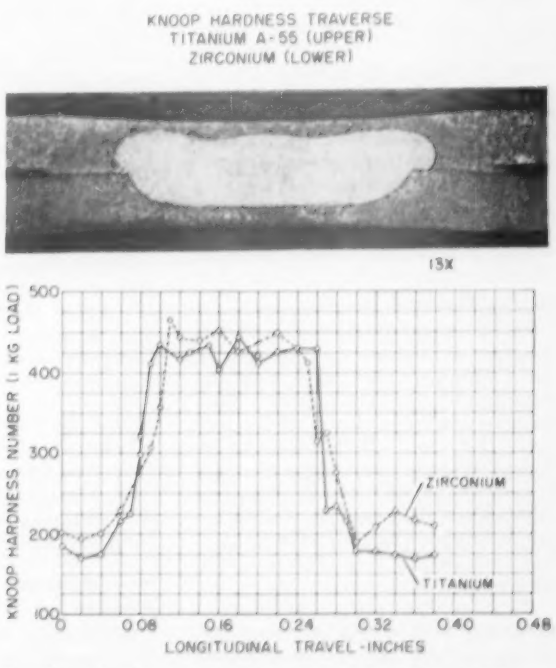

Fig. 10 Hardness study of a titanium-zirconium weld

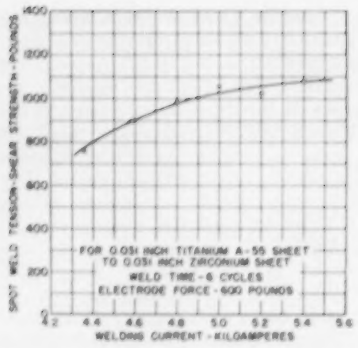

Fig. 11 Effect of variable weld current upon the tension-shear strength of titanium-zirconium welds

stainless steel 301 welds.

Contrary to what might be expected, the hardness of the titanium-nickel nugget material dropped somewhat from that of the base metals. This material, however, exhibited very strange properties when subjected to the Knoop indenter. Acting in a sponge fashion upon removal of the indenter, the material tended to "close" along the axis of the indention leaving a long slender hardness mark. Fracture of the weld revealed that nugget material greatly resembled in appearance the nugget material of the titanium-stainless steel weld. The hardness of the titanium-nickel nugget material, however, was only a Knoop of about 150 compared to 786 for titanium-stainless steel.

Miscellaneous Bimetallic Welds Involving Titanium

Included in this section are the results of investigation of a varied group of bimetallic welds of titanium. The object of this phase of study was to determine the feasibility of any type of satisfactory bimetallic welds utilizing titanium. Tension-shear curves and Knoop hardness traverses were obtained for several of the combinations used. Results from the application of such techniques as chromium plating of titanium and stainless 301 and titanium-chromium sandwiching are included.

Welds of Titanium to Zirconium

Zirconium was selected for use in this investigation because its properties in many ways resemble those of titanium. Reference to Table 1 shows the melting point of these two metals to be very nearly the same. Both have a close-packed hexagon lattice structure, are located in periodic Group IVa, and have atomic diameters that are not too far separated. Because of this similarity, it seemed very likely that the metals might produce satisfactory welds.

Figure 10 shows the typical titanium-zirconium weld nugget structure and Knoop hardness traverse. Hardness of the nugget material was approximately 430 compared to 786 for the nugget material of a high-heat titanium-stainless weld. Penetration was approximately 70%, indentation was low, and appearance of the weld was good. The polishing of this type of specimen proved to be among the most difficult as the nugget material, even though quite hard, abraded much more rapidly than either component metal. The nugget offset in this instance is due to the difference in electrical resistivity of the metals as RWMA class 1 electrodes were used adjacent to both metals.

Results from the shear strength weld current studies are shown in Fig. 11. Maximum spot-weld shear strength, obtained at about 5400 amp, was approximately 1100 lb. This value, the highest obtained for any combination of metals, was about twice the maximum obtained for titanium-stainless steel and as much as three times the value for certain other combinations. No practical value can be placed on this curve as the cost of zirconium is greater than that of titanium. It does, however, indicate that reasonable welds involving titanium and a dissimilar metal can be produced.

Welds of Titanium to Magnesium and Aluminum

Magnesium, located in Group II of the Periodic table, has a close-packed hexagon lattice structure, the same as titanium. Since the melting point and other properties of these metals are widely different, a different type of weld might be anticipated.

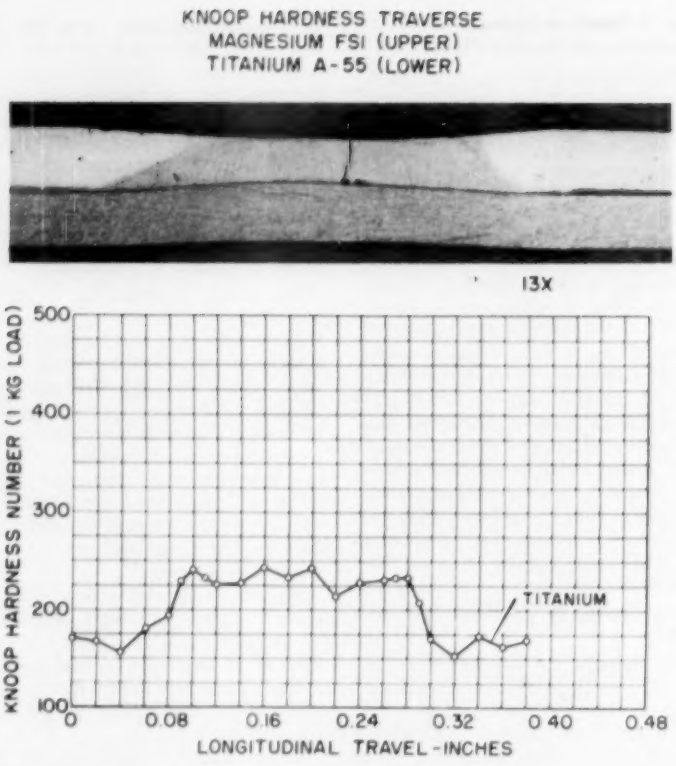

Fig. 12 Hardness study of a titanium-magnesium weld

Figure 12, a typical macrograph and hardness traverse of a titanium-magnesium alloy weld, shows clearly that a braze-type joint was formed with no intermingling of the metals whatsoever. This is attributed to the widely different melting points of the two metals. The hardness traverse was obtained only for the titanium and shows the expected hardening in the heat-affected zone. This hardness increase, however, is not nearly so great as for most combinations where mixing of the molten metals occurred.

The maximum magnitude of expected shear strengths for weld of this nature is about 525 lb as can be observed in Fig. 13. The expected minimum shear strength of a magnesium-magnesium weld of similar material is approximately 350 lb. Even though the electrode force was reduced to 290 lb, the indentation was quite high, and occasional cracking of the magnesium resulted as can be observed in Fig. 12. Welds at the higher heats produced consistent button-type failures. It was necessary, however, to thoroughly remove the oxide film from both the titanium and magnesium before a satisfactory weld could be produced.

Welds of titanium to aluminum

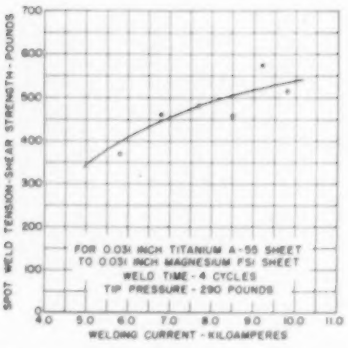

Fig. 13 Effect of variable weld current upon the tension-shear strength of titanium-magnesium welds

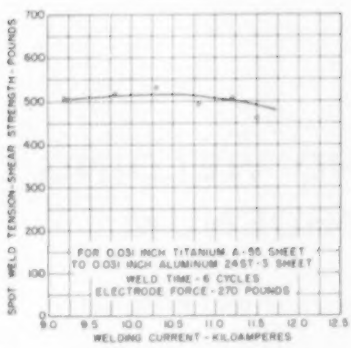

Fig. 14 Effect of variable weld current upon the tension-shear strength of titanium-aluminum welds

possessed the same general characteristics as titanium-magnesium welds. This again might be anticipated as the physical properties of titanium and aluminum, particularly the melting points, were greatly different. Hardness traverses were not obtained for this combination, but again a braze-type joint was formed with high indentation and occasional cracking of the aluminum. Electrode force and current were both reduced to alleviate this cracking.

Figure 14 is a curve of spot weld tension-shear strength versus weld current for titanium-aluminum welds. The maximum shear strength of this combination was 525 lb, comparing quite favorably to the RWMA Handbook's suggested minimum of 260 lb for an aluminum-aluminum weld of similar alloy and metal thickness. Although button failures were not common for this combination, the thorough removal of the titanium oxide film aided greatly in producing welds of consistent quality.

Titanium-Stainless Steel Welds with Increased Chromium Content

Based on a portion of the results of the titanium-chromium welds, three attempts were made to increase the chromium content of titanium-stainless steel welds and hence, it was hoped, increase the weld quality. The first efforts along this line were directed toward producing a titanium-chromium-stainless steel sandwich. Small pieces of pure chromium ground to 0.014 in. thick were placed between the titanium and stainless steel at the point where the weld was to be made. Shear tests indicated this type of weld had less strength than the conventional titanium-stainless steel welds. This weakening was attributed not to the chromium but to the fact that the titanium and stainless were separated by approximately 0.014 in. hence producing a moment on the weld when placed in shear. The additional chromium did not materially alter the intermetallic compound formation, as the weld nugget had the same characteristic appearance as in the titanium-stainless steel weld.

Chromium platings were applied to both titanium and stainless steel and this combination tested for improved weld quality. Difficulties were encountered in the case of titanium and the plated specimens were poor; however, the stainless steel specimens were very good. Weld quality showed no improvement over unplated specimens.

The third attempt at increasing the nugget chromium content was through the use of 446 stainless, a high-alloy steel without nickel. Chromium content of this alloy was about 25% compared to 18% for stainless 301. Shear strength of this weld showed no increase over the titanium-stainless steel 301 weld.

The average tension shear strength of the increased chromium content welds are as follows:

Titanium-chromium-stainless sandwich, lb.	165
Titanium-chromium-plated stainless, lb.	630
Chromium-plated titanium-stainless, lb.	405
Titanium-stainless 446, lb.	545

One Cycle Welds

A few titanium-stainless steel specimens were welded at fairly high currents with a weld time of only one cycle, the theory being to reduce the time of contact between the molten metals and hence the time for formation of undesirable weld materials. Shear strength result showed no improvement over the conventional welds. Average strength of these welds was 625 lb.

Conclusions

The following conclusions have been established on the basis of experimental observation described herein:

1. Attempts to effect a better heat balance through the use of a high-resistance electrode produced little or no improvement in the characteristics of titanium-stainless steel welds. The maximum tension-shear strength, obtained for welds of solid phase or plastic state bond, was 640 lb. Increasing heat caused cracking of the nugget material and formation of an intermetallic compound of crystalline appearance. The cracking was accompanied by a rapid decrease in tension-shear strength of the weld.

2. Investigations relative to the components of stainless steel indicate that the incompatibility of the titanium-stainless steel weld is probably due to the iron content of the stainless.

3. Of the three principal components of stainless steel, chromium produced a far better weld with titanium than either iron or nickel. No theory for this can be advanced at present.

4. Because of the like properties of titanium and zirconium, welds of this nature produced the highest strength of any combination tested. Ductility remained poor; tension-shear strength reached a value of about 1100 lb.

5. Magnesium or the aluminum, when spot welded to titanium, produced braze-type joints of fair characteristics. By carefully removing oxide film from both titanium and magnesium, welds with a tension-shear strength of 525 lb can be produced. Aluminum welds with a tension-shear strength of 525 lb can also be made provided the oxide film is carefully removed from the titanium.

6. Using the techniques described herein, the injection of additional chromium into the titanium-stainless weld has little effect on the weld characteristics.

Bibliography

Abkowitz, S., Burke, John J., and Hiltz, Ralph H., Jr., *Titanium in Industry*, D. Van Nostrand Co., Inc., New York (1955).

Barksdale, Jelks, *Titanium, Its Occurrence, Chemistry, and Technology*, The Roland Press Co., New York (1949).

Begeman, M. L., McBee, Frank W., Jr., and Fontana, J. C., "The Physical and Metallurgical Characteristics of Spot Welded Titanium," THE WELDING JOURNAL, 30 (9), Research Suppl., 429-s to 434-s 1951.

Guy, Albert G., *Elements of Physical Metallurgy*, Addison-Wesley Press Co., Cambridge, Mass. (1951).

Resistance Welder Manufacturers' Association, *Resistance Welding Manual*, Philadelphia, Resistance Welder Manufacturers' Association (1948).

Titanium Metals Corporation of America, *Handbook on Titanium Metal*, New York (1950).

FABRICATION AND WELDING OF ARC-CAST MOLYBDENUM

Study aimed at developing materials and procedures for making fusion weldments in molybdenum sheet with improved bend ductility at low temperature

BY R. E. MONROE, N. E. WEARE AND D. C. MARTIN

ABSTRACT. The objective of this investigation was the development of improved methods and procedures for producing molybdenum weldments with good room-temperature ductility. Sheet materials and fusion weldments made in a dry box from $^1/_{16}$- and $^1/_8$-in.-thick arc-cast molybdenum had good bend properties at low temperatures. The best ductility was obtained from 0.7% titanium alloys and carbon-deoxidized molybdenum with a low-carbon content (>0.025%).

The effects of variation in composition and fabrication procedures on the ductility of fusion weldments were studied for titanium-neutralized and carbon-deoxidized molybdenum. The titanium-neutralized alloy containing 0.7% titanium had better weldment ductility than alloys containing 0.5 and 1.0% titanium. Simplified melting and fabricating procedures did not adversely affect the ductility of titanium-neutralized molybdenum weldments, although double melting of the ingots was required to avoid weld porosity. Better weld ductility was obtained from lower carbon content material in commercial carbon-deoxidized arc-cast molybdenum. However, the ductility of sheet and weldments in experimentally rolled carbon-deoxidized molybdenum was not affected by the carbon content. Rolling sheet in a protective jacket did not affect the ductility in either type of molybdenum. An over-all improvement in weldment ductility was obtained by welding in a high-purity helium atmosphere and grinding the weld surface after welding.

Introduction

This study was made to develop materials and procedures for making fusion weldments in molybdenum sheet with improved bend ductility at low temperatures. Arc-cast alloys of molybdenum containing titanium and/or carbon additions were found to have good bend properties at room temperature in welds made in a helium atmosphere. The effects on bend properties of variations in composition, purity and fabrication procedures on ductility were determined by comparing the results of a simple bend test.

Molybdenum has several properties which recommend it for high temperature use. It has a high melting point and good strength at high temperatures. The modulus of elasticity of molybdenum at 1600° F is a third greater than steel at room temperature. The low thermal expansion of molybdenum gives it exceptional thermal shock resistance. Other properties which make molybdenum advantageous for many uses are good electrical conductivity and good corrosion resistance in many mediums.

Poor oxidation resistance and difficulties with welding are at present the main deterrents to the immediate use of molybdenum in many applications. The poor oxidation resistance of molybdenum can be offset by design modifications or by the use of claddings, but only an improvement in the weldability will make it possible to use the metal for many applications. The object of this investigation, therefore, was the development of a weldable molybdenum alloy.

Molybdenum weldments may be poor because of two things: (1) porosity in and around the welds, and (2) lack of room-temperature ductility in the weld and heat-affected zone. Earlier studies have shown that welds in arc-cast molybdenum alloys normally do not have a great amount of porosity and that welds have good ductility at around 400° F and above. However, very poor ductility was obtained at room temperature and some means of improving the room-temperature ductility was needed.

Molybdenum welds have the same deficiency in room-temperature ductility as arc-cast molybdenum before it is fabricated due to the similarity in structure. Information gained on the factors affecting the room-temperature ductility of cast molybdenum is therefore valuable in the development of a weldable molybdenum. An extensive study of the effects of impurities and alloying elements on the ductility of cast molybdenum was summarized in a recent report to the Office of Naval Research.[1] The most important findings were as follows:

1. The low-temperature ductility of arc-cast molybdenum is very sensitive to minute quantities of oxygen, less sensitive to nitrogen and much less sensitive to carbon.

2. Additions of titanium in the range of 0.5 to 1.0% overcome the deleterious effects of small amounts of oxygen.

Figures 1 and 2 show the effects of impurities and of titanium on the minimum temperature at which specimens of arc-cast molybdenum showed initial plastic deformation in bending.

A program was initiated to extend these findings to molybdenum weldments. Alloys containing from 0.5 to 1.0% titanium were carefully prepared to exclude as much oxygen, nitrogen and carbon as possible. These alloys were fabricated by extrusion and rolling into sheet, and weldments were made for evaluation by bend testing. Effects of minor relaxations in requirements for purity and fabrication were included in this study to determine if simpler methods could be substituted for the more costly steps used in the alloy fabrication without having a detrimental effect on the weld ductility.

Initially, commercially-available carbon-deoxidized molybdenum was selected as the base material for determining the effectiveness of titanium-neutralized alloys in improving weld ductility. Arc-cast carbon-deoxidized molybdenum is available as a commercial product and can easily be welded to produce crack- and porosity-free welds in thin sheet. Carbon-deoxidized molybdenum is considered an unalloyed material and the carbon present in this material is limited to the

R. E. Monroe and **N. E. Weare** are Principal Welding Engineers and **D. C. Martin** is Consultant, Metals Joining Research Division, Battelle Memorial Institute, Columbus, Ohio.

Presented at 1956 AWS National Fall Meeting in Cleveland, Ohio, October 8th to 12th.

Work performed under AEC Contract W-7405-eng-92.

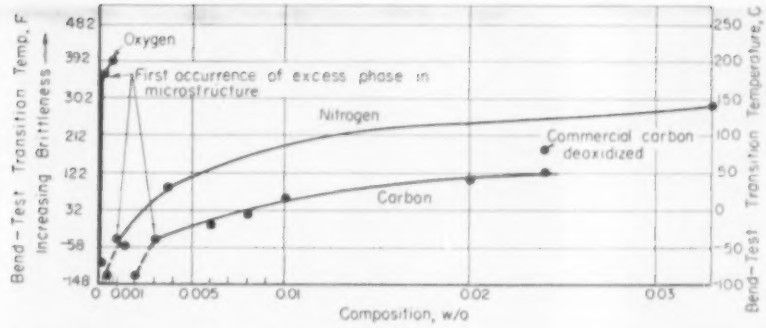

Fig. 1 Effect of oxygen, nitrogen and carbon upon bend-test transition temperature of cast molybdenum

minimum residual content consistent with good deoxidation practice. Improvements in the melting procedures have steadily lowered the amount of residual carbon to a current value of about 0.02%.

A study of ductility of a commercial sheet containing 0.046% carbon was made while the titanium-neutralized alloys were being fabricated. Results of this study showed a vast improvement in the weld ductility when using the welding methods used for this program on material tested several years ago[2] using different welding methods. These results prompted a more extensive study of carbon-deoxidized molybdenum to determine if changes in fabrication procedure and composition would improve weld ductility in this type of molybdenum.

Commercially-available sheet was used for some of this work, but for some studies it was necessary to fabricate sheet from commercial extrusions. The ductility of weldments from pilot extrusions made at Oak Ridge National Laboratory also was determined. Tests also were made on a commercial alloy containing a nominal 0.5% titanium addition and on a commercial carbon-deoxidized sheet of $^1/_8$-in. thickness.

All weld specimens were prepared by tungsten-arc welding in a helium-atmosphere chamber. Fusion welding was used, since it appears to be the most practical method for constructing many components of molybdenum.

Good bend ductility was obtained in weldments produced from both the titanium-neutralized and carbon-deoxidized molybdenum. The greatest improvement in weld ductility came from grinding the weld surface, increasing ductility at room temperature in most cases from completely brittle to fairly ductile. Of the titanium-neutralized alloys studied (0.5, 0.7 and 1.0% titanium), the 0.7% titanium alloy had the best ductility in weldments.

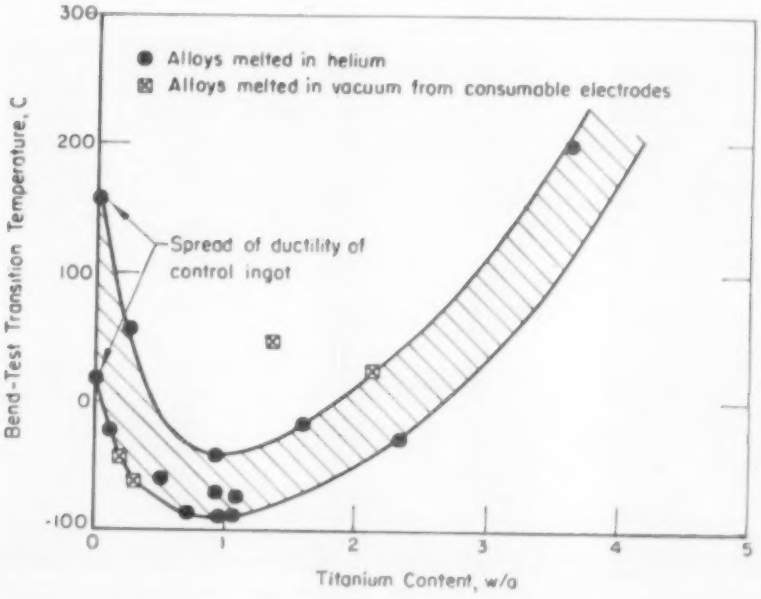

Fig. 2 Effect of titanium on bend-test transition temperature of cast molybdenum

Lowering the carbon content of the carbon-deoxidized alloys increased the weld ductility in commercially rolled sheets, but did not affect the weld ductility in experimentally rolled sheet.

The paper has been divided into sections on experimental procedures and factors affecting the ductility of sheet and weldments. The section on experimental procedures contains descriptions of the preparation of titanium-neutralized and carbon-deoxidized sheet and welding and testing procedures. In the section on factors affecting the ductility of sheet and weldments, the titanium-neutralized and carbon-deoxidized alloys are handled separately. These are followed by a summary of the results and conclusions derived from the results.

Experimental Procedures

Special procedures had to be developed for the preparation and handling of the materials used for this study. These procedures include the fabrication of sheet, welding and testing procedures.

Preparation of Titanium-Neutralized Molybdenum Sheet

The various steps and variables studied in the preparation of titanium-neutralized molybdenum sheet are tabulated below:

(1) Preparation of ingots—composition, purity and number of melts varied.
(2) Extrusion—temperature varied.
(3) Recrystallization.
(4) Forging.
(5) Rolling—surface preparation, canning, and atmosphere during heating varied.
(6) Stress relief—time and temperature varied.
(7) Testing—surface of sheet varied.

Commercial molybdenum ingots could not be used to make the titanium-neutralized alloys because of their inadequate purity. Sintered molybdenum was purified by two methods to lower the oxygen content to a more acceptable level. In the first method, crushed bars were slowly melted in a vacuum of less than 0.2 micron of mercury using a tungsten electrode.[3] By melting just once, the oxygen content was lowered to below 0.0005%, and the carbon content was about 0.002%. As an alternate method, other sintered bars were vacuum arc melted as a consumable electrode in a commercial furnace. From fractographic examination of these ingots, the oxygen content was estimated to be below 0.0010 and 0.0015%, and the carbon content was below 0.005%. For alloy preparation, master alloys of the purified molybdenum with iodide titanium and spectrographically pure graphite were prepared.

Titanium-neutralized molybdenum ingots were prepared in a special arc-melt-

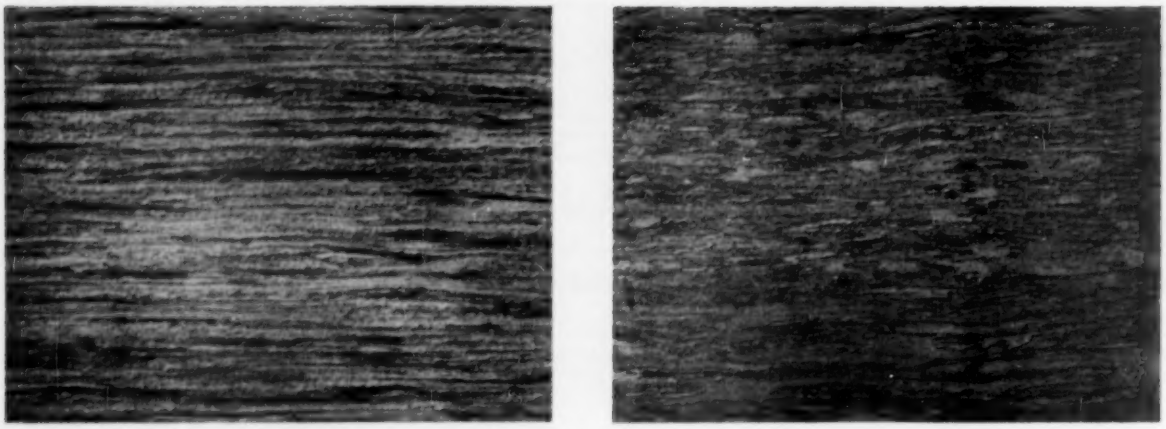

Murakami's etch. X 100. (*Left*) Longitudinal section and (*right*) transverse section.

Fig. 3 Typical microstructure of titanium-neutralized molybdenum sheet

ing furnace under an atmosphere of purified helium. Most ingots were melted twice to insure a uniform composition, others were melted only once. Macroporosity was present in ingots melted only once indicating the presence of gas which was not removed by a single melting. All ingots were stress relieved in hydrogen for at least 1/2 hr at 2000 or 2200° F and then scalped for extrusion.

Extrusion by the Ugine-Sejournet process was used for the initial ingot breakdown, since forging usually results in cracking of molybdenum ingots. The extrusions were made on a 750-ton horizontal extrusion press at Oak Ridge National Laboratory. Two pilot extrusions of carbon-deoxidized molybdenum from a single ingot were made to establish conditions. Extrusion ratios of 4:1 and 5.8: were used with a mixture of Pyrex and window glass for a lubricant. Initially, an extrusion temperature of 2300° F was used; however, temperatures of 2550 to 2600° F produced a greater recovery of sound metal and were used for later extrusions. Two ingots containing 0.008% added carbon (0.01% total carbon) failed to extrude entirely. However, the extruded portion of these ingots was more sound than the lower carbon billets. The extruded billets were recrystallized for 1 hr at 2600° F in hydrogen before any further fabricating operations were performed.

The cylindrical recrystallized bars were then flattened for rolling in a forge hammer to a thickness of 3/4 or 1 in. The forging temperature was 2200 to 2300° F. Billets to be rolled in a cladding were forged to tighten the jackets before rolling.

Initially, it was thought that the best rolling schedule for these alloys was to start at 2000° F and gradually reduce the temperature to 1350° F. Sheet rolled using this schedule was found to be severely laminated, so higher rolling temperatures were used (2000 to 2300° F). All rolling was done on a 8 by 12 two-high mill with reductions of 20 to 25% per pass. Samples were reheated between passes in a hydrogen atmosphere, except for some clad specimens rolled below 2000° F. Most of the sheet was stress relieved for 1 hr at 1800° F after rolling. Microstructures of typical titanium-neutralized sheet are shown in Fig. 3.

Preparation of Carbon-Deoxidized Molybdenum Sheet

The general fabrication procedures for commercial arc-cast carbon-deoxidized molybdenum sheet have been described by Deuble.[4,5] Specific information on the commercial materials used in this study is given in Table 1. All sheet was rolled on a commercial mill without any cladding. In commercial practice, reheating is done in a slightly reducing atmosphere when it is considered necessary by the rolling foreman. The oxide coating was removed prior to delivery of this material.

Two commercial extrusions containing 0.015 and 0.042% carbon were obtained to study the effects of cladding and composition on material rolled under known conditions. Both of these extrusions were made at 2300° F with a reduction from 6 1/8 in. in diameter to 4 in. in diameter. The extruded bars were annealed 1 hr at 2600 to 2700° F. Each extrusion was cut into pieces approximately 1 3/8 by 2 by 2 in. and rolled as

Table 1—Data on Commercially Rolled Molybdenum Sheet

Alloy specimen	*Composition, w/o*	*Initial breakdown*	*Intermediate working*	*Finish rolling temperature, ° F*	*Final thickness, in.*
C3	0.041 C	Extruded from 6 1/2 in. diam to 3 3/4 in. diam at 2300° F*	Forged to 1 1/8 by 4 1/8-in. sheet bar at 2350° F*	2300–1900	1/8
C12	0.046 C	Forged from 5 25/32-in. diam casting to 3 1/4 in. diam at 2450 to 2580° F*	Rolled to 1 by 1 1/2-in. bar at 2300 to 1900° F	2300–1900	1/16
C16	0.020 C	Same as C3	Rolled† to 1 1/8 by 4-in. sheet bar*	2300–1900	1/16
C19	0.029 C 0.46 Ti	Extruded from 6 3/8 in. diam to 4 1/4 in. diam at 2300° F‡	Forged† from 3 3/4 to 1 1/8 in. by 4 3/8-in. sheet bar*	2300–1900	1/8

* Annealed 1 hr at 2600° F.
† Temperature for rolling not given.
‡ Annealed 1 hr at 2750 to 2900° F.

shown in Fig. 4. Between passes, the material was reheated in a helium atmosphere. No difference in strain hardening, as determined by hardness measurements, was found in sheets fabricated by slightly different rolling procedures. Both extrusions had a hardness of 182 DPH, while the hardness of all the sheet ranged from 260 to 265 DPH.

Additional material for this study was obtained from the initial extrusions made at Oak Ridge National Laboratory. This sheet was rolled by the same procedures used for the first titanium-neutralized alloys, which were described earlier.

Microstructures of the sheet materials were similar to those shown in Fig. 3 for titanium-neutralized molybdenum.

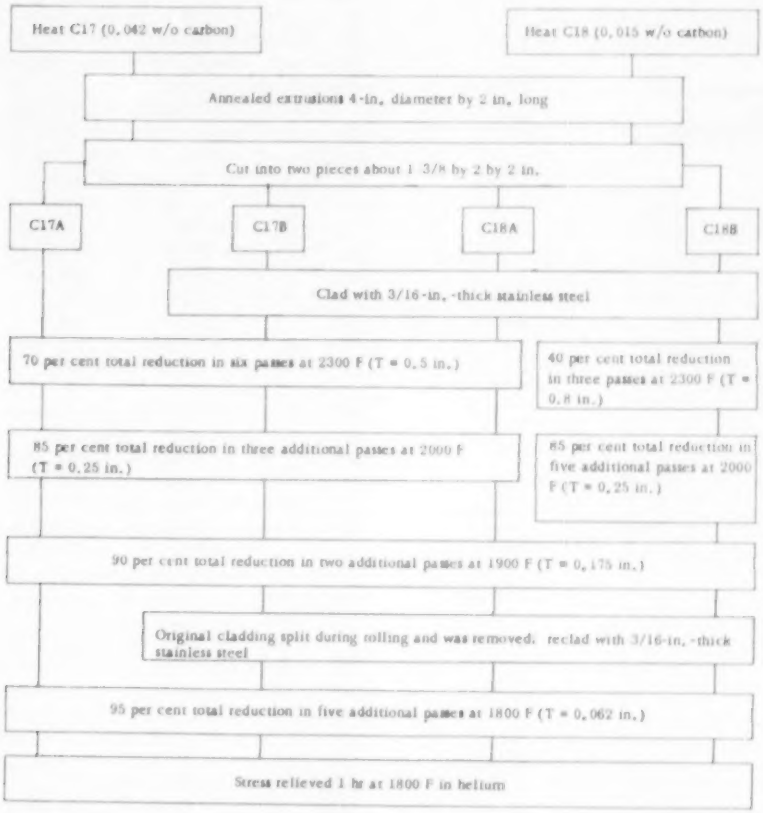
Heat C17 (0.042 w/o carbon)
Heat C18 (0.015 w/o carbon)
Annealed extrusions 4-in. diameter by 2 in. long
Cut into two pieces about 1 3/8 by 2 by 2 in.
C17A
C17B
C18A
C18B
Clad with 3/16-in. -thick stainless steel
70 per cent total reduction in six passes at 2300 F (T = 0.5 in.)
40 per cent total reduction in three passes at 2300 F (T = 0.8 in.)
85 per cent total reduction in three additional passes at 2000 F (T = 0.25 in.)
85 per cent total reduction in five additional passes at 2000 F (T = 0.25 in.)
90 per cent total reduction in two additional passes at 1900 F (T = 0.175 in.)
Original cladding split during rolling and was removed; reclad with 3/16-in. -thick stainless steel
95 per cent total reduction in five additional passes at 1800 F (T = 0.062 in.)
Stress relieved 1 hr at 1800 F in helium

Note: All rolling with 20 per cent reduction per pass and five-min reheating time between passes.

Fig. 4 Flowsheet for rolling experimental carbon deoxidized molybdenum sheet

Welding Procedures

Special equipment and procedures were developed to minimize the contamination of molybdenum alloys during fusion-welding operations. Inert-gas-shielded tungsten-arc welding was used in this work since it is versatile, it can be controlled closely and contamination is primarily a function of gas purity. The equipment used in welding and the procedures for handling the molybdenum before, during and after welding are described in the following section.

All welding was done in helium contained in a vacuum-purged dry box. The dry box was cylindrical, 4 ft long by 30 in. in diameter. Figure 5 shows the exterior of the dry box. The dry box was purged to a vacuum of 0.1 micron of mercury by a forepump diffusion-pump system. During the evacuation period, hot water was circulated through water jackets to speed outgassing of the chamber walls. After purging, the pumps were isolated from the working chamber, and gas was admitted directly from a high-pressure cylinder. This technique insured that the dry-box atmosphere was as pure as the gas in the cylinder.

For this program, an automatic welding setup was used to produce uniform

Fig. 5 Vacuum-purged dry box for welding in inert atmospheres

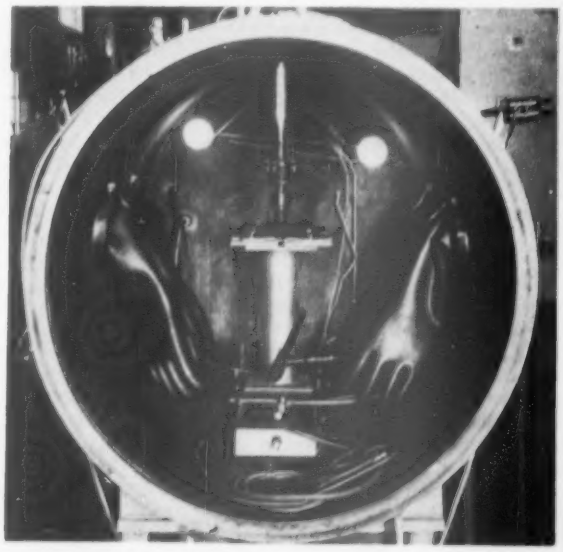

Fig. 6 Setup for automatic welding in helium atmosphere

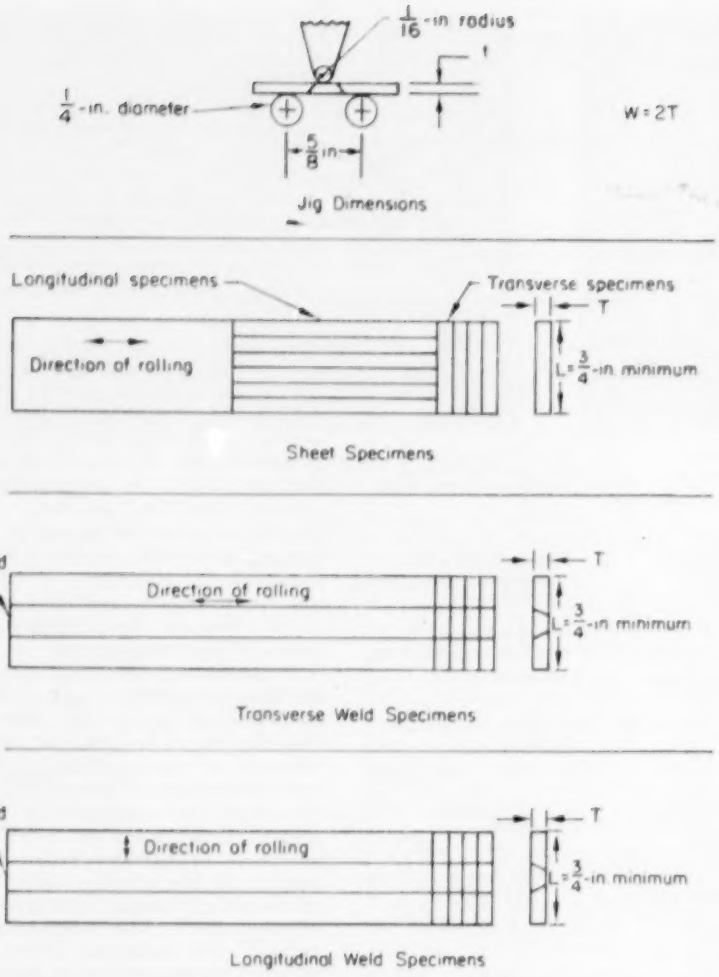

Fig. 7 Nomenclature and dimensions for bend-test jig and specimens

welds. The dry box was equipped with a constant-voltage welding head which controlled a water-cooled electrode holder passing through O-ring seals at the top of the chamber. Molybdenum sheet specimens were clamped to a screw-driven carriage which traveled under the electrode. Figure 6 shows the interior of the chamber set for automatic welding. Welding current was supplied by a 400-amp direct-current rectifier. The control circuit of the welding head struck the arc, started the carriage in motion and maintained a constant arc voltage during welding. This arrangement gave a minimum variation of the welding conditions during the test program.

The importance of meticulous procedures in the handling of molybdenum before and during joining have been reported by other investigators.[6] However, in the work reported here, consideration also was given to the practicality of the various procedures. Methods were developed which were precise enough to produce satisfactory welds without being impractical for the construction of useful welded structures. The cleaning of joint surfaces before welding is particularly important in welding molybdenum. Even slight oxide films and possibly higher impurity levels at the sheet surface can cause brittleness in molybdenum weldments.

Molybdenum sheet which was rolled in air had a heavy oxide coating on the sheet surfaces. This oxide coating was removed by immersing the molybdenum in a molten sodium-potassium nitrate salt bath. For rapid removal of the oxide, the temperature of the salt bath was held at 700° F, although lower temperatures could be used. Any surface defects in the sheet were removed by grinding.

When the jacket was peeled off the titanium alloys which were clad for rolling, the sheet generally had a rough surface. This surface probably was caused by the tearing of laminations which were present in sheet rolled at low temperatures. This rough surface was ground smooth before the final cleaning operations. In some cases, the final sheet thickness was 0.040 in. after grinding. Weld specimens about 1 by 4 in. were cut from the titanium-neutralized and carbon-deoxidized sheets after the initial cleaning and grinding.

To insure a clean surface for welding, the molybdenum was etched in a solution containing 95 parts H_2SO_4, 4.5 parts HNO_3, 0.5 part HF and 18.8 g per liter Cr_2O_3. The specimens were immersed in the hot etchant (140° F) for 30 sec, then rinsed in hot water and acetone. The specimens were then placed in the dry box for welding.

Weld specimens were clamped to a steel jig by two copper hold-down plates. There was no backing for 1/4 in. on each side of the joint. The dry box was loaded with several specimens for each run. After vacuum purging, the dry box was rapidly filled with Grade A helium. A weld bead was made on zirconium plate for several minutes to gather the atmosphere and to check its purity. No discoloration or tinting of the zirconium was observed before any of the molybdenum welds were made.

Welding conditions which produced full penetration were selected after several trial weldments on scrap molybdenum had been made. Both bead-on-plate and square-butt-joint welds were used in this work. There was no difference in the weld shape or penetration in weldments made from either type of specimen. The welding conditions established to give full penetration for various sheet thicknesses are given in Table 2. All welds were made without the addition of any filler metal. In some cases, this caused slight irregularities in the weld surface.

Table 2—Welding Conditions for Inert-Gas Tungsten-Arc Welds in Molybdenum Sheet

Welding current, amp	65 for 0.040 in. thick 120 for 1/16 in. thick 160 for 1/8 in. thick
Arc voltage, v	20
Travel speed, ipm	12 for 0.040 and 1/16 in. thick 8 for 1/8 in. thick
Voltage sensitivity control	Normal
Electrode	1/8-in.-diam. Zirtung
Atmosphere	Grade A helium
Current type	Straight-polarity direct current

After welding, all specimens were stress relieved for 1 hr at 1800° F in flowing tank hydrogen. The need for this stress relief was never determined in this study and is probably unnec-

essary for small specimens, but it has been shown that this treatment will relieve some of the stresses in more complex weldments.

Test Procedures

Molybdenum exhibits ductile-to-brittle transitions similar to those found in ferrous metals. Such transitions are usually defined by arbitrary tests which are eventually useful in the design of structures through the correlation of test results with success or failure in service. The temperature at which such an arbitrary transition occurs is dependent on a number of factors which can usually be defined as strain rate and on other factors which must be determined experimentally. Loss of ductility in molybdenum is most apparent when the metal is subjected to bending stresses transverse to the direction of working in wrought metal or grain orientation in the cast metal. For the evaluation of the changes in bend ductility of sheet and weldments, a simple bend test was used. In this test, the thickness of the bend specimen was the thickness of the sheet or weldment being tested and the width was twice the thickness. The terms used to describe the specimens and the dimensions of the test equipment are shown in Fig. 7. All welds were tested with the face of the welds in tension during bending. Normally, only the transverse specimens were used, since they defined the worst conditions. The load was applied at the center of the specimen at a deflection rate of 1 ipm. At this deflection, the strain rate was faster than a normal slow bend test, but slower than an impact test. The strain rate at the start of bending was 0.010 in. per inch per second for a 0.040-in. thickness, 0.016 in. per inch per second for a $^1/_{16}$-in. thickness and 0.032 in. per inch per second for a $^1/_8$-in. thickness. These slight differences in strain rates would not cause a significant change in transition temperature.

Specimens were bent until fracture occurred or to a maximum angle of 90 deg* in the temperature range from −75 to +250° C. The variable measured was the permanent bend angle after fracture, giving an indication of the amount of plastic flow which occurred during bending. For conveniences in interpretation, the data were plotted on rectangular coordinates and an envelope was drawn to contain all points.

The transition temperature of a given sample was chosen as the lowest temperature at which plastic flow occurred. Transition temperature is probably a measure of purity as it influences plastic flow in coarse-grained material. Figure 8 shows the differences that exist in the bend-test plots for cast, welded and wrought materials. The range between the temperatures at which all specimens bent 0 to 90 deg appears to be a good measure of differences in microstructure. Increasing the grain size broadens the temperature range in which the transition occurs from 0 to 90-deg bending. However, in this work, the most important consideration in evaluating different materials was the ductility around room temperature.

Metallographic and radiographic examinations were made to round out the data needed to evaluate the effects of variables on the ductility of molybdenum samples.

* Limit of test equipment.

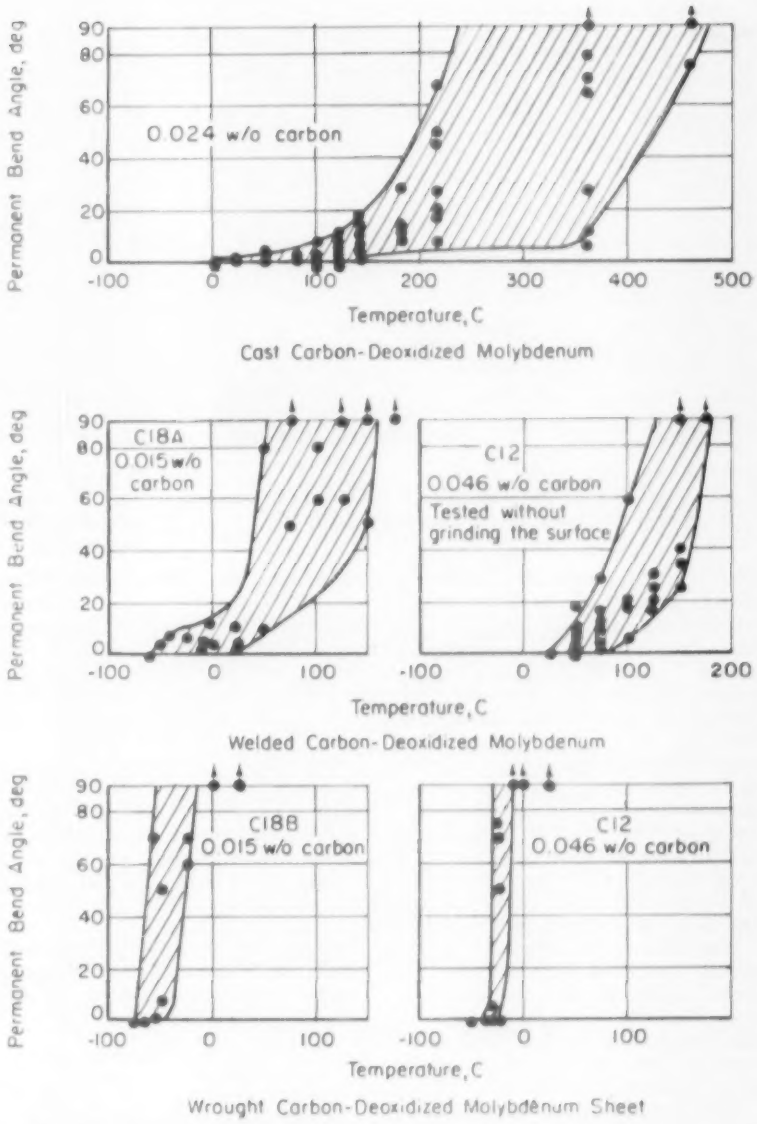

Fig. 8 Typical bend-test plots

Factors Affecting Ductility

Bend tests were made on the molybdenum sheet prior to welding to determine the effects of composition and fabricating variables on the ductility of the sheet. The two sections described the effects of variables on the ductility of the sheet and weldments for titanium-neutralized and carbon-deoxidized molybdenum.

Titanium-Neutralized Molybdenum

The ductility of the titanium-neutralized molybdenum sheets was generally good. Most sheet materials had transition temperatures below −75° C and nearly always bent 90 deg at room temperature. As previously mentioned, ductility of wrought sheet was largely governed by microstructure. Thus, the variables which changed the microstructure exerted the greatest influence on ductility. Sheet rolled by starting at 2000° F and gradually reducing the rolling temperature to

Murakami's etch. 0.7% titanium. X 100

Fig. 9 Typical weld-metal structure in titanium-neutralized molybdenum. (Reduced by 1/2 upon reproduction)

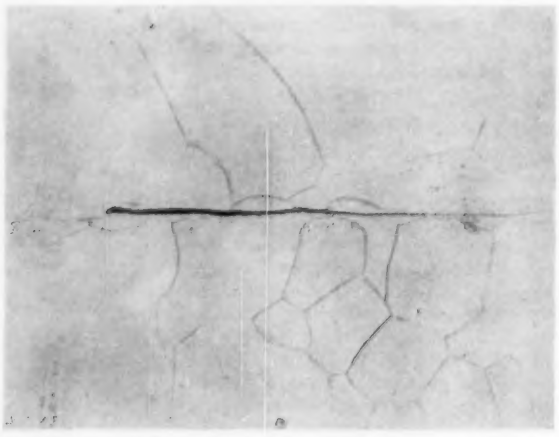

Murakami's etch. X 100.

Fig. 10 Lamination in the weld heat-affected zone of titanium-neutralized molybdenum rolled at low temperatures. (Reduced by 1/2 upon reproduction)

1350° F had good ductility but had a strong tendency to laminate. Sheet rolled by starting at 2300° F and finishing at 2000° F had about the same degree of ductility but much less tendency to laminate. Sheet rolled by starting at 2400° F and finishing at 2200° F, or recrystallized at 1/4-in. thickness before final rolling, was brittle at low temperatures. Removal of 0.001 in. from the surface of the sheet finish rolled at 2000° F was necessary to obtain good ductility. Cladding the alloys for rolling was not necessary to obtain good ductility. Stress relieving the sheet at 1800 to 2000° F after rolling improved the ductility of the sheet. Variations in the titanium content from 0.5 to 1.0% did not affect sheet ductility and slight variation in the purity of the initial molybdenum melting stock had no effect on the sheet ductility.

The ductility of the titanium-neutralized weldments varied much more than the sheet materials. Variations in composition and purity produced more noticeable differences in welds, because of the coarse grain structure in the fused and heat-affected zones. The greatest improvement in weld ductility was caused by removing the as-welded surface by grinding. Metallographic examination did not disclose any noticeable changes between weldments with good and bad ductilities. Figure 9 shows the typical structure of welds in titanium-neutralized molybdenum. The structure appears free of impurities at the grain boundaries and within the grain. The variables studied are discussed in the following sections.

Originally, bend tests were made on samples cut from as-welded joints. The surface of these joints were fairly smooth, although at times small depressions were present along the fusion line. Following a study of the effects of grinding the surface with a hand grinder, made on carbon-deoxidized molybdenum, all bend-test samples were cut from weld joints which were ground smooth. A comparison of the bend properties of the materials which were tested under both surface conditions is given in Table 3. The vast improvement in the surface-ground specimens is obvious. The effects of surface treatment are explained more fully in the section on carbon-deoxidized molybdenum. Studies of all other effects were made with surface-ground specimens.

Table 3—Effect of Surface Grinding on the Ductility of Welds in 0.7 w/o Titanium Alloys

Alloy specimen	*Specimen condition**	*Transition temperature, ° C*	*Bend at 25° C, deg*
B2	AW	10	4–10
	SG	−55	12–35
B3	AW	25	2
	SG	−60	12
B4	AW	80	0
	SG	−20	4–8
B5	AW	60	0
	SG	< −25	10–40

* AW, tested as-welded; SG, tested after hand grinding.

The composition of the titanium-neutralized alloys was varied to study three titanium levels, two levels of initial molybdenum purity, and a slight addition of carbon.

Alloys containing nominal additions of 0.5, 0.7 and 1.0% titanium were made to determine the effects of titanium additions on the ductility of molybdenum weldments. Welds in the 0.7% alloy had ductility better than either the 0.5 or 1.0% alloys. This finding followed the same trend found with cast molybdenum, where an optimum composition existed. The bend-test data used to compare the effects of titanium content are shown in Table 4. Below the optimum addition, there probably was not enough titanium present to combine with all the oxygen present, and over the optimum addition the alloys may be embrittled by solid-solution hardening.

Table 4—Effects of Titanium Content on Weld Ductility

Alloy specimen	*Titanium content, w/o*	*Transition temperature, ° C*	*Bend at 25° C deg*
Rolled in air above 2000° F			
B11A	0.5	60	0
B8A	0.7	−60	6–90
B10A	1.0	5	4–14
Rolled in cladding above 2000° F			
B11B	0.5	−35	10–20
B8B*	0.7	−10	2–18
B10B	1.0	−10	14–16
Rolled in cladding at or below 2000° F			
B11C	0.5	−20	0–30
B2	0.7	−55	12–35
B10C	1.0	− 5	0–4

* Cladding fused to alloy during stress relief and may have caused excessive contamination of this material.

The effects of melting-stock purity could not be isolated, since all of the high-purity alloys were rolled below 2000° F, while the low-purity alloys were rolled above this temperature. Bend ductility of the welds did not appear to be affected by changing the initial melting-stock purity. In some instances, low-purity alloys had slightly better weld ductility than corresponding welds in high-purity alloys.

Table 5—Effect of 0.01 w/o Carbon on Weld Ductility in 0.7 w/o Titanium Alloys Rolled in Air

Alloy specimen	Carbon content, w/o	Bend angle, degree at temperature, ° C											
		−50	−40	−25	−20	−10	0	25	50	75	100	125	150
B4	0.002			0	4	30	30	4	2	20	30	25	25
								8	30				
B7	0.010	0	10	0		20	12	6	18	30	50	90	30
		0						8					
								30					

The addition of 0.01% carbon to the 0.7% titanium alloy appeared to improve the weld ductility over comparable welds made in this alloy without the carbon addition, as shown in Table 5. Unfortunately, the carbon addition also increased the resistance to deformation by extrusion above the press capacity and very little of this material was available for study.

Only two sets of material (B10B and B10C, and B11B and B11C) were available to study the effects of rolling temperatures on weld ductility independent of other variables. Data for these materials were presented previously in Table 4. In both sets, the difference in weld ductility was slight when the rolling procedure was changed from rolling at 2300° F and finishing at 2000° F to complete rolling at 2000° F.

Although exact comparisons could not be made, the general effect of rolling at the low temperatures which produced serious laminations was to lower weld ductility and increase the scatter within the transition range. One type of flaw that results from bad laminations is shown in Fig. 10. Such defects would not be desirable in any material, particularly one as notch sensitive as molybdenum.

The ductility of welds in titanium-neutralized alloys was not affected by cladding the material during rolling. Evidently, when sheet was rolled in air and reheated in hydrogen, oxygen did not diffuse into the alloy in sufficient quantities to harm weld ductility, provided the contaminated surfaces were removed before welding. However, another possibility is that enough diffusion occurred during extrusion, which was always done without cladding, to overshadow the effects of diffusion during further working without cladding.

Slight fusion-line porosity was found in many of the titanium-neutralized alloys. This porosity slightly lowered weld ductility and caused much of the scatter in bend-test results. Several factors influenced the amount of porosity obtained. No porosity was observed in any welds made on sheet initially made from low-purity melting stock. This sheet was rolled at higher temperatures than the sheet made from high-purity stock. It is more likely that porosity was associated with the difference in rolling temperature, which, in turn, controlled the extent of laminations in the sheet. Laminations could cause porosity by several mechanisms.

The number of times that the ingots were melted also affected porosity in sheet rolled at low temperatures. Welds in material which was melted only once contained substantially more porosity than similar welds in twice-melted material. Weld porosity in the single-melted material could be reduced by remelting the weld. The reason for this difference in the tendency to form porosity was probably caused by the entrapment of gas in sheet rolled from single-melted ingots. Macroporosity was also present in the single-melted ingots.

Carbon-Deoxidized Molybdenum

Of the variables studied for carbon-deoxidized sheet, only specimen orientation, thickness and the titanium addition had much effect on sheet ductility. Commercially-rolled sheet

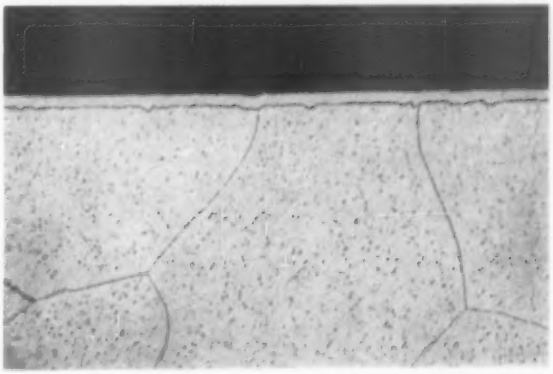

Murakami's etch. X 250.

Fig. 11 Weld surface before grinding. (Reduced by 1/3 upon reproduction)

Table 6—Bend-Test Results for Carbon-Deoxidized Molybdenum Weldments

Alloy specimen	Carbon content, w/o	Surface condition	Transition temperature, ° C	Bend at 25° C, deg
		1/16-in. commercial sheet		
C12A*	0.046	As-welded	0	0–8
C12B		As-welded	25	0
C16A	0.020	As-welded	−10	0–40
C16B		Ground	< −40	70–90
		1/16-in. experimental sheet from experimental extrusion		
C14A	0.036	As-welded	−25	0–20
C14B	0.036	Ground	−40	10–25
		1/16-in. experimental sheet from commercial extrusion		
C17A1	0.042	As-welded	50	0
C17A2		Ground	−50	8–25
C17B		Ground	−60	2–30
C18A	0.015	Ground	−60	2–10
C18B		Ground	−60	25–30
		1/8-in. commercial sheet		
C3	0.041	Ground	−25	6–18
C19	0.029†	Ground	−10	4–12

* Longitudinal-bend specimens; all other tests made with transverse-bend specimens
† Titanium content, 0.5 w/o.

had better ductility longitudinal to the direction of rolling than transverse to the rolling direction. Experimentally-rolled sheet showed little effect of specimen orientation. Commercial sheet $^1/_2$ in. thick had about the same ductility as commercial sheet $^1/_{16}$ in. thick, but the temperature for 90-deg bends was higher for the $^1/_2$-in.-thick sheet. The addition of 0.5% titanium to the carbon-deoxidized molybdenum increased the strength of this alloy to the point that no bend greater than 60 deg was obtained up to temperatures of 225° C. Changing the carbon content of experimentally rolled sheet did not affect the ductility of the sheet. Slight changes in the rolling procedure and cladding for rolling did not affect the sheet ductility. Experimentally rolled sheet generally had better transition temperatures than commercial sheet. However, commercial sheet had a more abrupt transition as determined by the temperature range between 0- and 90-deg bending. Not enough information was available about the commercial rolling procedures to allow an explanation of this difference in behavior.

Bend tests were made on weldments in carbon-deoxidized sheet to determine the effects of weld surface, carbon content, specimen orientation, weldment thickness, titanium additions and fabrication variables (in the case of experimental sheet). Results of these tests are summarized in Table 6. The greatest improvement in weld ductility was obtained by grinding the weld surface. Lower carbon contents in commercial sheet also gave better weld ductility at low temperatures. In experimental sheet, however, there was no effect on weld ductility from varying the carbon content. Tests made on welds in commercial sheet indicated a slight improvement in weld ductility for specimens bent in a direction longitudinal to the rolling direction. The other variables studied had little effect on weld ductility. Analysis of all the factors studied is presented in the following paragraphs.

Originally, tests were made using bend specimens cut from as-welded strips. Metallographic examinations of these strips showed slight surface irregularities, as shown in Fig. 11. Tests were made in which the weld surface was ground with a small hand grinder. A marked lowering of the transition temperature occurred as shown by comparing the data for C16A and B, C14A and B, and C17A1 and A2. Irregularities on the as-welded surface, while slight, still might act as notches and raise the temperature at which plastic flow initiates in molybdenum weldments. The welds were ground with a fine abrasive wheel in a direction such that any scratches would have the least effect as notches.

Previous work at Battelle[1] indicated that lowering the residual carbon content of molybdenum castings increased the ductility at low temperatures. The first test made on weldments in commercial sheet tended to confirm this. Welds in 0.020% carbon sheet (C16A) had better ductility than

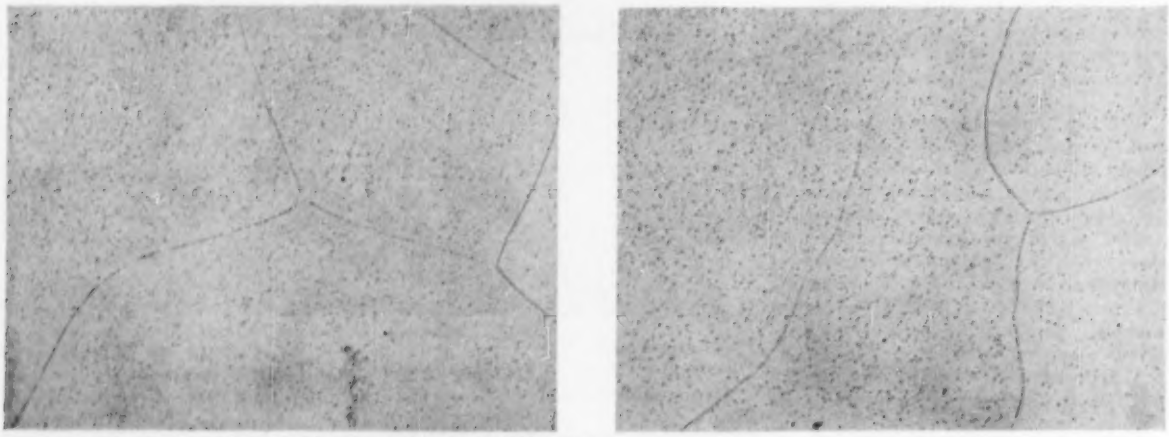

Murakami's etch. X 250. (*Left*) 0.015% carbon and (*right*) 0.042% carbon.

Fig. 12 Carbon-deoxidized molybdenum weld metal. (Reduced by $^1/_2$ upon reproduction)

Murakami's etch. 0.036% carbon. X 250.

Fig. 13 As-cast carbon-deoxidized molybdenum. (Reduced by $^1/_2$ upon reproduction)

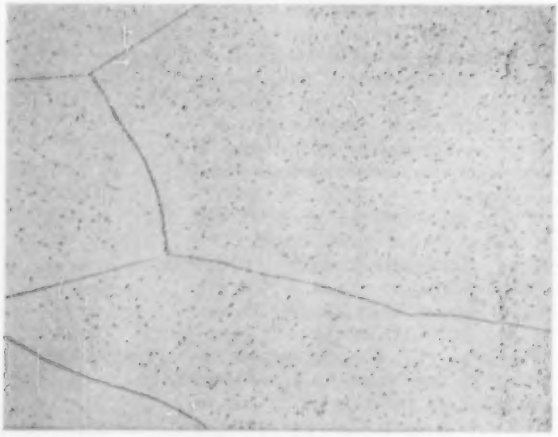

Murakami's etch. 0.029% carbon. X 250.

Fig. 14 Weld metal in carbon-deoxidized 0.5% titanium-molybdenum alloy. (Reduced by $^1/_2$ upon reproduction)

welds in 0.046% carbon sheet (C12B). Further testing of experimentally rolled sheet in which the carbon content varied from 0.015 (C18A) to 0.042% (C17B) failed to indicate any effect on ductility.

The photomicrographs in Fig. 12 show the weld-metal structure of welds containing varying amounts of carbon. In all cases, a carbide precipitate is shown in the grains and grain boundaries. Increasing the carbon content appears to lower the number of carbide particles and increase the size of individual particles. However, because of the rapid quench rate after welding, the structure does not reach the typical structure formed in slow-cooled molybdenum castings (Fig. 13) containing the same carbon content. This would explain the apparent discrepancy between transition temperature data in the welding studies and those obtained in previous studies of the effect of carbon in arc-cast ingots.

The tendency for commercial molybdenum sheet to exhibit better ductility in the direction of rolling was retained in weldments. The ductility of welds made in commercial sheet containing 0.046% carbon was definitely better in the longitudinal weld specimen (C12A). The effects of specimen orientation on weld ductility in experimental sheet were not determined.

Weld ductility at low temperatures appeared to be lowered slightly by increasing the weldment thickness. A direct comparison of this effect could not be made, however.

The weld ductility of the commercial titanium-molybdenum alloy (C19) was slightly lower than that of welds in comparable unalloyed molybdenum sheet (C3). The carbide phase in this weld metal was precipitated in acicular form, as shown in Fig. 14. This was in contrast to the spheroidal carbide phase found in the weld metal of unalloyed carbon-deoxidized molybdenum. Acicular precipitates generally give lower ductility in metals than spheroidal precipitates.

The following variables did not affect the ductility of weldments in carbon-deoxidized sheet:

1. Changing the rolling procedure slightly for the two 0.015% carbon sheet (C18A and C18B).
2. Rolling the 0.042% carbon sheet in a cladding (C17B) as compared with rolling in air (C17A).

Summary and Conclusions

Many variations in composition, purity and fabrication procedures of arc-cast molybdenum were studied in this program. Table 7 lists the important information on the materials studied. Definite conclusions on the effects of specific variations were limited to materials which were essentially the same except for the variation being studied. The values given for bend ductility generally should be viewed merely as comparative figures, since it is doubtful if any one material was ideal in all respects. It is significant, however, that almost all materials showed low-temperature ductility in sheet and weldment form.

The experimental titanium-neutralized alloys were not much better than commercial carbon-deoxidized molybdenum in the thicknesses studied. Future welding work should be limited to the commercial material until it is definitely established that a desired end product cannot be fabricated from this material. Carbon-deoxidized molybdenum may not have adequate weldability for the welding of thick plate where slow cooling rates may allow the carbide to precipitate in a more harmful form, or for weldments which must be made outside of dry-box facilities. Titanium-neutralized molybdenum may be required for these applications.

In general, it was found that grinding of the weld surface gave the most significant increase in low-temperature ductility. It was also shown that factors which did not affect the bend ductility of sheet had a significant

Table 7—Summary of Data and Results for Molybdenum Sheet and Weldments

		Bend-test transition temperature, ° C		
			Weldment	
*Identification**	*Cladding material*	*Sheet*	*As-welded*	*Surface removed*
	Titanium-neutralized molybdenum			
Group A				
B2	Stainless steel	< −75	10	−55
B4	None	−50	80	−25
B5†	None	<0	60	< −25
B7‡	None	< −75		−50
B9	Stainless steel	< −75		−10
Group B				
B3	Stainless steel	−60	25	−60
B6	None	−65		−25
Group C				
B8A	None	< −75		< −60
B8B	Mild steel	< −75		−10
Group D				
B10A	None	−35		5
B10B	Stainless steel	< −75		−10
B10C	None	< −75		−5
Group E				
B11A	None	−60		60
B11B	Stainless steel	< −75		−35
B11C	None	< −75		−20
	Carbon-deoxidized molybdenum			
Group F				
C12	None	−35	25	
C16	None		−10	< −40
C3§	None	−40		−25
C19§	None	−70		−10
Group G				
C14A	Stainless steel	−90	−25	
C14B	Stainless steel	< −75		−40
Group H				
C17A	None	−60	50	−50
C17B	Stainless steel	−70		−60
C18A	Stainless steel	−75		−60
C18B	Stainless steel	−75		−60

* *Group A.* 0.7 w/o titanium, high-purity molybdenum, ingots remelted. Rolled starting at 2000° F with temperature gradually reduced to 1350° F. *Group B.* Same as Group A except ingots not remelted. *Group C.* 0.7 w/o titanium, low-purity molybdenum ingots remelted. Rolled at 2300° F. *Group D.* 0.5 w/o titanium, low-purity molybdenum, ingots remelted. B10A rolled at 2300° F to a 1/4 in. thickness, recrystallized at 2600° F, and finish rolled at 2000° F. B10B rolled at 2300° F to 1/4 in. and finish rolled at 2000° F. B10C rolled at 2000° F. *Group E.* Same as Ground D except 1.0 w/o titanium. *Group F.* Commercial sheet. (C12 — 0.046 w/o carbon; C16 — 0.020 w/o carbon; C3 — 0.042 w/o carbon; C19 — 0.029 w/o carbon, 0.5 w/o titanium). *Group G.* Experimental extrusion and sheet; 0.036 w/o carbon, rolled with Group A. *Group H.* Experimental sheet from commercial extrusion (C17 — 0.042 w/o carbon; C18 — 0.015 w/o carbon). Rolled starting at 2300° F with temperature gradually reduced to 1800° F.

† Extrusion billet not scalped before rolling.

‡ Contained 0.01 w/o carbon addition, rolled at 2300° F.

§ This material 1/8 in. thick, all other material 1/16 in. thick.

effect on the bend ductility of weldments.

Welds made in titanium-neutralized alloys containing 0.7% titanium had much better ductility than either 0.5 or 1.0% titanium alloy weldments. Addition of 0.01% carbon to a 0.7% titanium alloy had little effect on weld ductility. A change from double to single melting for the ingots increased the amount of porosity in arc welds.

The study of carbon-deoxidized molybdenum weldments brought out several important findings. Lowering the carbon content from 0.046 to 0.020% in commercial material improved the weld ductility. A similar change from 0.042 to 0.015% carbon in experimental material did not affect the weld ductility. The addition of 0.5% titanium to carbon-deoxidized molybdenum had little effect on weld ductility. In commercial sheet, bend tests show certain directional properties, i.e., the sheet is more ductile in a direction parallel to the rolling direction. The directional property was retained in weldments in commercial sheet. Cladding of the sheet material during rolling did not improve the weld ductility. Increasing the weldment thickness to $^1/_8$ in. did not affect weld ductility.

Acknowledgments

The authors wish to acknowledge the work done by G. W. Rengstorff and L. E. Olds, of Battelle Memorial Institute, for the fabrication of the titanium-neutralized alloys, and H. Inouye, of Oak Ridge National Laboratory, for producing the experimental extrusions.

References

1. Case, S. L., "A Metallurgical Study of Molybdenum," NP-5420 (Oct. 15, 1954).
2. Jacobson, M. I., Martin, D. C., and Voldrich, C. B., "Production of Sound Ductile Joints in Molybdenum," Progress Rept. ND-4718 (July 17, 1953).
3. Rengstorff, G. W. P., and Fischer, R. B., "Cast Molybdenum of High Purity." *Jnl. Metals* **4** (2), 157 (1952).
4. Deuble, N. L., "Large Molybdenum Ingots by Arc Casting," *Metal Prog.*, **67** (4), 87–90 (1955).
5. Deuble, N. L., "Arc Cast Molybdenum—Ingot to Bar, Sheet or Wire," *Ibid.*, **67** (5), 89–92 (1955).
6. Kearns, W. H., Eichen, E., Martin, D. C., and Voldrich, C. B., "The Effect of Purification on Welds in Molybdenum." The Welding Journal, **32** (11), 1082–1088 (1953).

A WELD CRACKING SUSCEPTIBILITY TEST FOR SHEET MATERIALS

DISCUSSION BY E. H. KINELSKI AND G. R. PEASE

The author is to be commended for his sincere attempt to develop a weld cracking susceptibility test for sheet materials. Whereas a number of more or less satisfactory test specimens and procedures are available to welding engineers for the evaluation of weld cracking tendencies in heavy section welding, a need has existed for a long time for a suitable test for sheet alloys.

However, it is questionable whether or not the test as described by Mr. Boudreau has been developed to the point where confidence can be gained from his results for evaluating the relative ease of welding substantially different alloy compositions. The test, for instance, characterizes Inconel with poor weldability in sheet form. This seems to defy the rather widespread impression throughout the welding industry that Inconel sheet can be welded without undue difficulty. As an example, literally miles of Inconel sheathed, Calrod-type heater elements

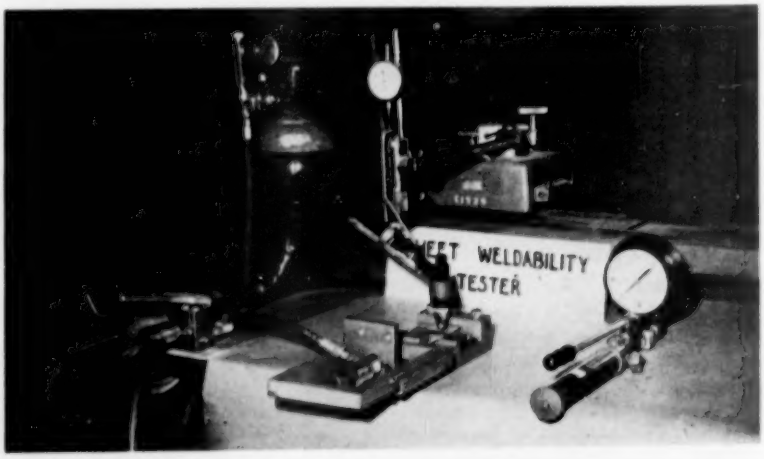

Fig. 1 Sheet weldability tester

E. H. Kinelski and **G. R. Pease** are associated with the Research Laboratory of the International Nickel Co., Bayonne, N. J.

Paper by J. S. Boudreau was published in the April 1956 issue of The Welding Journal, Research Suppl., **35**, (4) 164-s to 168-s.

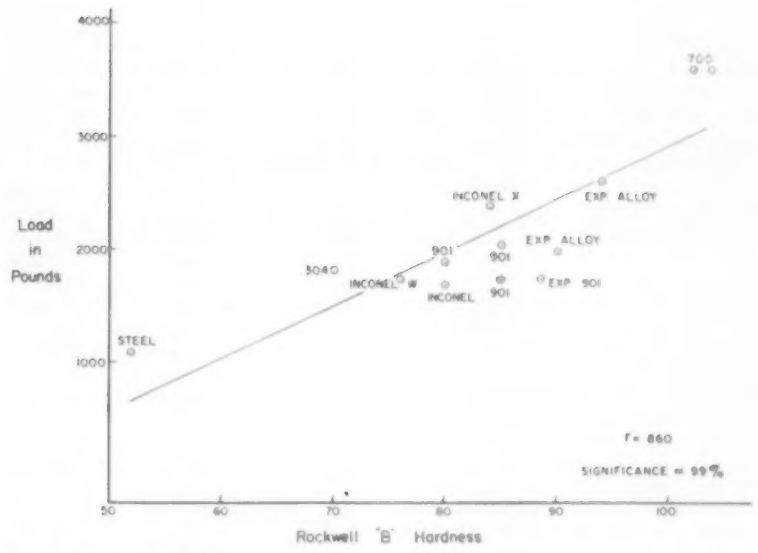

Fig. 2 Sheet weldability test. Load vs. hardness

have been welded with a minimum of difficulty. Although production welding experience with Incoloy 901 has been rather limited so far, nothing in our testing has suggested that its welding response can be expected to be as poor as that indicated by the results of Mr. Boudreau's tests.

It was our privilege to witness this test about a year ago. Its potential usefulness was thought of so highly that, with the approval of its proponents, we undertook to adapt it to our own needs. With only three modifications, which are believed to be of minor importance, we have been making similar tests. The modified testing device is shown in Fig. 1. The modifications consist of (1) using a hydraulic loading system in place of the mechanical system, (2) loading the specimen by means of a steel pin inserted through a hole in the specimen instead of serrated grips, and (3) preparing the test weld without a crater-eliminating device. Crater cracks were ignored when they occurred since they could be shown to be independent of the applied load.

Using this modified, but similar, testing procedure, "weldability" ratings were determined for a series of alloys ranging in composition from ordinary mild steel to a high-temperature alloy designated Inconel 700. It was disappointing, however, to find that the ratings failed to correlate at all with our concept of the comparative weldability of these alloys. For example, mild steel had a very low index, which suggested that it would be almost impossible to weld mild steel without cracking it. Inconel 700 alloy, a complex age-hardenable nickel-base alloy, had an index over three times as high as that of mild steel. It would be difficult to believe that steel is three times more susceptible than Inconel 700 to weld hot cracking.

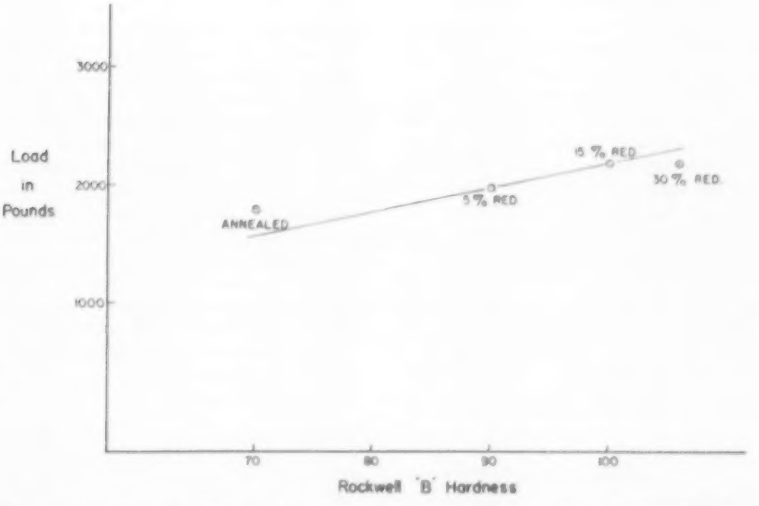

Fig. 3 Sheet weldability test for Type 304 stainless steel. Load vs. hardness

In attempting to interpret the data from this "weldability" test, it was apparent that some other property in addition to weld hot cracking was being measured. It was reasoned that the resistance to deformation under load, or possibly resistance to deformation under load at high temperature could be the factor contributing to the high indices. A graph of weldability load values versus Rockwell "B" hardness values appears to confirm this reasoning, as shown in Fig. 2. A statistical correlation of the data in Fig. 2 resulted in a relationship which had a level of significance of 99% with a correlation coefficient of 0.860. This surprisingly highly significant correlation indicated that the test was influenced markedly by the hardness of the test specimen.

A further demonstration of the influence of the hardness upon the test results was made in a series of "weldability" tests on specimens of type 304 stainless steel, cold rolled to various hardness levels. As shown in Fig. 3, the test index load increases with increasing hardness of the alloy sheet. A poll of experienced welding engineers would, it is believed, show that the reverse is true; namely, that the best welding response would be expected with material in the annealed condition.

The test has so much potential merit that it appears desirable to modify it to the point where it can be depended upon to do the things expected of it, that is, to rate unknown alloys without expensive shop experience. Almost certainly, the influential hardness component will have to be factored out of the index. A redesign of the test specimen has already shown some promise of being able to do this, in our experience.

The variable indices indicated by Mr. Boudreau for certain of the "fickle" alloys—those which vary considerably in welding response in shop practice from heat to heat—suggest that the test as now constituted may be extremely valuable in sorting out good heats from poor ones of a given alloy heat treated to a given hardness. It is difficult to believe, however, that it is possible to predict the welding response of a new, untried sheet alloy without further modification of the test.

AUTHOR'S REPLY

The author wishes to thank Mr. Kinelski, Mr. Pease and the International Nickel Co. for the interest shown in this test, as reported in the April 1956 issue of THE WELDING JOURNAL, and for their prepared discussion presented at the National Spring Meeting. It is gratifying to learn that such interest has existed and it is hoped that further investigations along these lines by other laboratories might suggest improvements in the technique of the reported test.

The test as devised in the Thomson Laboratory is an attempt to supply information, heretofore unavailable, which might lead to a better understanding and solution of welding and metallurgical problems. It would be presumptuous of the author to imply that the test as reported is the last word in the quantitative measurement of welding behavior. Considerably more development may be required before this test or similar tests are universally accepted.

With regard to the discussion presented, there are several comments which the author feels are in order.

The hydraulic-type loading system was rejected on the advice of several testing machine manufacturers because of the inability of such a system to maintain a steady load, automatically, under the testing conditions. However, an hydraulic system should be satisfactory, provided that good manual control of the load level can be effected.

Use of the steel pin in place of the serrated grips should be satisfactory, provided that the holes in the specimen are lined up in such a manner that no moments are introduced into the specimen in the weld area. Of course, this is an extra step in test preparation.

It can be argued that crater cracking is independent of the applied load; nevertheless, the crater eliminating device was employed to compensate for the variations in crater severity of the alloys tested and also because most actual welding operations of this nature with these alloys require the use of such a device.

The author is in complete agreement with the statement that the greatest value of this test at the present time, in its present form, is in sorting out good and bad heats of a given alloy under specific conditions. In attempting to standardize on a technique for all high-temperature alloys tested, certain specified conditions such as arc length, speed, gas coverage, backing, penetration, etc., had to be held constant. It may be necessary to adjust these and other factors for each alloy or family of alloys in order to arrive at the best set of conditions for a more acceptable comparison between alloys.

Concerning the suggested inability of the reported test to evaluate different alloy compositions or to predict the welding response of a new untried sheet alloy, it is necessary to consider the following:

As stated in the paper, along with the development of the technique, a program of material evaluation was simultaneously undertaken. Many of the results were obtained from tests on single heats and with slight variations in technique. However, a certain reliability of the test was indicated. Several heats of Type 321 and of A-286 alloys were evaluated. The former resulted in consistently high index values, while the latter resulted in consistently low values. Many other alloys were evaluated using essentially the same technique; most were rated on the basis of single heats. Since those alloys on which actual welding experience is available seemed to fall within a range compatible with their apparent "weldability," it was felt that the test had possibilities.

In the case of Inconel, the results on a single heat showed an index of 1000, which falls on the borderline of the arbitrarily-designated "poor-fair" zones. Inconel, by past experience, has been successfully welded consistently, but it cannot be considered as weldable as Type 321 alloy, and it certainly is a better welding material than A-286 alloy. The rating of Inconel somewhere in between Type 321 and A-286 did not, therefore, seem unreasonable. Its actual index level, however, would depend on the results of tests on several heats. It would appear that either this particular heat of Inconel had unique welding characteristics, or that the technique employed at the time was not ideal.

As for the results on mild steel, the test, as stated, was designed for the evaluation of high temperature alloys, and the information was to be applied to the fabrication of components for aircraft gas turbines. Mild steel can hardly be classed as a "super" alloy. This is not a fair comparison.

Tests on Inconel 700, which were not included in the paper, indicate a level of 1400. This is considerably lower than the value of 3600 appearing in the written discussion. This seems to suggest that the penetration in the latter case may have been low, as the specimens do not indicate failure at a stress in excess of 30,000 psi, which seems unlikely under ideal test conditions. The alloy, however, should be weldable.

On the basis of the previous statements, the data on mild steel and on Inconel 700 should be deleted from Fig. 2 of the discussion. The remaining data now show a correlation coefficient of 0.320 which does not justify the use of any regression. The conclusions on the basis of this information do not suggest the test to be influenced to any great degree by specimen hardness.

When attempting to correlate welding behavior with hardness, consideration must also be given to the mechanism of hardening. The author found that the age-hardenable alloys, Inconel X and A-286, exhibit lower index values in the aged condition than in the annealed condition. This is not in agreement with the conclusions drawn in the discussion. If hardness were the only criterion, the aged alloys should have higher index values. Results in the Thomson Laboratory suggest that these alloys in the aged condition should not weld as readily as in the annealed condition. Actual experience with this type of alloy seems to substantiate this.

The results on the effect of cold working on the index of Type 304 alloy, as shown in the discussion, indicate a rise in value with an increase in hardness. Industrial experience with this alloy and the range of index levels found indicate that this is a readily weldable material in almost any condition. A series of similar tests on alloys of a lower "weldability" rating might reveal some interesting information.

The test in its present form subjects the materials to temperatures in excess of their annealing temperatures within the weld zone and tends to cancel out all previous thermal history in this zone. The only effective portions of the specimen not reaching peak temperatures are the two areas in the base metal at the ends of the weld. The role of these areas must be explored further. Investigations to determine the effect of welding heat on the structure and properties of these areas in several alloys is planned. Further specimen modifications designed to eliminate these areas have also been arranged.

THERMAL STABILITY OF COLD BUTT WELDS IN COPPER AND ALUMINUM

Test program surveys the properties of cold welds and indicates the conditions under which these welds have the most useful application

BY W. H. BRUCKNER AND J. H. SAYLES

Introduction

Cold welding of nonferrous metals is not new, yet it is a newcomer to the welding field since one of the first references to a lap welding operation involving cold welding appeared in THE WELDING JOURNAL for February 1949. This JOURNAL paper by A. B. Sowter describes and illustrates equipment for cold welding and sections of aluminum and copper so welded. Sowter's paper relates the development of the cold welding process at the General Electric Co., Ltd., of England while another paper by W. Dubilier in THE WELDING JOURNAL for December 1950 describes further development and applications in the United States, but again for lapped welds.

Another paper which was of considerable interest to the investigation of cold welding was one by John M. Parks and entitled "Recrystallization Welding" in THE WELDING JOURNAL for May 1953. This paper describes the welding of nonferrous metals under various conditions of temperature and pressure. While Parks used fairly elevated temperatures for welding, the relationship of deformation levels and recrystallization to the success of the welding operation has an important bearing on the cold welding process. Ultimately, the research program in cold welding has for its objective a description of the instantaneous processes at the welding interface during welding. When this can be done there will be available a better understanding of the role of interface recrystallization and localized temperature rise in the success of the cold welding process.

The reason for choosing to study the thermal stability of cold butt welds is actually twofold; first, to survey the properties of cold welds as an initial step in discovering the fundamental mechanics of bonding and, secondly, to provide information which would indicate the conditions under which cold welds would have most useful application.

The present widespread substitution of aluminum for copper as electrical conducting material in electrical machinery and for cooling coils in refrigerating machines has posed a difficult joining problem. Previously, for copper, soldering provided an easily made and satisfactory joint. With the advent of a successful cold butt-welding process, a section of copper can now be joined to the aluminum conductor or tubing and the soldered joint made at the copper extension.

During the soldering, the cold-welded joint can be subjected to elevated temperatures unless the soldering is done remote from the joint or other means are used. In service also a temperature rise could occur due to malfunction of a service unit. Thus it appeared desirable to establish limits of time and temperature for the occurrence of any appreciable change in the properties of cold butt welds.

Materials

Two 4-in. long sections of $^1/_8$-in. wire were cold butt welded at the plant of the Utica Drop Forge and Tool Corp. to form an 8-in. long specimen. A large number of such cold-welded specimens made by joining aluminum wires, copper wires and aluminum to copper were made by the company on a power machine and were then sent to the campus. The welds were therefore made under ideal conditions representing present practice.

Methods of Investigation

The as-received welds were surveyed for hardness gradients, tensile behavior to fracture and electrical conductivity. The microstructure at the weld interface and neighboring areas was also surveyed.

The hardness tests were made with a Vickers diamond pyramid and hardness values are given in DPH units for a load of 100, 200 or 300 g. The plane of hardness testing was usually the diametral, longitudinal plane through the welded wire which was prepared by mounting the appropriate section of the cold weld in a plastic mounting material, then grinding and polishing down to the desired level. The plane of microexamination was the same as that for hardness testing.

The tensile tests were made in a horizontal machine used for determining tensile properties of wires of small diameter. No stress-strain curves were obtained since the only significance that was desired for the tensile tests was the maximum load and site of failure.

The electrical conductivity across the weld joint in comparison with the conductivity of unwelded wires was the data sought; thus, the conductivity of both types of specimens was measured. Two K2-type potentiometers were used to determine conductivity. One potentiometer was used to measure the current through the test sample. The other potentiometer measured the IR drop across either the weld or a uniform section of the wire.

The above tests were also made on the welded specimens which were heated to elevated temperatures for various periods of time and were then cooled to room temperature before testing.

Data Obtained

The as-welded specimens were examined for external characteristics peculiar to cold butt welding. It was noted that the fin or extruded portion at the site of the weld had been trimmed off

W. H. Bruckner is Research Associate Professor of Metallurgical Engineering, Department of Mining and Metallurgical Engineering, and **J. H. Sayles** is Graduate Student, Metallurgical Engineering, University of Illinois, Urbana, Ill.

Presented at 1956 AWS National Fall Meeting in Cleveland, Ohio, October 8 to 12.

Fig. 1 Macrograph at X 2 of aluminum wires cold butt welded in hand tool

before the specimens were sent to the campus. In order to obtain some concept of the amount of material extruded into the fin during welding, a cold weld was made by means of a hand tool designed for this purpose.

Figure 1 is a macrograph of the $^1/_8$-in. aluminum wires cold butt welded in the hand tool. This illustration shows clearly the extent of the extrusion fin at the site of the weld; also, it shows the slight longitudinal fin produced by the gripping dies which hold both sides of the wire material during the push-up for welding.

of the aluminum weld, it appears to be the principal reason (together with low ductility) for the failure which occurs at the weld interface in tension. The existence of some slight interface porosity in the cold welds of copper is suspected from the appearance of the microstructures examined. However, no microradiographic confirmation has been obtained to date. More detailed data on microstructure will be given later in the paper in conjunction with hardness and tensile data for welded specimens heated to elevated temperature.

Hardness Data

The hardness tests were made across the welds on the diametral plane and extended to at least $1^1/_2$ in. on both sides of the weld interface. The gripping dies extended along $1^1/_2$ in. on both sides of the weld; thus, any cold work due to gripping and at the interface would be represented in the hardness surveys. Figure 4 gives a general representation of the hardness contours obtained for the as-welded condition of the three types of weld; Al to Al, Cu to Cu and Al to Cu. The hardness surveys were repeated for the specimens which had been heated to elevated temperatures; thus, the hardness contours as a result of heating were available for study.

Figure 4 indicates that the maximum hardness of the as-cold-welded specimen was found at the interface. However, for the Al and Cu welds, as the heat-treatment temperature was increased the shape of the hardness con-

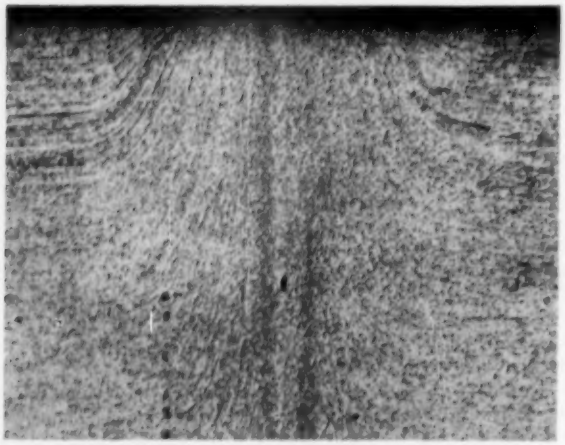

Fig. 2 Microstructure at X 50 of as-received, cold butt weld in aluminum wires

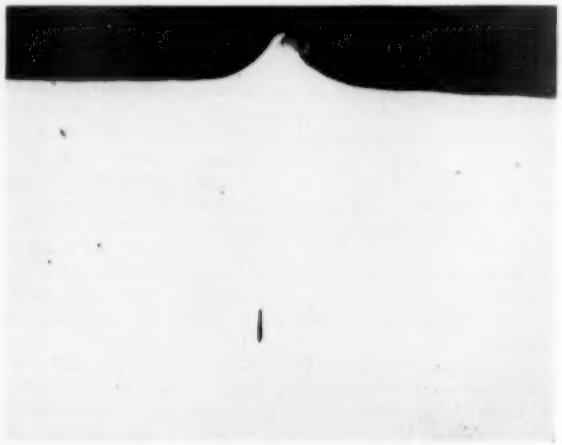

Fig. 3 Microradiograph at X 50 of interface porosity in aluminum cold weld

Figure 2 shows the microstructure of the as-received aluminum weld at $\times$ 50 magnification on a diametral plane. The out-bending of the fiber structure of the wire at the site of the weld is in evidence. Another microstructure characteristic of the aluminum welds is the region of apparent porosity at the weld interface shown in Fig. 2. Such apparent interface porosity was manifested quite generally in metallographic examination. Therefore, in order to distinguish between actual porosity and possible effects of polishing and etching, a microradiographic examination was made of thin longitudinal sections at the site of the weld.

Figure 3 shows the results of microradiography and leaves no doubt of the existence of lens-shaped porous areas at the weld interface of cold welds in aluminum. Although this porosity had little or no effect on the tensile strength

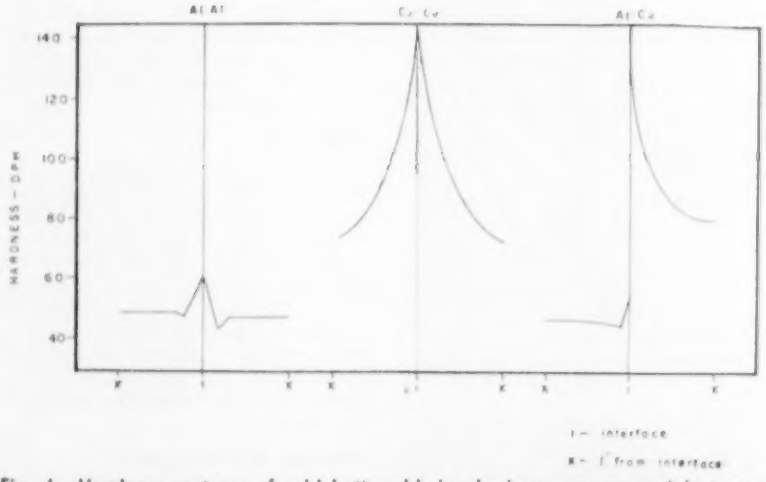

Fig. 4 Hardness contours of cold butt welds in aluminum, copper and between aluminum and copper

tours changed, i.e., instead of peak hardness occurring at the interface, two hardness peaks appeared at either side of the interface due to more rapid softening at the interface occasioned by recrystallization. This was not entirely the case for the Cu-Al welds for which the interface tends to retain a high hardness and the Cu side of the interface even increases slightly in hardness with increasing time at some temperatures.

The relationship of interface hardness to temperature of heating is given in the curves of Figs. 5 and 6.

When the tensile properties of the cold-welded materials was first investigated, the tensile grips were placed 5 in. apart with the weld interface equidistant at $2^1/_2$ in. from each pair of grips. The failures in the tensile tests with the 5-in. grip distance always occurred in the region between one of the pairs of grips and the cold-worked region produced by the gripping dies for cold welding. The initial wire material thus has a lower strength than the weld or the cold-worked region produced by the gripping dies.

The tensile grip distance required to determine weld strength was therefore of the order of 3 in. or less, since the cold work of the gripping dies for cold welding extended over this distance. Under these conditions, the as-received Al-Al welds fractured at the interface, but the as-received Cu-Cu welds could not be made to fracture at the weld, even when shorter and shorter grip distance was used.

Tensile Tests

The general trend of the tensile data is to follow the hardness versus temperature curves quite closely only for the aluminum welds. Another general trend for as-welded joints was for failure to occur at the weld interface in Al-Al welds, away from the interface in Cu-Cu welds and in the Al away from the interface in Al-Cu welds. As the heating temperature is increased, the Al-Al welds tend to fail away from the interface whereas the Cu-Cu welds have a higher frequency of weld interface failure and the Al-Cu failures still occur in the Al away from the interface.

Figures 7 and 8 show the sensitivity of the strength of Al welds to heating temperature and the insensitivity of the Cu welds. The Al and Al-Cu welds are sensitive to heating temperature irrespective of whether or not the failure occurs at the interface, thus indicating that all the cold-worked volume of Al included within the gripping dies and at the weld interface participates in the tensile response to elevated temperature heating after welding.

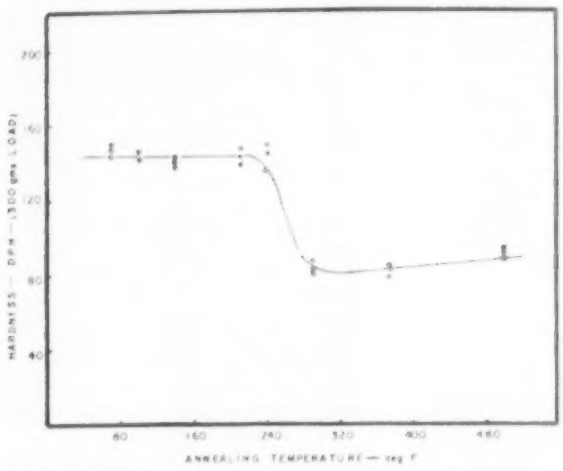

Fig. 5 Interface hardness (DPH) versus annealing temperature for cold welds in copper heated for 30 min

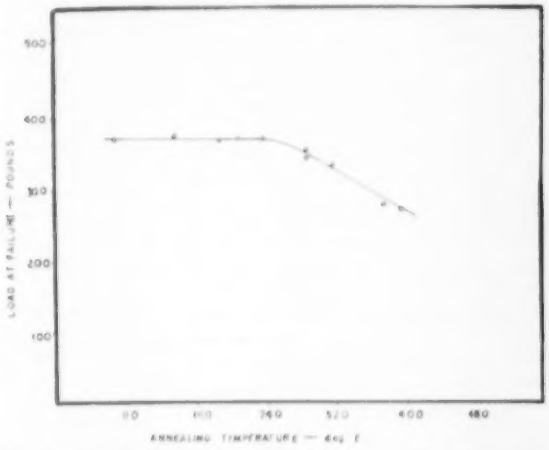

Fig. 7 Maximum tensile load versus annealing temperature for cold welds in aluminum (weld failures) heated for 30 min

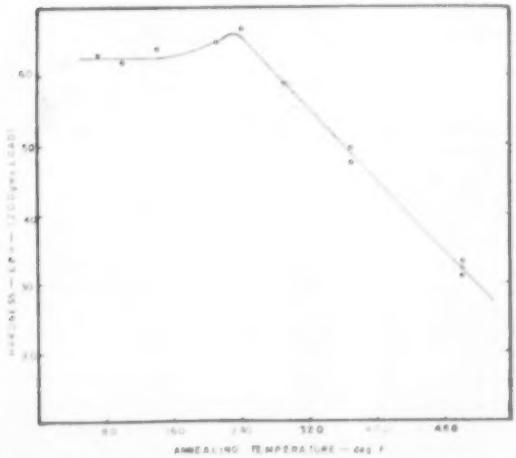

Fig. 6 Interface hardness (DPH) versus annealing temperature for cold welds in aluminum heated for 30 min

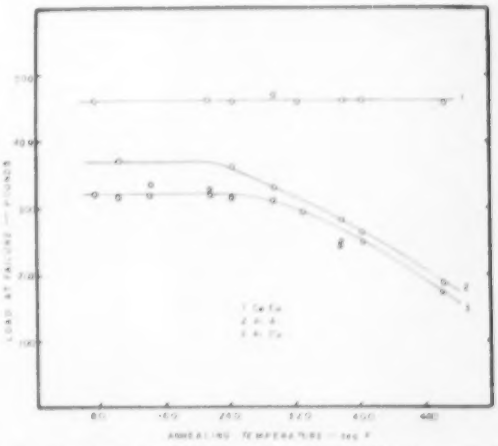

Fig. 8 Maximum tensile load versus annealing temperature for cold welds in aluminum, in copper and between aluminum and copper heated 30 min (only noninterface failures are included)

Microstructural Studies

In an effort to interrelate interface porosity in Al-Al welds with interface tensile failure, several specimens were loaded in tension to incipient failure. The specimens were then polished in the diametral plane and examined under the microscope. The general appearance of the interface is shown in Fig. 9, where it is seen that voids of rectangular shape have been opened up by the tensile load. As the welded specimens are heated to increasingly higher temperature before tensile testing, these voids become more circular and apparently less effective in causing weld-interface failure. As the heating temperature is raised, the highly cold-worked region at the interface also softens and becomes more ductile, thus reducing the stress-concentrating effect of the lens-shaped porous areas.

In general, it was difficult to detect any fine detail in the microstructure of the aluminum alloy used for cold welding. The reason for the difficulty was an inability to develop grain boundary areas by even the most refined etching methods. Consequently the evidence of recrystallization had to be supported entirely by hardness data.

For the cold welds in copper, the microstructure was easily developed and examined, thus evidence of recrystallization and coalescence could be found. It was apparent that the interface material was the first to recrystallize but retained a fine grain size while the material on either side next to the interface was next to recrystallize, with higher temperature or longer time, but developed maximum grain size.

At the highest power of the optical microscope, it was possible to discover lens-shaped areas at the interface of Cu-Cu welds which may have been formed by recrystallization and growth during the cold welding. The reason for assuming such causality was that the lens of material was positioned just at the interface while the surrounding material was extruded around both sides of the lens. Such an area is illustrated in Fig. 10. At elevated temperatures, such areas tend to grow mainly in a direction normal to the axis of the welded wire, whereas interface areas free from the lens shapes grow randomly and with small grain size.

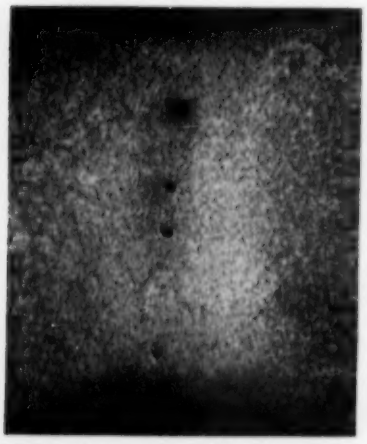

Fig. 9 Appearance of interface area at X 300 in cold-welded aluminum partially fractured in tensile test. (Reduced by 1/2 upon reproduction)

Fig. 10 Photomicrograph at X 700 of lens-shaped area at interface of cold weld in copper. (Reduced by 1/2 upon reproduction)

For the Cu-Al cold welds, no evidence of intermetallic compound formation could be found for any heating temperature after welding up to 500° F. Since the latter was the highest temperature employed, it is possible that higher temperatures might produce a brittle phase at the interface and change the mode of fracture which was consistently in the Al away from the interface.

Electrical Conductivity Studies

For the Al-Al welds a complete series of tests were made as shown in Fig. 11. The sudden decrease in resistance across the weld for an annealing temperature of 290° F and above indicates interface recrystallization. The other data on hardness and tensile strength show an inflection at the same temperature. The unwelded wire exhibited only a slight decrease in resistance after heating up to 500° F from about 275 microhms to about 271. The indications are that for the unwelded wire heating merely removed a small amount of strain or caused the loss of some grain boundary resistance due to grain growth.

For the Cu-Cu welds, less complete conductivity data were obtained since only the resistance across the weld of the as-received material and after heating to 500° F was measured. The decrease in resistance from 156.9 to 116.3 microhms after heat treatment is a considerable change however. The indications from the large decrease in resistance are that the large incidence of interface fracture in tensile testing of Cu-Cu welds as the annealing temperature is increased is not due to the formation of copper oxide at the interface. The oriented growth at the interface of the lens shaped areas and extreme softening may be the principal cause of interface fracture and of loss of electrical resistance with higher annealing temperatures. Porosity may also be a factor in interface fracture.

The determination of conductivity of the Cu-Al welds has not progressed to a point of sufficient reproducibility of data thus requiring more extended effort for the measurements.

Discussion of the Data

In surveying the tensile data, it must be noted that the weakest part of the weld, the un-cold-worked base metal, was purposely excluded from the tests in order to assay the relative strength of the cold-worked area at the interface and that included in the gripping dies for cold welding. In the light of this procedure for tensile testing, it is seen that the cold butt-welding process provides welds with high efficiencies such that even with a decrease in strength occasioned by annealing at higher temperatures the strength of the weld is merely brought down to that of the unwelded wire. It would seem therefore that we should be less concerned about the thermal stability of the cold butt welds than with a controlled, deliberate heat treatment after welding in order to obtain higher ductility in the cold-worked regions.

The conductivity tests also indicate the benefits in increased conductivity which could be derived from heating the welds subsequent to welding. Since the weld has greater strength than is needed to behave as a unit with the unwelded wire, a relatively low-temperature heat treatment subsequent to welding could provide greater conductivity across the weld and improve the ductility without sacrifice of the weld efficiency.

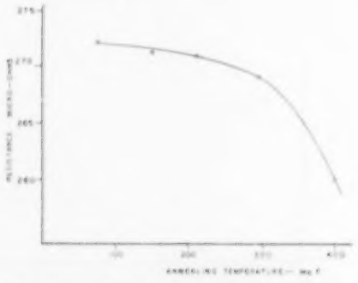

Fig. 11 Electrical resistivity versus annealing temperature for cold welds in aluminum heated for 1 hr

Acknowledgments

The research program on cold butt welds was made possible by a grant of $1000 from the Welding Research Council by direction of the University Research Committee. We wish to thank Professor R.D. Stout, chairman, W. Spraragen, secretary, and the other members of this committee for the financial help given to initiate the project. The supply of cold-welded specimens by the Utica Drop Forge and Tool Corp. is acknowledged herewith, and we wish also to thank W. A. Barnes, vice-president of the Corporation, for his interest in the research and the efforts he made in supplying the cold welds and the loan of a cold welding tool.

A number of students in Metallurgical Engineering were employed in assisting the authors in obtaining the data presented in the paper. Special acknowledgment is made of the services of Dallas Pasley for the excellent metallographic work and hardness tests. Charles A. Robertson, graduate student in Metallurgical Engineering, also assisted in the electrical conductivity tests and in the preparation of drawings for illustrations.

THE ARC WELDING OF 2.25% CR–1.0 MO ALLOY STEEL PIPE

DISCUSSION BY R. A. HUSEBY AND M. A. SCHEIL

As the author pointed out in his paper, the chromium-molybdenum steels have become increasingly important in process equipment and in the steam power industry. The original addition of molybdenum to carbon steel was made to increase high temperature strength. Subsequently, chromium additions were made to inhibit graphitization and attack by high temperature hydrogen. Inevitably the welding of these air hardenable chromium-molybdenum steels pose welding problems not previously encountered.

Two years ago, in the A. O. Smith Corp. research laboratory, a long-time investigation of the high-temperature properties and high-temperature stability of welded joints in these steels was initiated. A-301 Grade B (1 Cr, $^1/_2$ Mo) and A-387 Grade D ($2^1/_4$ Cr, 1 Mo) plate material welded with electrodes covering the range 1% chromium, $^1/_2$% molybdenum to 8% chromium, 1% molybdenum were included. After about a year of testing it was observed that, if a difference of chromium level existed between deposit and plate, there was a strong tendency for the carbon to diffuse to the higher chromium alloy. This diffusion takes place to such an extent that a decarburized zone will appear adjacent the higher chromium alloy. This weakened decarburized zone provides a source for stress rupture failure as shown in the illustrations. The rate of diffusion and severity of decarburization are mainly dependent on two conditions:

Table 1—Chemistry of Welds, %, and Plate Tested

	C	*Mn*	*Si*	*P*	*S*	*Cr*	*Mo*
A-301 Plate	0.12	0.43	0.16	0.023	0.043	0.91	0.54
A-387 Plate	0.14	0.57	0.38	0.015	0.019	2.23	1.00
SW-90 Weld	0.05	0.66	0.31	0.016	0.028	1.03	0.50
SW-89 Weld	0.09	0.64	0.32	0.013	0.027	2.08	1.08
SW-151 Weld	0.09/0.14	0.60/0.90	0.30/0.55	0.03 max.	0.03 max.	4.0/6.0	0.40/0.70

1. Difference in chromium level. (The action of other strong carbide formers such as vanadium, tungsten and titanium remain to be assessed.) 1% chromium, $^1/_2$% molybdenum plate will rapidly decarburize at 1000° F

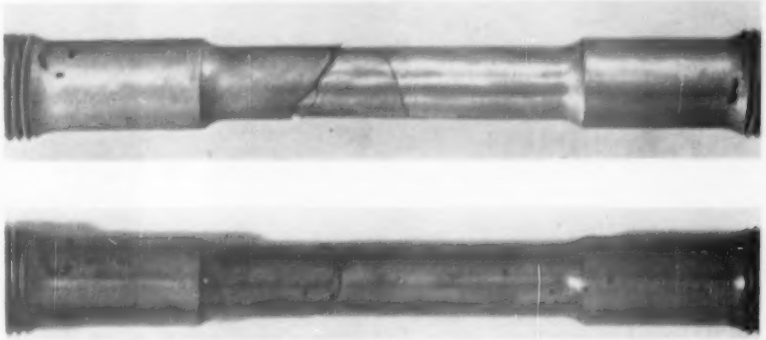

Fig. 1 Standard 0.505-in. diam welded stress-rupture specimen. SW151 (4–6 Cr, $^1/_2$ Mo) weld in 1 Cr, 0.5 Mo stock. Fracture in decarburized zone of stock at weld junction after 1983 hr at 30,000 psi and 1000° F

R. A. Huseby is Metallurgical Engineer and **M. A. Scheil** is Director of Metallurgical Research, A. O. Smith Corp., Milwaukee, Wis.

Paper by Jay Bland was published in The Welding Journal, 35 (4), 181-s to 194-s (1956).

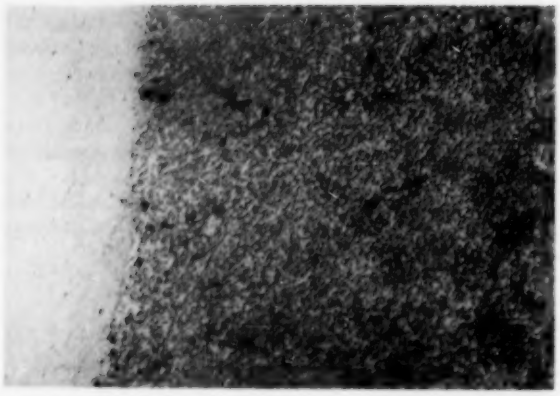

Fig. 2 SW151 (4–6 chrome, 1/2 Mo) weld on left. A301 G.B. 1 chrome, 1/2 Mo stock right. As-welded. X 100. (Reduced by 1/3 upon reproduction)

Hardness, Vhn, 2 1/2 kg load. Stock, 155–168 Vhn. Heat-affected zone, 213–218 Vhn. Weld, 387–390 Vhn

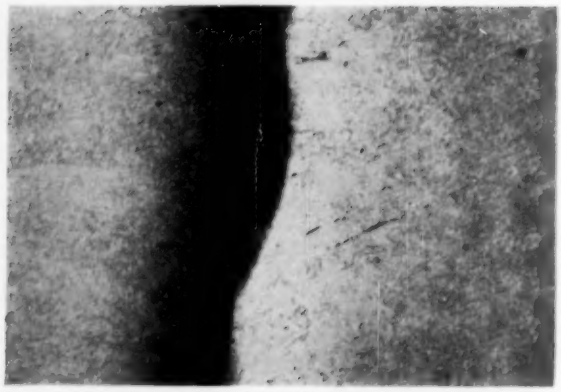

Fig. 3 SW151, left, in A301 stock after stress rupture test 1983 hr at 1000° F. Carbon has diffused from the stock adjacent the weld into the higher chromium weld to form the dark etching high carbon band. Fracture took place in the decarburized weakened stock adjacent the weld. X 100. (Reduced by 1/3 upon reproduction)

Hardness, Vhn, 2 1/2 kg load. Stock, 157–159 Vhn. Decarburized zone, 162–183 Vhn. Weld, 243–262 Vhn

when welded with 8% chromium, 1% molybdenum electrode. When the same plate is welded with 2 1/4% chromium, 1% molybdenum electrode the action is much slower, as can be seen in Fig. 6.

2. Temperature of exposure. The carbon diffusion from low to higher chromium steel occurs at 900° F and above and more rapidly at the higher temperature. At the present time we have no information on temperatures below 900° F.

Figure 1 illustrates the type of fracture obtained in stress rupture tests where carbon diffusion and decarburization resulted in a weakened zone adjacent the weld. Figure 3 shows the carburized zone in the weld and the decarburized zone in the stock adjacent the weld. Figure 5 illustrates incipient intergranular stress rupture cracks in the decarburized zone. Figures 6, 7 and 8 show the same condition where difference in chromium level is less.

Chemistry of the plate and welds is shown in Table 1.

Table 2—Eberbach Microhardness After 2500 Hr at 100° F; 1 Cr, 1/2 Mo Plate with 7–9 Cr, 1 Mo Weld

Ferrite (unaffected stock), Vhr	176
Pearlite (unaffected stock), Vhr	280
HAZ,* not decarburized, Vhr	218
HAZ,* decarburized area, Vhr	176
Weld, carburized zone, Vhr	480
Weld, not carburized, Vhr	264

* Heat-affected zone

Microhardness tests were made on one section of 1 chrome, 1/2 molybdenum plate welded with 7–9 chrome, 1 molybdenum electrode after 2500 hr at 1000° F. The weld was exposed in the as-welded condition.

It can be seen that the decarburized zone reverts to the ferrite hardness and that the carburized zone becomes excessively hard. Some grain growth will occur in the decarburized zone.

Stress relieving at a temperature above the exposure temperature tends to increase the carbon diffusion observed.

It would appear, on the basis of the observed tendency toward carbon diffusion, carburization and decarburization, that for applications involving service above 900° F the chromium content of both plate and deposited metal should fall within the range specified for that particular grade of

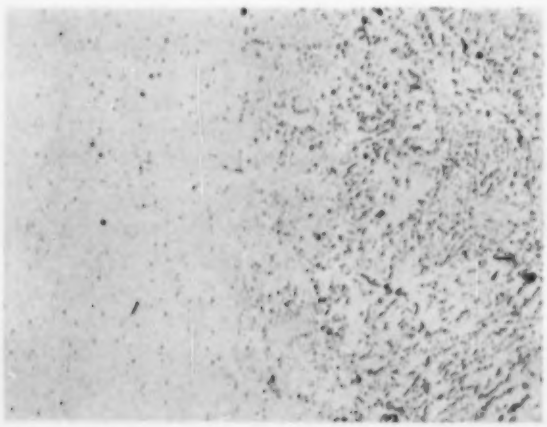

Fig. 4 Weld junction shown in Fig. 2 at higher magnification. Weld on left. X 500. (Reduced by 1/4 upon reproduction)

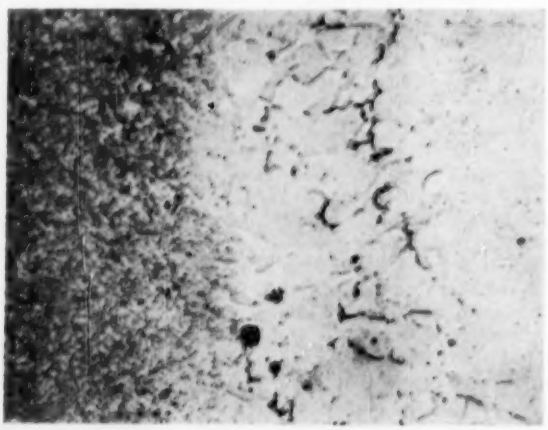

Fig. 5 Weld junction after 1983 hr at 30,000 psi and 1000° F. Stock on right. Incipient intergranular stress rupture cracks in decarburized zone are visible. X 500. (Reduced by 1/4 upon reproduction)

Fig. 6 SW89 ($2^1/_4$ chrome, 1 Mo), left, in A301 Grade B (1 chrome, $^1/_2$ Mo) stock after 3468 hr at 29,000 psi and 1000° F. Carbon diffusion has taken place from the 1 chrome stock to the $2^1/_4$ chrome weld. Fracture took place in the stock with incipient stress rupture cracks in the decarburized zone of the stock (see Fig. 7). X 100. (Reduced by $^1/_3$ upon reproduction)

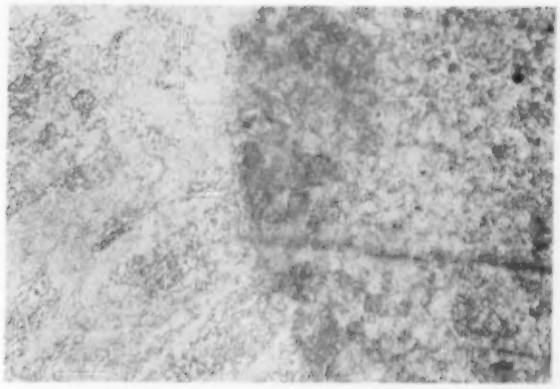

Fig. 8 Carbon diffusion from SW90 weld (*left*) (1 chrome, $^1/_2$ Mo) into $2^1/_4$ chrome, 1 Mo stock on right. Exposed 4100 hr at 1000° F not stressed. Carburized zone of stock is not as apparent because of the low (0.05–0.06%) carbon content of the SW90 weld. Carbon content of plate 0.14%. X 100. (Reduced by $^1/_3$ upon reproduction)

plate or pipe being fabricated. Optimum weld zone properties can probably be achieved by investigation of stress relieving temperatures.

AUTHOR'S REPLY

Messrs. Huseby and Scheil have presented some interesting data in their discussion of this paper. Based on these data, they have concluded "that for applications involving service above 900° F, the chromium content of both plate and deposited metal should fall within the range specified for that particular grade of plate or pipe being fabricated."

Fig. 7 Incipient stress rupture cracks in decarburized zone of A301 stock adjacent to $2^1/_4$ chrome weld after 3468 hr at 1000° F. SW89 weld on left. X 500. (Reduced by $^1/_3$ upon reproduction)

The author is aware of the phenomenon of carbon diffusion resulting in decarburization of the lower chromium-content material and carburization of the higher chromium-content material, for weldments involving dissimilar alloy contents exposed for long times at elevated temperatures. Unpublished work done at the Engineering Research Department, Standard Oil Co. (Ind.), which involved various chromium-molybdenum base metals welded with both ferritic and austenitic electrodes, indicated that the decarburized zone in the base metal produced little, if any, significant effect on the short-time tensile properties or impact properties of the weldment. The paper "Carbon Migration in Welded Joints at Elevated Temperature and Its Effect on Certain Mechanical Properties," by R. J. Christoffel, R. M. Curran and J. E. Corr, General Electric Co., which was presented during the May 1956 meeting of the AMERICAN WELDING SOCIETY, discussed the carbon diffusion phenomenon in detail. These authors concluded that carbon diffusion resulted in little noticeable effect on the mechanical properties of dissimilar metal weldments, at least up to 100 hr of stress rupture testing.

It appears to this author that the interesting data presented by Messrs. Huseby and Scheil do not warrant the conclusion which they indicated. For example, the fracture in Fig. 1 of their discussion does not continue 100% through the decarburized area of the weld. Further, stress rupture after 1983 hr at 30,000 psi and 1000° F is somewhat above the quoted figures for the 1% Cr – 0.5% Mo material, noted in ASTM special technical publication No. 151, "Report on the Elevated-Temperature Properties of Chromium-Molybdenum Steels." In the published ASTM data, a stress rupture life of approximately 2000 hr would be expected at about 24,000 to 25,000 psi load. Similarly, Fig. 6 of the discussion which indicates the condition of the fusion zone after 3468 hr at 29,000 psi and 1000° F, would not indicate an abnormal reduction in stress rupture properties for the combination of alloy materials noted.

Figure 8 of the discussion is most interesting. This represents a condition similar to that proposed in the paper, in which 1 or $1^1/_4$% Cr – $^1/_2$% Mo weld metal and $2^1/_4$% Cr – 1% Mo pipe material was investigated. The discussors note "that the carburized zone of stock is not as apparent because of the low (0.05–0.06%) carbon content of the SW-90 weld. Carbon content of plate 0.14%." The sample represented by Fig. 8 of the discussion was exposed 4100 hr at 1000° F, not stressed; this would be significant only in so far as stress rupture was concerned but not necessarily in so far as carbon diffusion is concerned. It is difficult to see any significant effect of carbon diffusion in this diffusion zone.

It seems to the author that, for the low-carbon-content alloy materials involved, differentials in chromium content of about 1% would have little, if any, significant effect on the stress rupture properties of the weldment. The comments which author made in the paper, relative to the use of dissimilar-alloy-content weld metal versus base metal, was not intended to apply to 9% Cr–1% Mo weld deposits in 1% Cr–$^1/_2$% Mo base metals.

WETTABILITY OF STEEL WITH PURE SILVER AND VARIOUS SILVER-BRAZING ALLOYS

Experimental program with silver alloys containing strong deoxidizers indicates new possibilities for development of self-fluxing, airproof brazing alloys

BY NIKOLAJS BREDZS

ABSTRACT. In the course of the investigation of wettability of low-carbon steel by pure silver and some silver-base brazing alloys under a layer of molten flux, a new phenomenon was observed. It was named "rotation phenomenon." The "rotation phenomenon" demonstrated the influence of oxygen diffusion through layers of molten silver and various silver-base brazing alloys on the wettability of the steel surfaces.

A fundamental study of oxygen diffusion through layers of molten silver with and without deoxidizing additions has been carried out. The mechanism of the formation of iron-oxide layers and nucleation of CO bubbles on the steel-filler metal interface has been investigated.

The experiments performed on silver alloys containing strong deoxidizers open vistas of future research on self-fluxing brazing alloys. They indicate new possibilities for the development of self-fluxing, airproof brazing alloys.

Introduction

One of the principal objectives of the research on the fundamentals of brazing is the improvement of the quality of brazed joints. The first, and most important prerequisite for obtaining sound and voidless brazed joints is perfect wetting of the solid base metal surfaces by the molten filler metal. For this reason the investigation of the wettability of solid metals by liquid metals is one of the most important aspects of the theory of brazing and, accordingly, it was chosen right at the beginning as the first objective of this work. In view of the practical implications of this problem, it was decided to start the wettability studies with the investigation of the wettability of steel by pure silver and some silver-base brazing alloys. In the course of these studies a series of quite interesting new phenomena were observed which appeared to be quite helpful for the fundamental understanding of the mechanism of wettability. The most interesting observations, however, have been made during the studies of the process opposite to wettability, namely, dewetting of the base metal by liquid filler metals. It has been proved that the process of dewetting is determined by a rather intricate series of chemical reactions taking place on the base metal–filler metal interface. Accordingly, a great part of this work is devoted to the investigation of the whole complex of physicochemical processes taking place on the steel-filler metal interface while the molten filler metal layer, spread over the base metal surface, was exposed to the air.

Finally, after the mechanism of the diffusion of oxygen from the air through a layer of molten silver to the steel surface and the mechanism of the oxidation of the steel surface had been clarified sufficiently, it was decided to investigate the possibilities of developing air brazing alloys which would braze steels in air without any fluxes or protective atmospheres. Some experiments indicated that it might be feasible to develop such alloys by adding to the filler metals some strong deoxidizers and other metals which would considerably decrease the rate of oxygen diffusion through layers of the molten filler metals. These experiments are described in the last section of this paper.

Spreading Experiments in Various Atmospheres But with No Flux

The investigation of the wettability of liquid metals on solid metals started with studies of wetting of low-carbon steel surfaces by the following four filler metals: pure silver, pure copper, BAg-8* and BAgMn.* The experimental apparatus used for these studies is illustrated in Fig. 1. For the wettability tests, 3/4 in. diam cylindrical low-carbon steel bars, 3 in. long, were used. The end surfaces of these bars were ground and polished. Each of the steel bars, *B*, with a polished top surface, was placed vertically in the induction coil, *C*. A small filler metal nodule was placed precisely on the center of the polished upper surface of the bar, *B*. The weight of each nodule was exactly 1.5 g. The nodules were prepared by melting 1.5 g of the filler metal wire in a small porcelain crucible under 10% H_2 + 90% N_2 atmosphere.

After placing the filler metal nodule in the center of the top surface of the steel bar, *B*, the apparatus was covered by the glass jar, *J*, and a slow flow of 10% H_2 + 90% N_2 gas was turned on for 10–15 min. This amount of time was sufficient to replace all air with the protective gas; the high-frequency

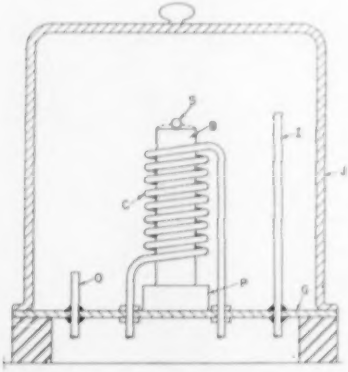

Fig. 1 Experimental apparatus for wettability tests

B, Cylindrical low-carbon steel bar; C, water-cooled induction coil; G, glass plate; I, gas inlet tube; J, glass tar; O, gas outlet tube; P, transite block; S, filler metal nodule (dotted line indicates the shape of the filler metal drop after melting)

Nikolajs Bredzs is Research Metallurgist, Armour Research Foundation of Illinois Institute of Technology, Chicago, Ill.

Presented at the 1955 AWS National Fall Meeting in Philadelphia, Pa., October 17 to 21.

* The brazing filler metals are identified, when applicable, by designations established in the AWS-ASTM specifications for brazing filler metals.

Table 1—Molten Filler Metal Drop Diameters in Air and in 10% H_2 + 90% N_2 Atmosphere on Polished Low-Carbon Steel Surfaces

Filler Metal	*Temperature of the filler metal*	*Drop diameter, in.* — *in air*	*Drop diameter, in.* — *in 10% H_2 + 90% N_2*
Pure silver	Slightly over the mp of the filler metal	0.397	0.496
Pure copper	Slightly over the mp of the filler metal	0.610	0.750
BAg-8	Slightly over the mp of the filler metal	0.550	0.675
BAgMn	Slightly over the mp of the filler metal	0.393	0.672

unit was then activated. Just after the molten filler metal drop was formed on the end surface of the bar, the power was turned off, the bar cooled down to room temperature, and the diameter of the solidified filler metal drop was measured in several directions. From these measurements an average diameter of the area of spread of the drop was determined.

The experimental results of the wettability tests are summarized in Table 1. Some wettability tests were performed in dry helium atmosphere and also in air. In these atmospheres the molten filler metals did not wet the oxidized steel surfaces.

From the theoretical point of view, these tests served only to confirm the well-known fact that if the steel surface is sufficiently reduced by hydrogen, then the molten filler metal will readily wet the steel, and completely sound and voidless base metal-filler metal interfaces will result.

Spreading Experiments Under Molten Flux Layer—"Rotation Phenomenon"

Experimental Procedure

After the rather preliminary investigation of the wettability of low-carbon steel by the four filler metals—pure silver, pure copper, BAg-8 and BAgMn—in air, dry helium and 10% H_2 90% N_2 atmosphere was completed, a series of experiments was run in which molten flux was substituted for atmosphere. Observations made during these experiments opened some new aspects for the investigation of the mechanism of wettability.

For the wettability tests under molten flux, the same experimental device as in the previous experiments (Fig. 1) was used. In order to avoid the runoff of the liquid flux from the top of the bar, a cylindrical cup was machined on the upper end of the bars, as shown in Fig. 2.

Small amounts of the commercial flux to be investigated were put into the preheated steel cup until the cup was almost full. Then the temperature was gradually raised until the flux was completely transparent and no gas evolution could be observed. In this way the braze metal was not subjected to the dehydration and gassing stages occurring prior to the flux fusion. Next, about 1.5 g of the pertinent filler metal wire, cut into small pieces, was dropped into the cup, the apparatus covered by glass jar, *J*, and a slow flow of protective gas was turned on. After the last traces of air were removed, the temperature was further increased until the filler metal was molten.

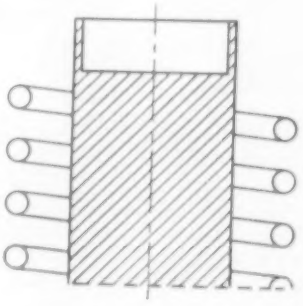

Fig. 2 Enlarged cross section of the apparatus for wettability tests under a flux layer

A cup is machined on the upper end of the cylindrical steel bar

In helium and 10% H_2 + 90% N_2 atmosphere, all four filler metals—pure silver, pure copper, BAg-8, BAgMn—readily spread beneath the molten flux layer. However, the moment the glass jar was removed and the steel cup—with the molten flux and the molten filler metal in it—was exposed to the air, the flux layer parted almost instantly, exposing a part of the molten filler metal surface to the air. In the next second the filler metal ran beneath the flux drop, exposing a part of the bottom surface of the steel cup to the air. Shortly afterward the piled-up flux spilled over the dewetted steel surface, and from this moment a rapid rotation of the flux and filler metal drops followed and continued for about two to three minutes until the flux layer was completely saturated with iron oxides. In the first seconds of the exposure to the air the speed of the rotation was the fastest: about two revolutions per second.

Significance of the Rotation Phenomenon

Since the rotation phenomenon was observed not only on the four investigated filler metals but also on a great number of other commercial brazing alloy-flux combinations, it was evident that the rotation experiment proves in a quite effective manner that in the brazing of steel the flux cannot completely protect the molten filler metal against exposure to the air. Furthermore, the rotation experiments indicated that an incomplete protection against exposure to the air might be an important factor causing imperfections in the brazed joints under practical brazing conditions. The speed of the rotation in these experiments proves quite effectively that under certain conditions on exposure to the air, times as short as $^1/_2$ sec are sufficient to cause dewetting of the steel surfaces.

Considering these practical consequences, it was decided to investigate the nature and the causes of the rotation phenomena somewhat more thoroughly.

Experiments were initiated to examine the possibility that the parting of the flux layer after exposure to the air might be caused by oxygen diffusion through the molten flux layer to the molten brazing-alloy surface. These experiments are reported in the following section.

Investigation of Oxygen Diffusion from the Air Through a Layer of the Molten Flux to the Filler-Metal Surface

Small amounts of eutectic silver-copper brazing alloy (BAg-8) were melted under a layer of pure borax. The melting of these samples was done in quartz glass test tubes under a glass jar filled with 10% H_2 + 90% N_2 atmosphere (see Fig. 3). Under this

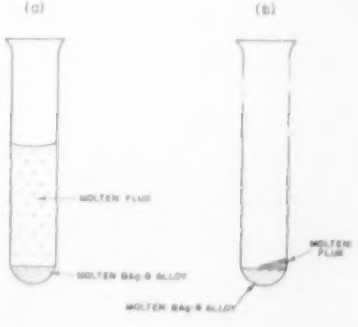

Fig. 3 Two quartz glass test tubes with molten silver-copper alloy (BAg-8) under a layer of molten flux, after 10 min exposure to the air

(a) Thick layer of flux (flux is colorless and transparent). (b) Thin layer of flux (red color of the cuprous oxide solution in borax).

atmosphere oxygen was excluded from the flux and the flux layers did not show any signs of oxidation; they were absolutely colorless and transparent. Ten minutes after melting the brazing alloy, the glass jar was removed and the liquid melts exposed to the air for five to ten minutes and then cooled down to room temperature. In the test tubes, where the flux layer was very thin, the flux layer parted, and thus the surface of the molten copper-silver alloy was exposed to the air. After cooling to room temperature the characteristic red color of the cuprous oxide solution in borax, well known from the borax-bead test of qualitative chemical analysis, could be observed in the flux layer, indicating that the oxidation of copper took place.

However, in the other test tubes, where the flux layer was thicker and had not parted after exposure to air, the red color did not appear and the flux remained colorless and transparent, even after exposure to air in a molten state for an additional ten minutes. This diffusion experiment has been repeated with some commercial fluxes. The results were always the same.

From these experiments it has been concluded that the investigated fluxes at a temperature slightly above the melting temperature of the eutectic silver-copper brazing alloy do not transfer oxygen to the surface of the molten brazing alloy, at least not in an amount which would cause the very sensitive red color reaction, provided that the flux layer is sufficiently thick.

Since, on the other hand, the rotation experiments showed that the same fluxes at the same temperature after exposure to the air parted and formed globules on the surface of the molten brazing alloy, even with a considerable thickness of the flux layer, this phenomenon can be explained only by assuming that the partition and the globule formation were caused by a considerable change of surface tension of the molten flux associated with the saturation of the flux layers adjacent to the walls of the steel cup by iron oxides.

The following experiment gave a more solid basis to this assumption. A globule of a glasslike, completely dehydrated flux is melted on top of a red hot steel bar (Fig. 1) in air and without the presence of any filler metals. The flux globule spreads readily over the polished end surface of the bar. In the next few seconds the flux pellet becomes increasingly saturated with the iron oxides until it starts to dewet the steel surface and finally shrinks to small round globules.

In order to investigate the mechanism of the rotation phenomenon somewhat more thoroughly, some rotation experiments have been recorded by means of high-speed movies. An examination of these films was helpful

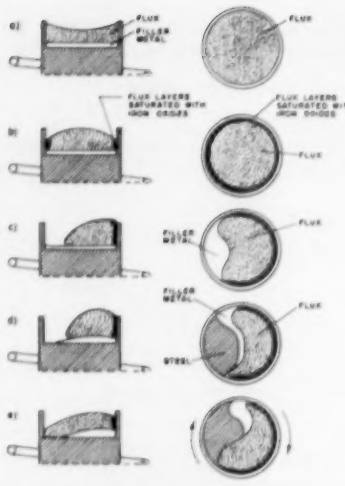

Fig. 4 Various phases of the "rotation experiment"

for a more detailed analysis of the rotation phenomenon. This analysis is presented in the following section.

Explanation of the Rotation Phenomenon

In the first phase of the rotation experiment (Fig. 4a), before removal of the glass jar, the steel cup is surrounded by a protective gas atmosphere. The surface of the molten flux in the steel cup is motionless, almost flat in the center and slightly concave at the walls of the cup. The molten filler metal—also motionless—forms a flat layer beneath the flux.

During the second phase of the rotation experiment (Fig. 4b), following removal of the glass jar, the glowing steel cup is exposed to the air. The edges are oxidized rapidly, and the iron oxides from the steel cup walls are quickly dissolved by the molten flux. In the next few seconds the flux layers adjacent to the steel cup walls become more and more saturated with iron oxides until finally they start to dewet the oxidized steel cup walls, turning the shape of the molten flux surface from concave to convex. Three to four seconds after exposure to the air, the flux forms a completely round globule floating on the molten filler metal. Suddenly, due to the altering surface-tension forces, the flux globule moves from the center to one or another side of the cup, exposing the molten filler-metal surface on the opposite side of the cup to the air (Fig. 4c). This moment can be considered as the starting point of the third phase.

The third phase of the rotation experiment is normally very short, not longer than $^1/_2$ sec. During this period, the exposed filler-metal surface readily absorbs oxygen; the oxygen from the air is transferred extremely rapidly to the steel-filler metal interface. Thus the steel surface is oxidized, and a thin layer or iron oxide and a large number of small CO gas bubbles (resulting from oxidation of the carbon in the oxidized steel layer) form on the steel-silver interface. The filler metal dewets the oxidized steel surface, moving beneath the flux layer on the opposite side of the cup (Fig. 4d) and exposing the glowing steel surface on the bottom of the cup to the air. The molten filler metal moving beneath the flux sets the flux drop into motion, so that the flux starts to flow over the dewetted steel surface exposing a new section of the filler metal surface to the air on the opposite side of the cup (Fig. 4e). From this moment a rapid rotation of the flux and filler metal layers starts around the center of the cup, clockwise or in the opposite direction depending on the side to which the flux flows first. During each separate rotation cycle, the flux flows one time over the dewetted steel surface, dissolving the iron oxides, so that the molten filler metal which flows beneath the flux layer can again wet the deoxidized steel surface. Then the same spot is again dewetted by the flux, the oxygen transfer takes place, the steel surface is again oxidized and the oxidized surface dewetted by the filler alloy. At the moment the molten flux flows over this spot again one complete rotation cycle is accomplished. With each subsequent cycle the flux becomes more and more saturated with iron oxides and the speed of the rotation slows down until finally it ceases completely. The speed of the rotation is temperature dependent; it increases rapidly at higher temperatures. With certain filler metal-flux combinations and sufficiently high temperatures the

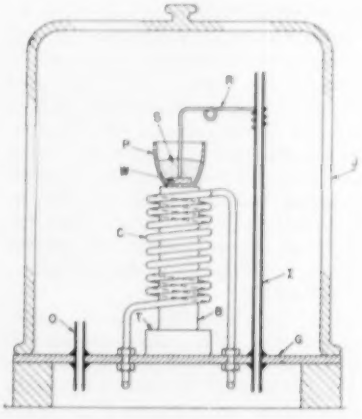

Fig. 5 Experimental apparatus for diffusion experiments

B, Cylindrical steel bar; *C*, water-cooled induction coil; *G*, glass plate; *I*, gas inlet tube; *J*, glass jar; *O*, gas outlet tube; *P*, porcelain crucible; *S*, molten silver layer; *T*, transite block; *W*, steel disk; *R*, steel wire (preventing the steel disk, *W*, from floating up in the molten silver)

speed of the rotation might reach two revolutions per second. The speed of the rotation is influenced only slightly by the high-frequency current. On switching off the high-frequency current for a short period no change in the speed of the rotation has been observed. The speed of the rotation was the same whether high-frequency current, furnace heating or torch heating was used.

Oxygen Transfer from the Air Through a Layer of Molten Silver to the Steel-Silver Interface

Scope of the Investigation

The rotation experiments effectively demonstrated a phenomenon which, as the previous investigations proved, could be caused only by an extremely high rate of diffusion of oxygen from the air through a layer of molten brazing alloy to the steel-brazing alloy interface. Consequently, it was concluded that a fundamental study of the diffusion of oxygen through thin layers of molten brazing alloys might be of great practical interest. Such a study might bring about a better understanding of the mechanism of formation of the imperfections in brazed joints resulting from an incomplete protection of the molten brazing alloys from the air by molten fluxes.

To exclude disturbing factors and influences, these studies were begun with the investigation of diffusion of oxygen through layers of pure silver.

The diffusion of oxygen through a layer of pure, solid silver has been investigated by K. W. Froelich[1] who used copper sheets electroplated with pure silver which were heated at 700° C (1292° F) in oxygen. The amount of oxygen absorbed at the copper-silver interface was proportional to the time and inversely proportional to the thickness of the silver layer.

Micrographs showed the formation of Cu and O compounds between the copper sheet and the silver layer.

According to Froelich's experiments, the rate of diffusion of oxygen through layers of pure silver should be considerable. The rates of diffusion of oxygen through thin plates of pure silver have been determined by Johnson and Larose.[2] They found a square-root relation between the rate of diffusion and the pressure. It has been shown that their data on the diffusion of the gas through the metal were in accord with Richardson's equation. Steacie and Johnson[3] investigated the solubility of oxygen in silver. They found that the solubility was proportional to the square root of pressure at pressures above 10 mm.

Since the purpose of the investigation presented here was not a study of the diffusion rates or a study of solubility of oxygen in silver, but rather of

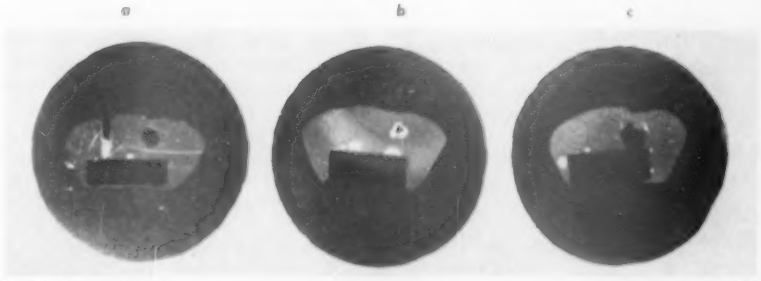

Unetched Mag. X 2

Fig. 6 Cross sections through steel disks covered by a layer of pure silver (10 g)
Material of the disks: (a) Armco iron (0.07% C); (b) low-carbon steel (0.20% C); (c) drill rod (1.00% C). The specimens were rapidly cooled after keeping the molten silver for 10 min in 10% H_2 + 90% N_2 atmosphere, cross sectioned and mounted in plastic. (Reduced by 1/4 upon reproduction)

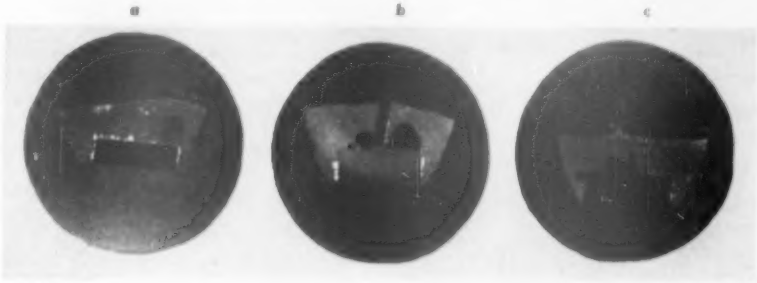

Unetched Mag. X 2

Fig. 7 Same as Fig. 6
The specimens were rapidly cooled after keeping the molten silver for 10 min in 10% H_2 + 90% N_2 atmosphere, and subsequent exposure to the air for 1 min. (Reduced by 1/4 upon reproduction)

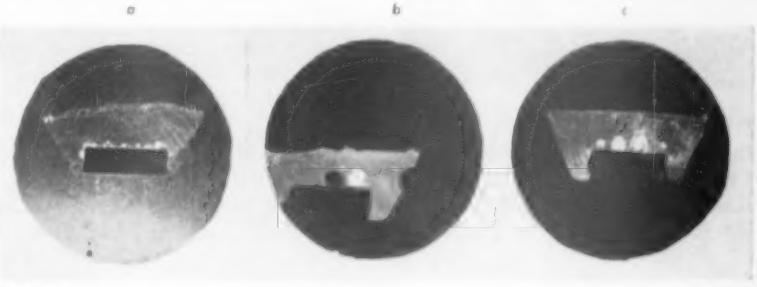

Unetched Mag. X 2

Fig. 8 Same as Fig. 7. Time of exposure to air, 3 min

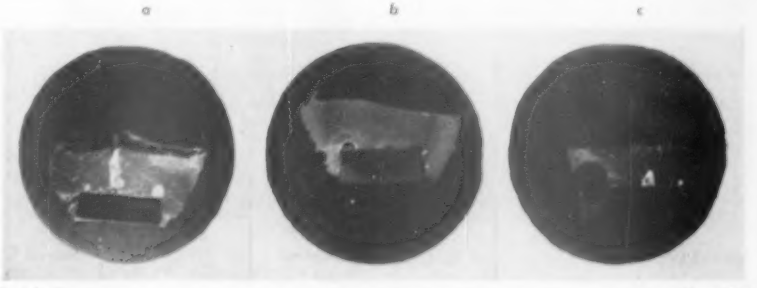

Unetched Mag. X 2

Fig. 9 Same as Fig. 8. Time of exposure to air, 5 min. (Reduced by 1/4 upon reproduction)

the mechanism of the diffusion and formation of iron oxide layers and CO gas bubbles on the steel-silver interface, there is no need to discuss the above-mentioned papers more thoroughly.

Experimental Apparatus and Methods

The experimental apparatus used for the diffusion studies is illustrated in Fig. 5. In this apparatus, the silver in the porcelain crucible, *P*, is brought up to the necessary temperature by heat conduction from the glowing steel bar, *B*, and not directly by induction heating. This has been achieved simply by positioning the steel bar, *B*, so that the por-

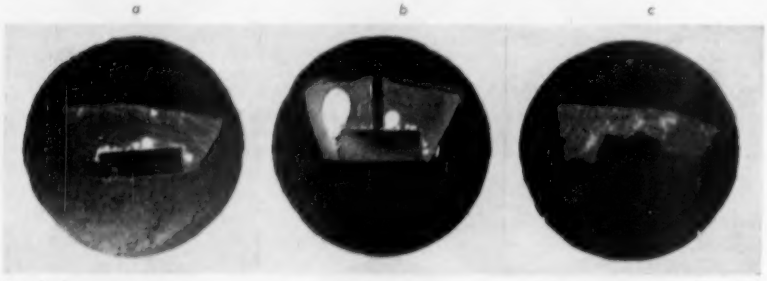

Unetched Mag. X 2

Fig. 10 Same as Fig. 8. Time of exposure to air, 10 min

Unetched Mag. X 150

Fig. 15 Steel-silver interface from the cross section shown on Fig. 10*a*

Material of disk: Armco iron (0.07% C). Time of exposure to air, 10 min

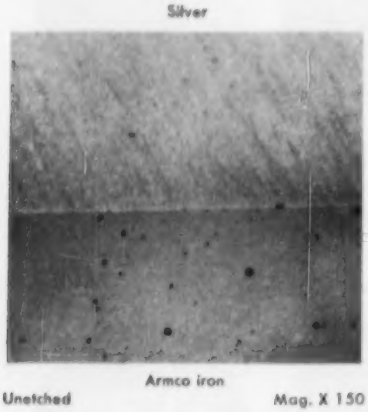

Unetched Mag. X 150

Fig. 11 Steel-silver interface from the cross section shown on Fig. 6*a*

Material of the disk: Armco iron (0.07% C). Time of exposure to air, 0 min

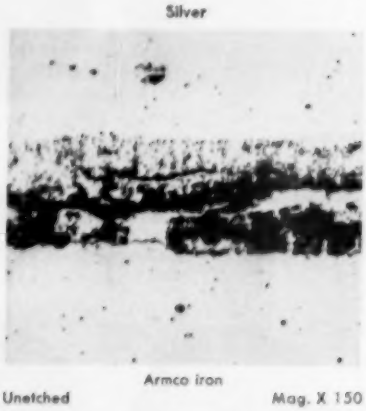

Unetched Mag. X 150

Fig. 13 Steel-silver interface from the cross section shown on Fig. 8*a*

Material of the disk: Armco iron (0.07% C). Time of exposure to air, 3 min

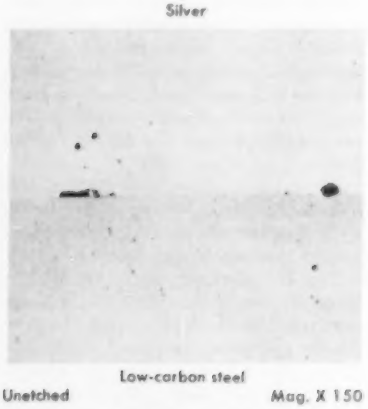

Unetched Mag. X 150

Fig. 16 Steel-silver interface from the cross section shown on Fig. 6*b*

Material of the disk: low-carbon steel (0.20% C). Time of exposure to air, 0 min

Unetched Mag. X 150

Fig. 12 Steel-silver interface from the cross section shown on Fig. 7*a*

Material of the disk: Armco iron (0.07% C). Time of exposure to air, 1 min

Unetched Mag. X 150

Fig. 14 Steel-silver interface from the cross section shown on Fig. 9*a*

Material of the disk: Armco iron (0.07% C). Time of exposure to air, 5 min

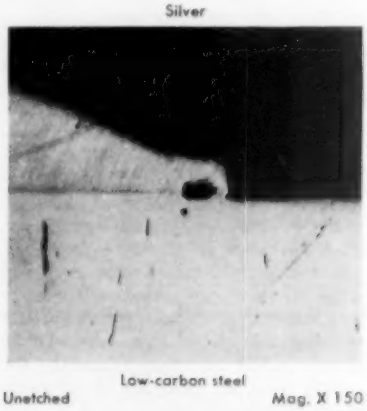

Unetched Mag. X 150

Fig. 17 Steel-silver interface from the cross section shown on Fig. 7*b*

Material of disk: low-carbon steel (0.20% C). Time of exposure to air, 1 min

celain crucible, P, is above the electromagnetic field of the coil, C.

The modified heating method produced samples which permitted the study of the mechanism of the diffusion of oxygen through molten silver layers to the steel-silver interface.

In the course of these experiments a series of steel disks ($^3/_8$ in. diam by $^1/_8$ in. high) was prepared from: (*a*) Armco iron (0.07% C), (*b*) low-carbon steel (0.20% C), (*c*) drill rod (1.00% C). The carefully cleaned disks were placed on the bottom of small porcelain crucibles, P (see Fig. 5), and covered by equal amounts (10 g) of pure silver. Since the density of molten silver is considerably greater than the density of solid steel, the steel disks, in order to prevent them from floating in the molten silver, were pressed down to the bottom of the crucible by a stainless steel spring, R. After melting the silver layer under 10% H_2 + 90% N_2 atmosphere, the crucibles were exposed to the air for a certain time (1, 3, 5 or 10 min) and then rapidly cooled to room temperature. Under the microscope the polished (unetched) cross sections of these samples showed a characteristic picture: the samples which were not exposed to the air yielded a straight, geometrical line representing the steel-silver interface. In all cases—Armco iron, Fig. 11; low-carbon steel, Fig. 16; and drill rod, Fig. 21—no oxide layers and only very few gas bubbles could be found on the steel-silver interface (see also Fig. 6).

All the samples which were exposed to the air for 1, 3, 5 or 10 min (Fig. 7, 8, 9 and 10) showed a layer of iron oxides on the steel-silver interface, and variable amounts of gas bubbles. The thickness of the oxide layers increased with increase of time of exposure to air. Under larger magnifications (Figs. 12 to 25), however, these oxide layers no longer appeared continuous, but divided into separate, thin oxide layers, which were parallel to the steel surface and were separated by quite thin intermediate layers of pure silver. These parallel layers of iron oxides separated by intermediate silver layers closely resembled the pattern of annual rings on a cross section of a stump of an old tree (see Figs. 13, 14 and 20). The number of these separated iron oxide layers was almost proportional to the time of the exposure to the air. It was found that a new oxide layer formed approximately every minute, so that, for instance, the samples which were exposed to the air for 5 min yielded, on the average, four to five separate oxide layers (see Fig. 14). These thin oxide layers again were not continuous, but were perforated by a large number of small holes which were apparently caused by CO-gas bubbles escaping from the steel-silver interface (Figs. 12 and 20). Accordingly, in the horizontal projection, these oxide layers would look like thin films punctured by a large number of small holes, resembling thin screens of very fine mesh.

Considering all these observations, the mechanism of formation of the lamellar oxide layers on the steel-silver interface might be explained as follows:

During the first phase of the diffusion experiment, before removal of the glass jar, J (Fig. 5), the crucible, P, with the molten silver is surrounded by 10% H_2 + 90% N_2 gas; there is no oxygen present in the molten silver, and the steel-silver interface is completely free from oxides (see Figs. 11, 16 and 21).

During the second phase of the diffusion experiment, following the removal of the glass jar, J, the molten silver surface is exposed to the air, and the oxygen—as was demonstrated in the rotation experiments—almost instantly is diffused to the steel-silver interface, where a rapid oxidation of the steel surface takes place. However, due to the formation of the CO bubbles beneath the growing FeO layer, this layer is separated from the solid steel surface and is forced by the developing gas to move upward. After a while, the gap between the steel surface and the lifted FeO layer is so wide that the molten silver may start to flow into the gap, pushing out the CO gas. In this way, the thin FeO layer will be disrupted, permitting the CO gas to escape through the gaps between the broken FeO layer pieces. It can be anticipated that with a higher carbon content of the pertinent steel disk, more CO gas will develop, and consequently the FeO layers will be more completely destroyed. The photomicrographs confirmed this reasoning: for instance, on the drill rod surface (Figs. 22 to 25) the FeO layers are much more thoroughly destroyed than on the Armco iron surface (Figs. 12 to 15). The silver layer exposed to the air for 10 min even broke off completely from the drill rod disk after solidification (see Figs. 10 and 25).

The molten silver which flows into the gap between the steel surface and the lifted FeO layer is saturated with oxygen. Consequently, the molten silver immediately will present oxygen to the steel surface, initiating the formation of the second FeO layer. About a minute after the silver has filled the gap, the second FeO layer will be separated from the steel surface, and again slightly lifted up, and the molten silver will again fill the gap between the second FeO layer and the steel surface, initiating the formation of the third FeO layer. The formation of the FeO layers will continue as long as the molten silver surface is exposed to the air. At the same time, each subsequent FeO layer will hinder the oxygen transfer

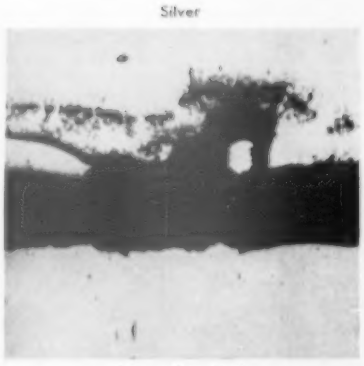

Unetched Mag. X 150

Fig. 18 Steel-silver interface from the cross section shown on Fig. 8b

Material of disk: low-carbon steel (0.20% C). Time of exposure to air, 3 min

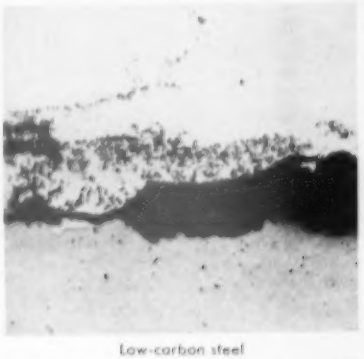

Unetched Mag. X 150

Fig. 19 Steel-silver interface from the cross section shown on Fig. 9b

Material of disk: low-carbon steel (0.20% C). Time of exposure to air, 5 min

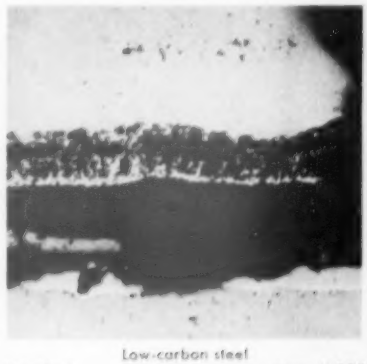

Unetched Mag. X 150

Fig. 20 Steel-silver interface from the cross section shown on Fig. 10b

Material of disk: low-carbon steel (0.20% C). Time of exposure to air, 10 min

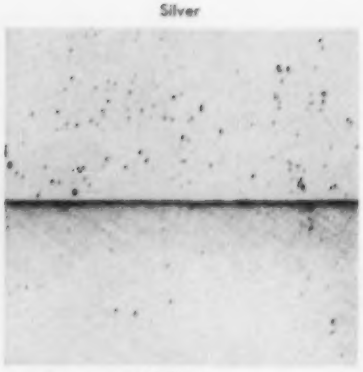

Fig. 21 Steel-silver interface from the cross section shown on Fig. 6c

Material of the disk: drill rod (1.00% C). Time of exposure to air, 0 min

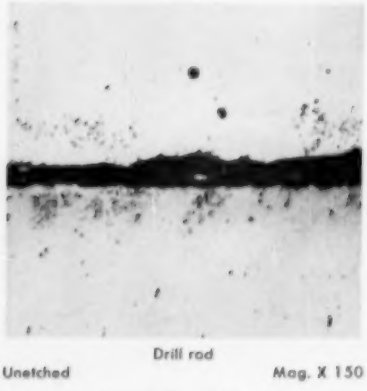

Fig. 22 Steel-silver interface from the cross section shown on Fig. 7c

Material of the disk: drill rod (1.00% C). Time of exposure to air, 1 min

Fig. 23 Steel-silver interface from the cross section shown on Fig. 8c

Material of the disk: drill rod (1.00% C). Time of exposure to air, 3 min

more and more, slowing down the oxidation of the steel surfaces.

Formation of Carbon Monoxide on the Steel-Silver Interface During the Diffusion Experiments

The diffusion experiments confirmed the hypothesis that by oxidation of the steel surface the carbon monoxide separates on the steel-silver interface in the form of small gas bubbles. When the diffusion experiments were started it was believed that the amount of the CO gas inclusions on the steel-silver interface must be proportional to the amount of diffused oxygen, and consequently, proportional to the time of the exposure to the air. However, this hypothesis had to be somewhat revised since the experimental observations were not in complete agreement with the expected behavior. Some additional studies have been made to clarify the causes of these discrepancies.

First of all, a stoichiometric calculation was conducted in order to evaluate the amount of CO gas which forms on the steel-silver interface, assuming that the carbon content of the steel is 1%, and that a 0.1 mm thick steel layer was completely oxidized to FeO. This calculation yielded 14.5 cc CO gas per square centimeter of steel surfaces. In other words, the volume of the CO gas is about 145 times larger than the volume of the steel layer before oxidation. Certainly the volume of the CO gas will decrease with the decrease of the carbon content of the steel. With 0.1% carbon, it will be 14.5 times larger, and with 0.01% carbon it will be only 1.45 times larger than the corresponding volume of the steel layer.

The results of this calculation demonstrate rather effectively that by an inadequate protection* of the molten brazing alloy from oxygen of the air by molten flux, the oxygen diffusion through the molten brazing alloy layer to the steel surface might cause not only oxidation of this surface, and consequently dewetting of the oxidized steel surface by molten brazing alloy, but also formation of a considerable volume of evolved CO gas at the steel-brazing alloy interface.

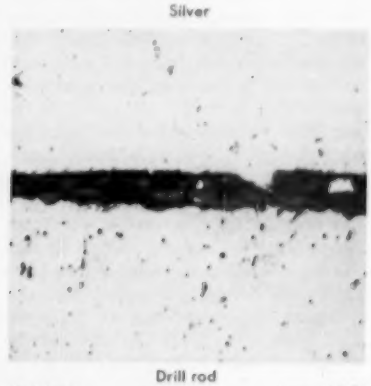

Fig. 24 Steel-silver interface from the cross section shown on Fig. 9c

Material of the disk: drill rod (1.00% C). Time of exposure to air, 5 min

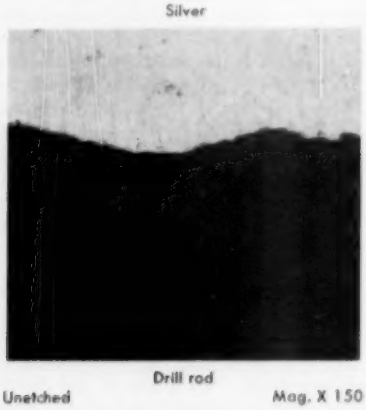

Fig. 25 Steel-silver interface from the cross section shown on Fig. 10c

Material of the disk: drill rod (1.00% C). Time of exposure to air, 10 min

* The inadequacy of such protection has been proved by the "rotation experiment" not only for the case of pure silver but also for a large number of different commercial brazing alloy-flux combinations.

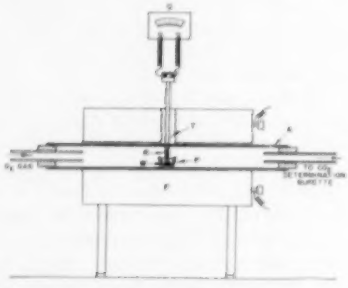

Fig. 26 Apparatus for determination of CO_2 gas formed by diffusion of oxygen through a layer of molten silver to the steel-silver interface

A, Porcelain tube; *F*, electrical furnace; *P*, porcelain crucible; *R*, Inconel wire (preventing the steel disk from floating in the molten silver); *W*, steel disk; *Q*, potentiometer; *T*, thermocouple

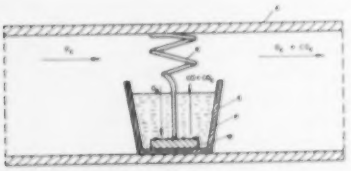

Fig. 27 Enlarged cross section through the porcelain crucible, *P*, shown in Fig. 26

A, Porcelain tube; *P*, porcelain crucible; *R*, Inconel wire; *S*, molten silver layer; *W*, steel disc

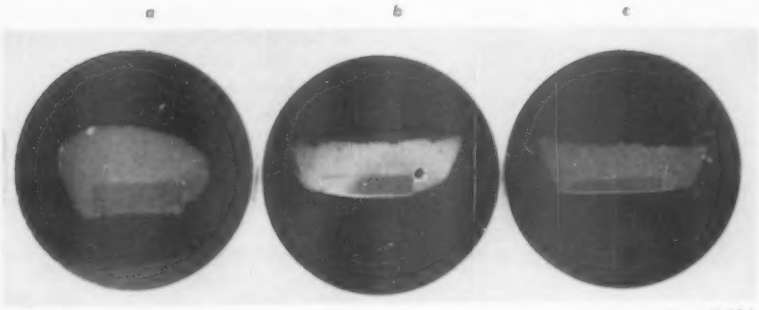

Unetched Mag. X 1 1/4

Fig. 28 Cross sections through drill rod disks covered by a layer of 1% Sn – 99% Ag alloy (10 g)

All the specimens were rapidly cooled down after keeping the molten alloy for 10 min in 10% H_2 + 90% N_2 atmosphere, and subsequent exposure to air: (a) for 0 min, (b) for 3 min, (c) for 5 min

This calculation indicates also that in the diffusion experiments where the molten silver surface was exposed to air for a shorter time, the amount of entrapped CO gas bubbles on the steel-silver interface might be proportional to the time of exposure to the air, but only in the case of very short time of exposure. With longer exposure times, the amount of CO gas will increase so much that the gas will begin to bubble out of the molten silver. The experimental observations fully confirmed this reasoning. It has been observed during the diffusion experiments that after exposure to air the molten silver began to "boil" almost instantly when a drill rod disk was on the bottom of the porcelain crucible. The "boiling" was much slower in the case of low-carbon steel or Armco iron disks, but "boiling" has never been observed without using steel disks.

Similar observations have been made also during the "rotation" experiments. The studies of the high-speed motion pictures of the "rotation" process have proved that by exposure to air the molten brazing alloy in 2 to 3 sec begins to dewet the steel surface, as the dewetting starts simultaneously on a large number of almost infinitely small spots which spread quite rapidly, removing the brazing alloy from the oxidized steel surface. It is quite possible that the large number of small spots, where the dewetting starts, is caused by nucleation of a large number of almost infinitely small CO gas bubbles, which grow rapidly and remove the molten brazing alloy from the steel surface. Consequently, it is possible that the high rotation speed in these experiments is caused not only by dewetting of the oxidized steel surface, but also by a rapid precipitation of large amounts of CO gas on the steel-silver alloy interface.

In the diffusioa experiments the amount of CO gas which forms in one unit of time on one square unit of the surface should be proportional to the carbon content of the steel, all other conditions being equal. In order to prove this it has been attempted to determine by means of gas analysis the amount of CO gas formed. For these quantitative determinations the porcelain crucible, *P* (see Figs. 26 and 27), with the steel disk, *W*, covered by 10 g of pure silver was placed in the center section of the porcelain tube, *A* inserted in the furnace of a carbon determination apparatus, normally used for determination of carbon in steel. By raising the temperature in the center section of the porcelain tube, *A*, to 1100° C, the silver pieces melt and the liquid silver covers the steel disk, exactly as in the previous diffusion experiments. The melting of silver was done in dry helium atmosphere. After the temperature in the porcelain tube, *A*, has been stabilized at 1100° C, the helium gas flow was turned off, the oxygen gas turned on and the porcelain tube, *A*, connected with the CO_2 absorption burette. The flow rate of oxygen was about 700 ml/min. The oxygen diffuses through the molten silver layer to the steel-silver interface and oxidizes the steel surface. The carbon of the oxidized steel layer yields carbon monoxide gas, which separates from the molten silver and is oxidized to CO_2. The CO_2 gas is absorbed in the carbon dioxide absorption burette. After 5 min of continuous flow the supply of oxygen gas is interrupted, and the amount of absorbed CO_2 gas determined.

The analytical results are summarized in Table 2. As these results show, in the first crucible was pure silver without any steel disk; this sample yielded 1.1 mg CO_2. In the second crucible was an Armco iron disk (0.07% C); this sample yielded 2.1 mg CO_2. The third sample, containing a low-carbon steel disk (0.20% C), yielded 3.2 mg CO_2; the fourth sample with a drill rod disk (1.00% C) yielded 4.4 mg CO_2. Though the amounts of the CO_2 gas are not quite proportional to the carbon content of the pertinent steels, the obtained results proved beyond doubt that carbon monoxide (and possibly also carbon dioxide) is formed by dif-

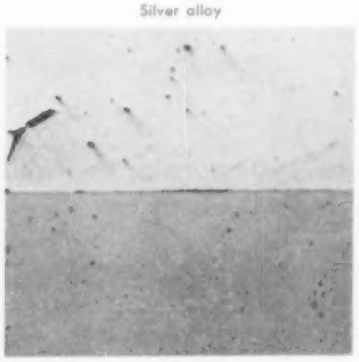

Unetched Mag. X 150

Fig. 29 Steel, 1% Sn – 99% Ag alloy interface from the cross section shown on Fig. 29a. Time of exposure to air, 0 min

Unetched Mag. X 150

Fig. 30 Steel, 1% Sn – 99% Ag alloy interface from the cross section shown on Fig. 29b. Time of exposure to air, 3 min

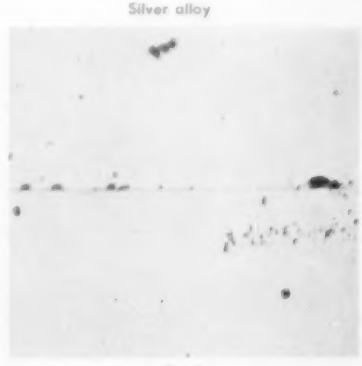

Unetched Mag. X 150

Fig. 31 Steel, 1% Sn – 99% Ag alloy interface from the cross section shown on Fig. 29c. Time of exposure to air, 5 min

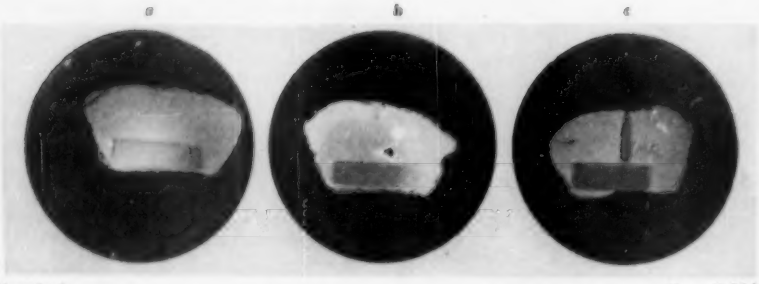

Unetched Mag. X 1 1/4

Fig. 32 Cross sections through drill rod disks covered by a layer of 1% Ni – 99% Ag alloy (10 g)

All specimens were rapidly cooled down after keeping the molten alloy for 10 min in 10% H_2 + 90% N_2 atmosphere, and subsequent exposure to air: (a) for 0 min, (b) for 3 min, (c) for 5 min

fusion of oxygen through layers of molten silver to the steel surface.

After the investigation of the mechanism of oxygen diffusion through layers of molten silver and of the mechanism of the oxidation of the steel surfaces had been accomplished, the next problem to be investigated was the influence of additions of various deoxidizing elements on the oxygen diffusion through layers of molten silver.

Table 2 Analytical Results of the Diffusion Tests in Oxygen Atmosphere

Material of the disk	*Carbon in steel, %*	*CO_2 in the O_2 gas, mg*
No disk (Ag only)	...	1.1
Armco iron	0.07	2.1
Low-carbon steel	0.20	3.2
Drill rod	1.00	4.4

Oxygen Transfer from the Air to the Steel-Silver Interface Through Layers of Molten Silver with 1% Additions of Various Deoxidizing Elements

Preparation of the Alloys

The purpose of the investigations reported in this section was to study the influence of the various deoxidizers on the oxygen diffusion through the molten silver layers and on the mechanism of oxidation of the steel surface. First, the pertinent silver alloys were prepared by melting 99 wt % (35 g) of pure silver with 1 wt % (0.35 g) of one of the following deoxidizing metals: Be, Mg, Al, Si, Ca, Ni, Cd, Ba and Sn. The melting was performed in porcelain crucibles under 10% H_2 + 90% N_2 atmosphere (see Fig. 5).

The 1% Li alloy was melted under dry helium atmosphere. The 1% Cu and 1% Zn alloys were prepared from master alloys (commercial brazing alloys BAg-8 and 75% Ag, 25% Zn, respectively) by adding the necessary amount of pure silver.

The literature search has proved that there is no reliable method known for preparing 1% P–99% Ag alloys. Accordingly, no attempts were made to prepare such alloys.

After remelting several times under 10% H_2 + 90% N_2 atmosphere the alloys were divided into three 10-g samples for the diffusion tests and one 5-g sample for the chemical analysis.

The chemical analyses of the prepared silver alloys yielded the following results:

Alloy	*Analysis*
Al-Ag	1.09% Al, balance Ag
Ba-Ag	0.56% Ba, balance Ag
Be-Ag	0.91% Be, balance Ag
Ca-Ag	0.89% Ca, balance Ag
Cd-Ag	0.87% Cd, balance Ag
Cu-Ag	1.16% Cu, balance Ag
Li-Ag	0.37% Li, balance Ag
Mg-Ag	0.85% Mg, balance Ag
Ni-Ag	1.23% Ni, balance Ag
Si-Ag	1.02% Si, balance Ag
Sn-Ag	0.75% Sn, balance Ag
Zn-Ag	0.98% Zn, balance Ag

As the results of the chemical analysis show, only in the case of Ag-Ba and Ag-Li alloys was the percentage of the deoxidizing ingredient considerably below 1%, presumably due to the lithium and barium losses during the remelting of the alloy in the protective atmosphere which was not absolutely dry. The content of all other deoxidizing elements was roughly around 1%.

Experimental Apparatus and Methods

The apparatus used for the diffusion experiments is illustrated by Fig. 5. In this apparatus, the given silver alloy is brought up to the necessary temperature by heat conduction from the glowing steel bar.

The diffusion experiments consisted of the following operations: first of all, a series of carefully cleaned drill rod (1% carbon steel) disks—3/8 in. diam, 1/8 in. high—were placed on the bottom of small porcelain crucibles and covered by equal amounts (10 g) of the pertinent silver alloy. For each of the 12 experimental alloys were reserved three crucibles, so that the total number of crucibles was 36. Since the density of molten silver is considerably greater than the density of solid steel, the steel disks, in order to prevent them from floating in the molten silver, were pressed down to the

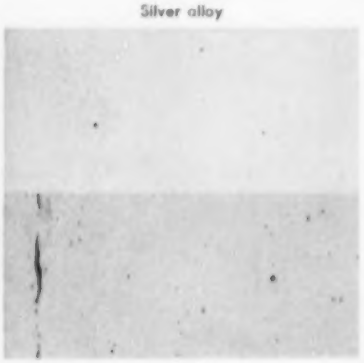

Unetched Mag. X 150

Fig. 33 Steel, 1% Ni – 99% Ag alloy interface from the cross section, shown on Fig. 33a. Time of exposure to air, 0 min

Unetched Mag. X 150

Fig. 34 Steel, 1% Ni – 99% Ag alloy interface shown on Fig. 33b. Time of exposure to air, 3 min

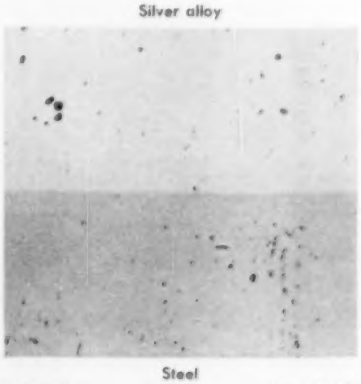

Unetched Mag. X 150

Fig. 35 Steel, 1% Ni – 99% Ag alloy interface shown on Fig. 33c. Time of exposure to air, 5 min

bottom of the crucible by a stainless steel spring, *R*.

After remelting for 10 min under 10% H_2 + 90% N_2 atmosphere, the first crucible with each particular alloy was cooled down to room temperature without exposing to the air, the second and the third crucibles were exposed to the air for 3 and 5 min, respectively, and then rapidly cooled down to room temperature.

The metallographic examination (see Figs. 28 to 53) yielded the following picture: only three of the deoxidizing elements, namely, nickel, tin and zinc, completely eliminated the oxygen diffusion through the molten silver layers even after exposure to the air for as long as 5 min. All the other deoxidizing elements did not prevent, or only partly prevented, the diffusion of oxygen to the steel-silver interface. In some cases, as for instance with the 1% Cu–99% Ag alloy the oxygen diffusion was even accelerated.

Discussion of the Diffusion Experiments

In the case of 1% Sn–99% Ag alloy (Figs. 28a, 28b, 28c, 29, 30 and 31), the samples which were exposed to the air (Figs. 28b, 28c, 30 and 31) as well as the one which was not exposed to the air (Figs. 28a and 29) yielded on the photomicrographs one straight, geometrical line, representing the steel-silver interface, without any signs of oxidation or gas inclusions.

Figure 28a shows the cross section of a drill rod disk covered with 10 g of the 1% Sn–99% Ag alloy, melted and cooled in 10% H_2 + 90% N_2 atmosphere without any exposure to the air.

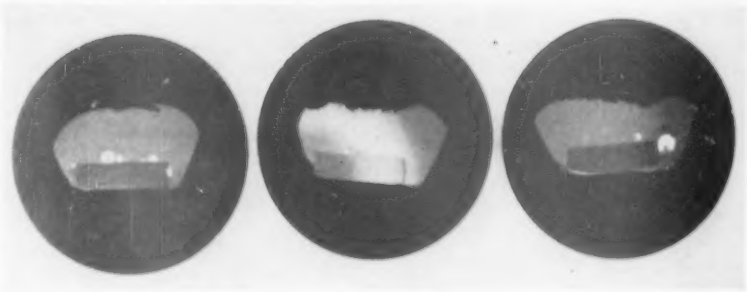

Unetched Mag. X 1 1/4

Fig. 36 Cross sections through drill rod disks covered by a layer of 1% Zn – 99% Ag alloy (10 g)

All of the specimens were rapidly cooled down after keeping the molten alloy for 10 min in 10% H_2 + 90% N_2 atmosphere, and subsequent exposure to air: (a) for 0 min, (b) for 3 min, (c) for 5 min.

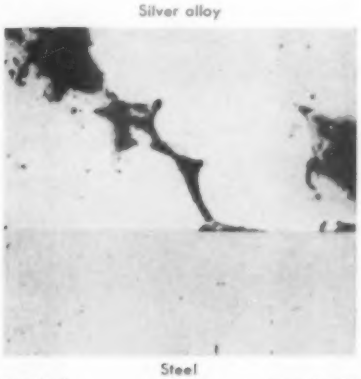

Unetched Mag. X 150

Fig. 37 Steel, 1% Zn – 99% Ag alloy interface from the cross section shown in Fig. 37*a*. Time of exposure to air, 0 min

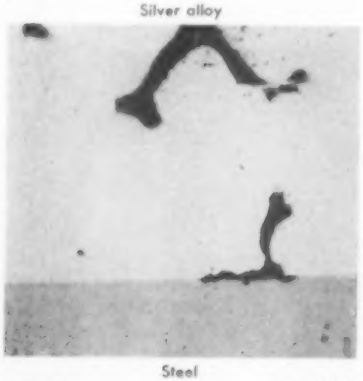

Unetched Mag. X 150

Fig. 38 Steel, 1% Zn – 99% Ag alloy interface shown on Fig. 37*b*. Time of exposure to air, 3 min

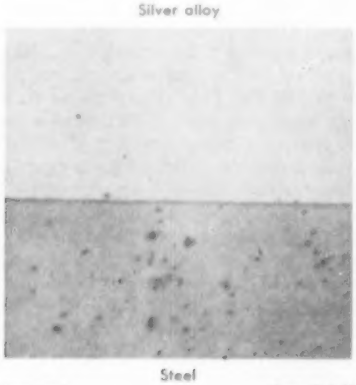

Unetched Mag. X 150

Fig. 39 Steel, 1% Zn – 99% Ag alloy interface shown on Fig. 37*c*. Time of exposure to air, 5 min

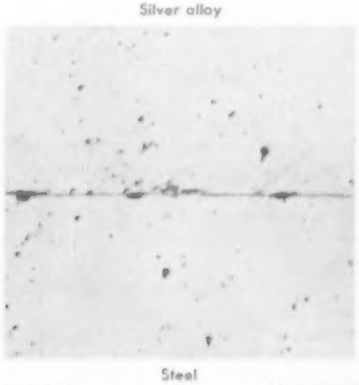

Unetched Mag. X 150

Fig. 40 Steel, 1% Cd–99% Ag alloy interface. Time of exposure to air, 0 min

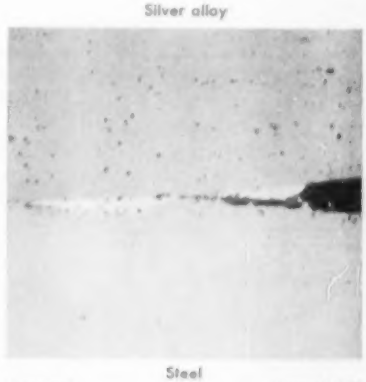

Unetched Mag. X 150

Fig. 41 Steel, 1% Cd – 99% Ag alloy interface. Time of exposure to air, 3 min

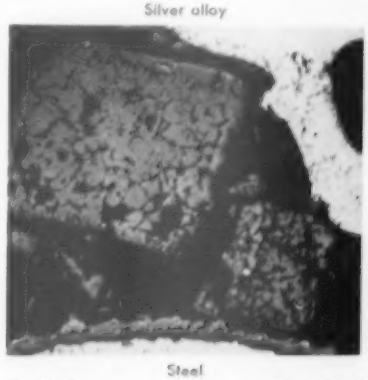

Unetched Mag. X 150

Fig. 42 Steel, 1% Cd – 99% Ag alloy interface

Time of the exposure to the air, 5 min. (Reduced by 1/4 upon reproduction)

Figure 28b shows the cross section of a drill rod disk covered with the same alloy after 3 min exposure to the air, and Fig. 28c after 5 min exposure to the air, respectively. The magnification of these photomicrographs is × 2.

Fig. 43 Steel, 1% Cu–99% Ag alloy interface. Time of exposure to air, 0 min

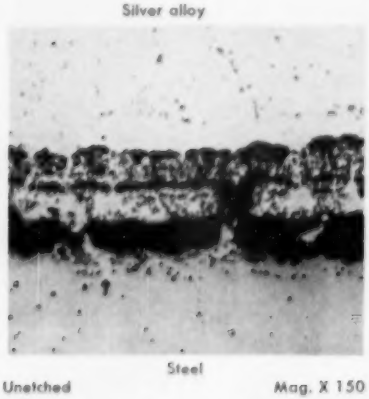

Fig. 44 Steel, 1% Cu–99% Ag alloy interface. Time of exposure to air, 3 min

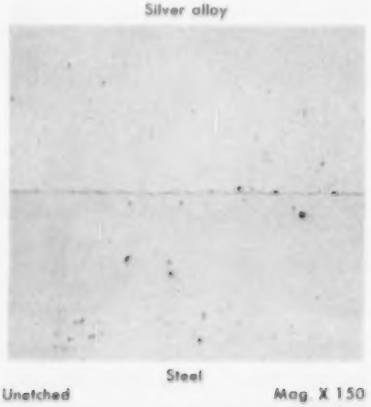

Fig. 45 Steel, 1% Ba–99% Ag interface. Time of exposure to air, 0 min

Under a larger magnification (× 150, Figs. 29–31) the steel-silver interfaces of the samples illustrated by Figs. 28a–28c still show no signs of oxidation or gas inclusions, and present one straight geometrical line (Fig. 29 is a magnification of a section of the steel-silver interface shown on Fig. 28a; Fig. 30 is a magnification of 28b; Fig. 31 of 28c, respectively).

Exactly the same pattern is shown by the 1% Ni–99% Ag alloy, without exposure to the air (Figs. 32a and 33) as well as after exposure to the air for 3 min (Figs. 32b and 34) and for 5 min (Figs. 32c and 35). The steel-silver interface again presents a straight line without any traces of oxides or gas inclusions.

The 1% Zn–99% Ag alloys also show no traces of oxides or gas inclusions, either on the samples not exposed to air (Figs. 36a and 37), or on the samples exposed to the air for 3 min (Figs. 36b and 38) and for 5 min (Figs. 38c and 39). However, on the micrographs obtained on 1% Zn–99% Ag alloy some large voids are visible in the layers of silver adjacent to the steel-silver interface. These voids are present in the sample exposed to air for 3 min (Fig. 38) as well as in the sample not exposed to air at all (Fig. 37). This type of void may be related to the fact that the boiling point of pure zinc (1665° F) is much lower than the solidus temperature of the 1% Zn–99% Ag alloy (about 1715° F). It is quite understandable also that in the case of 1% Cd–99% Ag alloys, where the boiling point of cadmium (1409° F) is also far below the melting point of the 1% Cd–99% Ag alloy (about 1735° F), the same type of large voids appear in the silver alloy layers adjacent to the steel-silver interface: the 1% Cd–99% Ag alloy samples exposed to the air for 3 min (Fig. 41) and for 5 min (Fig. 42) show large voids in the silver alloy layers.

All other alloys, e.g., 1% Al–99% Ag; 1% Ba–99% Ag (Figs. 45, 46, 47); 1% Be–99% Ag (Figs. 48–50); 1% Ca–99% Ag (Figs. 51, 52 and 53); 1% Cu–99% Ag (Fig. 43 and 44); 1% Li–99% Ag; 1% Mg–99% Ag; and 1% Si–99% Ag could not prevent the oxygen diffusion through the molten alloy layer, and, consequently, the pertinent photomicrographs show considerable oxidation of the steel-silver interface, even after exposure to the air for as short time as 3 min.

Thus, the diffusion experiments show that the elements which have the greatest affinity for oxygen, e.g., Li, Al, Mg, Ba, etc., are not able to prevent the diffusion of oxygen through the layers of molten silver. On the other hand, it is most interesting to note that the best performance in the prevention of oxygen diffusion is shown by the elements Ni and Sn, which are among the weakest deoxidizers. Especially interesting are the observations made in the course of the preparation of the 99% Ag–1% Ni alloy. According to the Ag-Ni phase diagram,[4] the solubility of nickel in solid silver is very low: 0.102% at

Fig. 46 Steel, 1% Ba–99% Ag interface. Time of exposure to air, 3 min

Fig. 47 Steel, 1% Ba–99% Ag interface. Time of exposure to air, 5 min

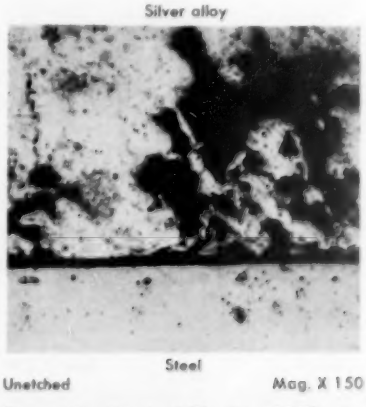

Fig. 48 Steel, 1% Be–99% Ag interface. Time of exposure to air, 0 min

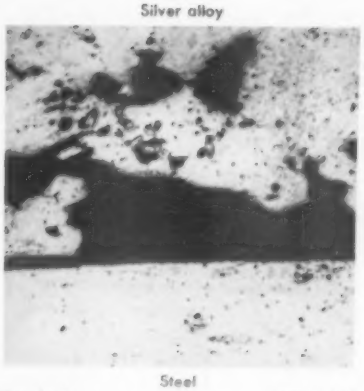

Fig. 49 Steel, 1% Be–99% Ag alloy interface. Time of exposure to air, 3 min

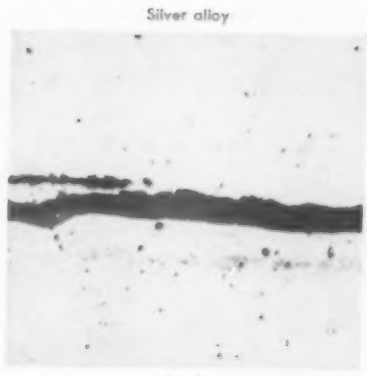

Fig. 50 Steel, 1% Be–99% Ag alloy interface. Time of exposure to air, 5 min

Fig. 51 Steel, 1% Ca–99% Ag alloy interface. Time of exposure to air, 0 min

952° C and 0.012% at 400° C. The solubility of nickel in liquid silver has not been determined precisely. In the course of the preparation of the 99% Ag–1% Ni alloy it has been observed that molten silver rather easily dissolves about 1% nickel. However, after cooling the molten alloy to room temperature and cross sectioning the solidified melt, it has been found that nickel has a tendency to concentrate in the upper layers of the melt. Consequently, it is quite possible that in the liquid melt, a nickel rich layer floats over the melt and protects the molten silver-nickel alloy from the oxygen of the air. That might explain why in the molten 99% Ag–1% Ni alloy the oxygen did not diffuse to the steel-silver alloy interface, even after exposure to the air for a time as long as 10 min. However, since no segregation has been observed in the 99% Ag–1% Sn melts, this hypothesis cannot be applied for the silver-tin alloy. In all events the practical aspects of these observations are quite promising; they show that in principle it is quite possible to prevent oxygen diffusion through layers of molten silver without any flux protection. Now, in addition to one of the two elements (Ni or Sn) which prevent the oxygen diffusion, a third strong deoxidizing element such as Li, K or Na might be added to the alloy in the right proportion. If this third element could reduce the oxides on the base metal surfaces, then it should be possible to use such an alloy to braze the given base metal in air, without using any fluxes, or reducing or protective atmospheres.

In order to investigate more thoroughly the possibilities of development of such self fluxing, "airproof" brazing alloys, it was decided to investigate: (1) the wetting of some base metals, such as low-carbon steel, drill rod, 18-8 stainless steel, etc., by molten silver with 1% addition of the above-mentioned 12 deoxidizing elements; (2) the ability to reduce the oxides on the surfaces of low-carbon steel by molten silver with 1% addition of the above-mentioned twelve deoxidizing elements.

The experimental results on the development of the self-fluxing, airproof brazing alloys have been published in the November 1955 issue of THE WELDING JOURNAL.[5] In the course of this study it has been shown, by comparing some chemical and physical properties of lithium with the properties of some other strongly reducing elements, that lithium appears to be the most suitable metal for developing self-fluxing brazing alloys.

The wettability tests performed with molten 1% Li–99% Ag alloy on low-carbon steel, drill rod and 303 stainless steel fully confirmed this theoretical postulation. Small additions of lithium not only reduce the oxides on the surfaces of these steels, but also considerably lower the wetting (contact) angle of molten silver thus promoting wettability and fluxidity.

The lithium bearing silver alloys and the lithium bearing copper alloys can be successfully used for brazing plain carbon steels, as well as stainless steel without flux or reducing atmospheres. The tensile strength of such joints is quite high.

Conclusions

In summary, the following conclusions are evident:

1. The experimental results obtained on the investigation of wettability of low-carbon steel with pure silver and various silver base alloys proved that an incomplete protection against exposure to the air might considerably impair the wettability. Under certain conditions on exposure to the air, times as short as $^1/_2$ sec are sufficient to cause dewetting of the steel surfaces by the molten filler metals.

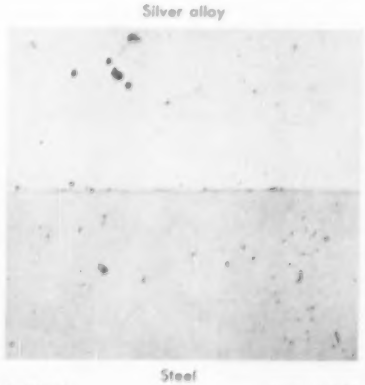

Fig. 52 Steel, 1% Ca–99% Ag alloy interface. Time exposure to air, 3 min

Fig. 53 Steel, 1% Ca–99% Ag alloy interface. Time exposure to air, 5 min

2. A study of the influence of small additions of various metals on the diffusion of oxygen through a layer of molten silver has revealed that:

(*a*) Some metals can considerably decrease the rate of diffusion of oxygen through molten silver; and some of them, as for instance Ni or Sn, might even completely protect the molten silver from the oxygen of the air.

(*b*) The metals which have the highest affinity for oxygen, e.g., Li, Al, Mg, Ba, etc., are not able to prevent, or appreciably slow down, the diffusion of oxygen through layers of molten silver.

(*c*) Small additions of copper to molten silver, apparently, can even accelerate the rate of diffusion of oxygen through layers of molten silver.

3. The wettability experiments performed with molten silver with small additions of various metals have proved that small additions of barium, and especially small additions of lithium, considerably improved the wettability of liquid silver on steel. The two metals, barium and lithium, both of which have a very high affinity for oxygen, apparently are able to reduce iron oxides at practical brazing temperatures. The wettability experiments also indicate that small additions of barium or lithium are able to reduce considerable the surface tension of the molten silver, thus promoting extremely good wettability and fluidity of the pertinent alloys.

4. The practical aspects of this investigation are quite promising. They indicate that it might be feasible to produce self-fluxing, airproof brazing alloys, which would braze steel in air without any fluxes or protective atmospheres. This could be done by combining the metals so that one metal (or combination of metals) would protect the molten filler metal against the oxygen of the air, and the other metal (or combination of metals) would reduce the iron oxides on the steel surfaces, thus providing the filler metal with self-fluxing properties.

For protection against oxygen diffusion, small additions of nickel or tin, or both of them, can be used for self-fluxing silver-brazing alloys.

The high affinity of lithium for oxygen and the comparatively low melting point of Li_2O make lithium especially suitable as an addition for self-fluxing brazing alloys.

Acknowledgments

The author wishes to express his appreciation to the Pitman-Dunn Laboratory of the Frankford Arsenal for sponsoring this investigation at the Armour Research Foundation, for granting their permission to publish this work, and specifically to Frank W. Hussey for his technical assistance.

In addition, the author wishes to acknowledge the assistance of Dr. John M. Parks, Dr. William Rostoker and Orville T. Barnett, who were in charge of this study, Edmund Klimek, Supervisor of the Metallographic Services, and Edward R. Roeder, Senior Technician at Armour Research Foundation. The author wishes to acknowledge the valuable assistance of Harry Schwartzbart in the preparation of this paper.

Bibliography

1. Froelich, K. W., *Z. Metallkunde*, **28**, 368–375 (1936).
2. Johnson, F. M. G., and Larose, P., *Jnl. Am. Chem. Soc.*, **46**, 1377 (1924), and **49**, 312 (1927).
3. Steacie, E. W. R., and Johnson, F. M. G., *Proc. Roy. Soc., London (A)*, **112**, 543 (1926).
4. Christie, John L., *Metals Handbook*, ASM 1151 (1948).
5. Bredzs, N., and Canonico, D. A., "Lithium Additions to Brazing Alloys," THE WELDING JOURNAL, **34** (11), 535-s to 543-s (1955).

Correction:

"The Effects of Zinc Phosphate Coating on Flash Welding of Steel Tubing"

by J. F. Young and A. Phillips

In the September 1956 issue of THE WELDING JOURNAL, *Research Supplement, page 420-s, table at top of page, second column, the Surface Condition for Specimens 7 through 11 reads incorrectly. It should state "Cleaned" instead of "Zinc phosphate."*

The Editor